MAREES TERRESTRES

BULLETIN D'INFORMATIONS

1 3 2

1 JUIN 2000

Association Internationale de Géodésie

Commission des Marées Terrestres

Editeur Dr. Bernard DUCARME
Observatoire Royal de Belgique
Avenue Circulaire 3
1180 Bruxelles

BIM 132

1 juin 2000

IN MEMORIAM

Hans Georg Wenzel (1945 – 1999)

The geodetic community lost an outstandig scientist: Hans-Georg Wenzel died on 11 November 1999. His colleagues and friends are shaken and speechless.

Hans-Georg Wenzel was born on 3 February 1945, in Hahnenklee/Harz, Germany. His professional education included the training for a technican in surveying (1962-1964), and studies of surveying engineering (School of Technology Essen, 1964 – 1967) and Geodesy (Technical University Hannover, 1968 – 1972), both finished with „summa cum laude".

He then entered the Institut für Theoretische Geodäsie (today Institut für Erdmessung) of the University of Hannover, and worked there from 1972 – 1988, as scientific assistant, chief engineer and senior scientist. At this young institut, Hans-Georg Wenzel could fully display his high qualification and deep knowledge. With great enthusiasm and admirable efficiency, he engaged himself in teaching and research, and became a driving element at most of the institut's research projects in physical geodesy and gravimetry. He received the Doktor-Ingenieur degree with a thesis on the accuracy of gravimetric earth tides observations (1976), and his Dr.-Ing. habil. thesis dealt with high resolution spherical harmonic models for the gravitational potential of the earth (1985). These fundamental publications and many other papers on earth tides research, relative and absolute gravimetry, instrumental developments, spectral analysis of the gravity field, geoid determination (a first gravimetric geoid for Europe was presented in 1983), and network adjustment showed his solid theoretical background and his abilities at the aquisition and processing of large different type data sets, as well as his capacity to develop new methods for data evaluation and modelling.

In 1988 Hans-Georg Wenzel became Professor at the Geodetic Instiute, University of Karlsruhe, and Director of the Schiltach Geodynamical Observatory. His research now concentrated on the analysis of earth tide measurements, including the determination of the pole tides and the nearly diurnal free wobble. Amoung the results of this period we find a new tidal potential catalogue, a world wide synthetic gravity tides model, and the earth tides data processing package ETERNA. In the last year, a remarkable step forward to the next generation of global gravity field models was done, with the development of the ultra high-degree (1800, 1800) geopotential models GPM 98. Altogether more than 150 papers, many of them presented on international meetings, document the scientific productivity of Hans-Georg Wenzel over more than a quarter of a century.

It was only natural, that IAG early recognized H.-G. Wenzels talents, and incorporated him into the world wide IAG network. He chaired the special study group „Global Gravity Field Approximation" (1987 – 1991) and the International Gravity Commission working group „Computation of Mean Gravity Anomalies" (1989 – 1991). He served as Secretary (1987 – 1991) and President (1991 – 1995) of Section 3 „Gravity Field Determination" and as President of the Earth Tides Commission (1995 – 1999). His management abilities were acknowledged in the Directing Board of the "Bureau Gravimétrique International" (1987 – 1995), and as Secretary of the Federation of the Astronomical and Geophysical Data and Analysis Services FAGS, since 1996.

In 1999 Hans-Georg Wenzel accepted a call from the University of Hannover, to become Professor for Physical Geodesy at the Institut für Erdmessung, and thus to return to his

previous sphere of activity, as the successor of his former teacher, colleague and friend, who has the sad duty to write this obituary. Hans-Georg was the ideal person to take over this chair, with the expectation to further develop well established research areas, and to build up new branches. With great energy he started work on the 1st of March 1999, and at many discussions with him I again admired his clear thinking, his energy and his visions on the challenges and the development of physical geodesy and the future of the Institute. Without any recognizable warning Hans-Georg Wenzel left us far to early. We shall miss him and we mourne with his wife Marion and his daughter Christine. His exellent scientific work will remain, as well as the manyfold personal reminescences of a kind colleague and a good friend.

Wolfgang Torge, Hannover

NDFW Analysis of Borehole Water Level Data from the Hot-Dry-Rock Test Site Soultz-sous-Forêts

Jörg Zaske
Geophysical Institute, Karlsruhe University, Hertzstr. 16, D-76187 Karlsruhe, Germany
Joerg.Zaske@gpi.uni-karlsruhe.de

Walter Zürn
Black Forest Observatory, Heubach 206, D-77709 Wolfach, Germany
Walter.Zuern@gpi.uni-karlsruhe.de

Helmut Wilhelm
Geophysical Institute, Karlsruhe University, Hertzstr. 16, D-76187 Karlsruhe, Germany
Helmut.Wilhelm@gpi.uni-karlsruhe.de

Abstract

Water level variations in boreholes which are in hydraulic contact with confined aquifers often reflect pore pressure changes of different origin. Two sources of natural pore pressure changes are the tides of the solid earth and barometric pressure variations. Knowing the transfer function between these forcing functions and the water level reaction, such natural pore pressure changes can be used to get important in-situ information about hydraulic aquifer properties. In the time period from 05/1994 to 02/1996 a 665 days quasi-continous dataset of well level variations was recorded in an observation borehole at the European Hot-Dry-Rock (HDR) test-site in Soultz-sous-Forêts, Alsace (France) with the purpose to monitor the aquifer pressure in the hydraulic far-field of the geothermal reservoir. These well level data include distinct reactions to massive hydraulic activities in the frame of the HDR project as well as air pressure and earth-tide induced water level variations. The transfer function between the water level variations and the earth tides has been derived using the earth tide analysis program ETERNA 3.21. Even though the data have been heavily disturbed by the mentioned hydraulic activities it was possible to perform an earth tide analysis and to use the results for the estimation of poroelastic aquifer parameters. The results of the tidal analysis and the high spectral resolution made it possible to consider all major wavegroups in the diurnal and semidiurnal tidal band separately, especially P_1, S_1, K_1, ψ_1 and ϕ_1. Our results clearly show the effect of the NDFW which emphasizes the sensitivity and the potential of borehole measurements as large scale volumetric strain meters. This fact encouraged us to perform additionally a more detailed analysis concerning the Nearly Diurnal Free Wobble (NDFW), the well-known mode of the rotating earth with an elliptical core-mantle boundary. The parameters of this mode reveal important information about the ellipticity of the core-mantle boundary. So far only very high quality gravity or strain measurements have been used to estimate NDFW parameters. Note that 100% of the total signal in case of the strain and only 16% in case of gravity tides is due to the response of the earth to tidal forcing. As the free core nutation period we determined $T_{FCN} \approx 380$ days, which is in disagreement with other studies.

Introduction

It is a well known phenomenon that pore pressure changes in confined aquifers can be observed as water level variations in boreholes intersecting such layers. Especially useful sources of such pore pressure variations are the tides of the solid earth as well as changes in the barometric loading. The tides caused by the gravitational forces of sun and moon are predictable to high accuracy, which makes it possible to calculate the transfer functions between the different theoretical tidal strain components and the water level reaction using an earth tide analysis program. The resulting transfer function between the large scale tidal deformation and the water level reaction can be used to derive in-situ petrohydraulic aquifer parameters assuming different simplistic model aquifers. This is a unique key to derive in-situ poroelastic rock parameters at natural strain and frequency conditions and many studies have been done (e.g. van der Kamp and Gale, 1983; Rojstacer and Agnew, 1989; Hsieh et al., 1987; Evans et al., 1991; Endom and Kümpel, 1994).

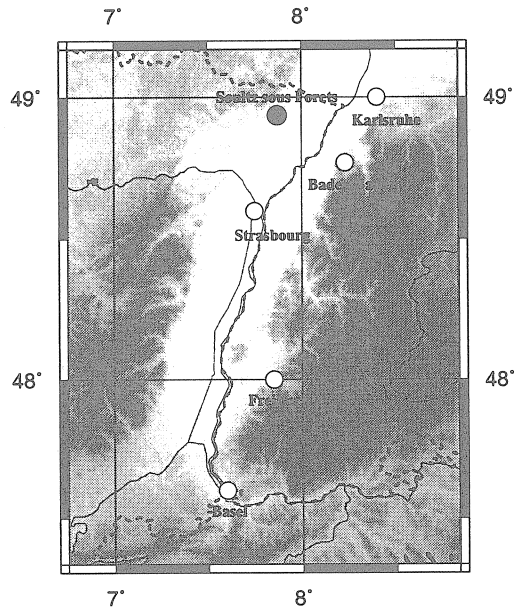

Figure 1: Location of the HDR test site Soultz-sous-Forêts, Alsace (France) in the Rhine-valley.

As part of the 'European Hot-Dry-Rock (HDR) Research Programme' for heat mining from deep granitic rocks in Soultz-sous-Forêts longtime water level measurements in different boreholes are carried out by GTC Kappelmeyer GMBH. Soultz is located in the Rhine Graben, 50 km north of Strasbourg, France (Fig. 1). The project was initiated in 1987 and has two deep production and four observation wells (Fig. 2). Mohr and Frey (1991) and Zaske (1997) used earth tide and barometric pressure induced well level variations of borehole GPK-1 and of borehole 4550, respectively, for the estimation of in-situ rock parameters.

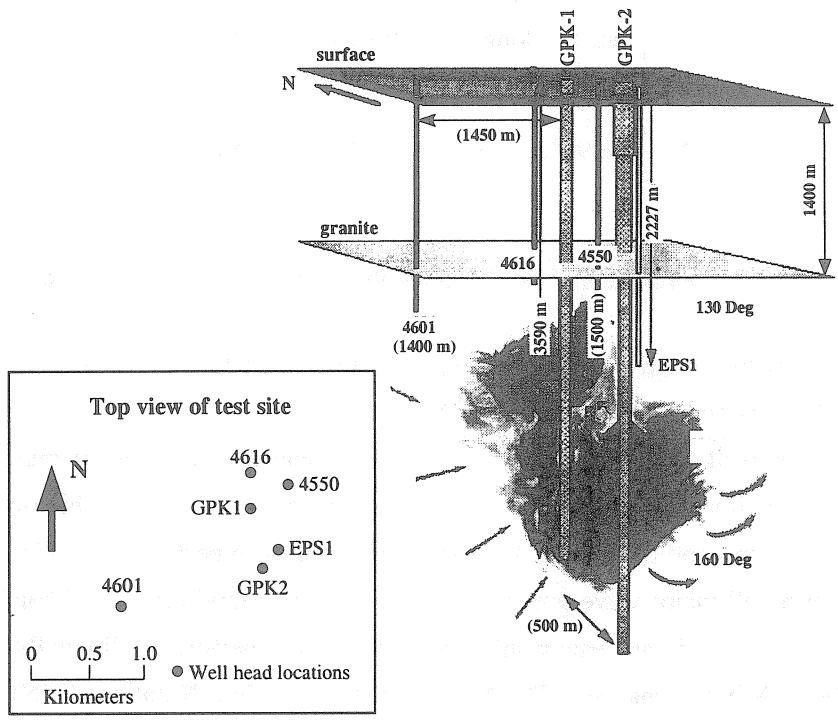

Figure 2: Schematic cross section of the HDR test-site in Soultz-sous-Forêts with the different wells as being available in March 1995 (modified from Baumgärtner et al. (1996)). The data series of this study stems from the observation borehole 4550. Additionaly the top view of the well network is shown.

The aim of the HDR project is to exploit heat stored in the rock mass rather than heat contained in hydrothermal waters. The realization of this idea is based on the 'Soultz-HDR-Concept' (Baria et al., 1995; Baumgärtner et al., 1996): In the first stage the existing fracture system in the granitic rocks, which is partly connected and partly not, is opened, extended and better connected. This is done by performing a large scale stimulation of the desired 'heat exchanger' by injecting cold water with high pressure in the involved boreholes. In the next stage water is circulated through the heat exchanger between at least two deep boreholes. By performing several large scale hydraulic stimulations in the years 1993 to 1995 a very large permeable volume was created. Additionally different circulation experiments between the two wells GPK-1 and GPK-2 (distance $\approx$ 500 m) of several months length have been performed. In order to observe the hydraulic far field of the 'heat exchanger' and to determine the impact of the hydraulic experiments on the rocks surrounding the involved boreholes (GPK-1 & GPK-2), the water level in the four peripheral wells EPS1, 4550, 4616 and 4601 has been monitored for many years now. In this manner water level variations due to pore pressure changes in the confined aquifer, which are caused by effects of hydraulic activities, barometric pressure variations as well as earth tide deformations have been monitored. The fact that the hydraulic activities have been restricted to the deep boreholes GPK-1 and GPK-2 made

Well	Position lat. [°]; long. [°]	Height [m a.s.l.]	Depth [m]	Open Hole [m]
4550	48.94°N; 7.87°E	151.17	1500	85

Table 1: Coordinates of Well 4550 at the HDR test site in Soultz-sous-Forêts.

it possible to record relatively long data series, with short interruptions at the observation wells. Between 05/1994 and 02/1996 a 665 day quasi-continous well level time series was recorded in the observation well 4550 (Fig. 2, Table 1). The disturbances due to the hydraulic stimulation and circulation experiments in this period could be effectively eliminated by high-pass filtering. The high spectral resolution of the long time series allowed us to perform a detailed earth tide analysis considering all major wave groups in the diurnal and semidiurnal tidal band separately. The quality of the earth tide analysis results encouraged us to perform additionally a Nearly Diurnal Free Wobble (NDFW) analysis. The NDFW or the Free Core Nutation (FCN) are two different aspects of the same free mode of the rotating earth with an elliptical core-mantle boundary. This effect is a well known phenomenon in gravity, strain or tilt observations of very high quality (e.g. Polzer et al., 1996). The goal of a NDFW analysis is to estimate characteristic NDFW parameters, which reveal important information about the core mantle boundary. Our results verify clearly the influence of the NDFW in the borehole water level data.

In this paper we present the data, the processing and earth-tide analysis results and focus on the NDFW analysis. More tidal analysis results and their use for the estimation of poroelastic aquifer properties as well as an investigation for possible changes in these properties due to the massive hydraulic experiments are considered in Zaske (1997) and Dornstädter et al. (1998).

Instrumentation

The data presented in this work have been digitally recorded at well 4550, which is an observation well located about 350 m north of the deep production well GPK-1 (Fig. 1). The borehole is 1500 m deep and cased except for the last 85 m in the granitic rocks (Fig. 2). A schematic diagram of the well site instrumentation is shown in Fig. 3. The piezometer utilized a quartz type differential pressure sensor with an absolute measurement accuracy of $\pm$ 0.1% of the full scale measurement range (Table 2). The relative accuracy is usually estimated to be better than 10% of the absolute accuracy. The sensor is calibrated to measure water level variations in the borehole. The pressure device was located at 45 m below wellhead, whereas the average water level was about 39 m below well head. The interior of the pressure sensor was kept at atmospheric pressure

through a breather tube incorporated in the electrical cable from the datalogger at the surface to the sensor in the borehole. For protection against rainfall the borehole was closed at the surface, however it was open to atmospheric pressure changes.

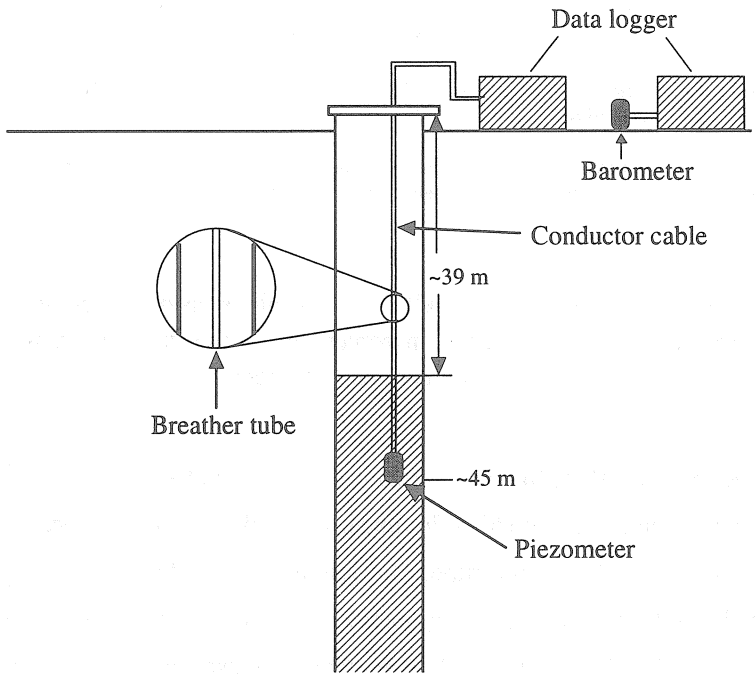

Figure 3: Schematic of well instrumentation. Water level variations and barometric pressure are measured on site. The borehole is closed against rain fall but open for barometric pressure variations. A breather tube compensates for air pressure variations.

The water level variations were digitally sampled every 10 minutes locally on site with date and time using a commercial data logger (MadoSolo; Iris Intruments). No anti-aliasing filter was used. The data have been retrieved irregularly but at the latest after 110 days. If necessary system time was manually adjusted using a DCF clock. The time accuracy is estimated to be better than 3 minutes. The use of an anti-aliasing filter and improved timing accuracy would certainly improve the data quality to some extent. The barometric pressure was digitally recorded at Soultz using a quartz absolute pressure sensor. In addition and independently from the HDR project barometric pressure was digitally recorded at 10 minute sampling intervals at the Research Center in Karlsruhe, Germany (Fig. 1). For periods higher than 11 hours the air pressure variations at Soultz and Karlsruhe were determined to be coherent. Therefore it was possible to use the Karlsruhe data for interpolation of gaps in the Soultz air pressure data.

Data and data processing

The well level data in borehole 4550 (Fig. 2) and the air pressure data at Soultz-sous-Forêts in the period from May 4, 1994, to February 27, 1996, were digitally recorded with a 10 min sampling

Purpose	Location	Pressure device *Company*	Full scale Pressure	 WL	Type	Acurracy (absolute)
Well Level	Soultz Well 4550	PDCR 940 (*Druck Messtechnik GMBH*)	1000 hpa	10 m	Difference	0.1% 1 cm
Air Pressure	Soultz Well EPS1	PDCR 940 (*Druck Messtechnik GMBH*)	1000 hpa	10 m	Absolute	0.1% 1 cm
Air Pressure	Karlsruhe Forschungszentrum	Baro Ferngeber 5010 (*Theodor Friedrichs GMBH*)	100 hpa	1 m	Absolute	0.2% 0.2 cm

Table 2: Pressure devices used for well level and air pressure observations at the different locations. The absolute accuracy is given in percentage of the full scale range. The relative accuracy can be estimated as 10% of the given absolute accuracy.

interval. The total length of the time series is 665 days. In the water level data only a few gaps, all shorter than one hour, had to be filled by linear interpolation. The air pressure recordings at Soultz-sous-Forêts were sometimes interrupted for longer periods due to technical problems, which were caused e.g. by lightning strikes. A comparable air pressure time series, recorded at the Research Center of Karlsruhe (Fig. 1) about 40 km away was used instead during these periods. Table 3 gives an overview of the used data. Fig. 4 (a) and (b) show the interpolated data series.

	Period [d]	Sampling [min]	Data gaps ($> 1\ h$) [days]	Length of gap [days]	Summed length
Well Level Soultz	04.05.94 (00:00 UT) - 27.02.96 (23:50 UT) 0-665 d	10	0	0	0.1 d 0.01%
Air Pressure Soultz	04.05.94 (00:00 UT) - 27.02.96 (23:50 UT) 0-665 d	10	38.6-51.3 68.3-100.1 155.8-169.7	14.6 31.8 13.9	60.4 d 9.1%
Air Pressure Karlsruhe	04.05.94 (00:00 UT) - 26.02.95 (23:50 UT) 0-299 d	10	241.5-243.4	1.9	1.9 d 0.7%

Table 3: Statistics of the used well level and air pressure data from Soultz-sous-Forêts (France) and Karlsruhe (Germany).

As an example the two air pressure recordings are shown over an undisturbed 70 day time span in Fig. 5a. The mean coherency function between both time series calculated from 5 non-overlapping data segments with a total length of about 230 days of undisturbed recordings at both stations is

shown in Fig. 5b. For frequencies larger than 2.5 cycles per day (cpd) the coherency decreases rapidly, but below 2.1 cpd it is larger than 0.8 and for frequencies smaller than 0.6 cpd it is almost 1. For the diurnal and semi-diurnal tidal band as well as for lower frequencies the coherency of the barometric pressure field between the two locations of air pressure registration is high enough to use the Karlsruhe data instead of the Soultz data. In order to investigate a possible phase shift between the two airpressure recordings the crosscorrelation function between both time series was calculated. Due to its maximum magnitude at zero time lag, no phase difference was considered when the gaps of the air pressure data at Soultz were filled with the corresponding data from the Research Center Karlsruhe.

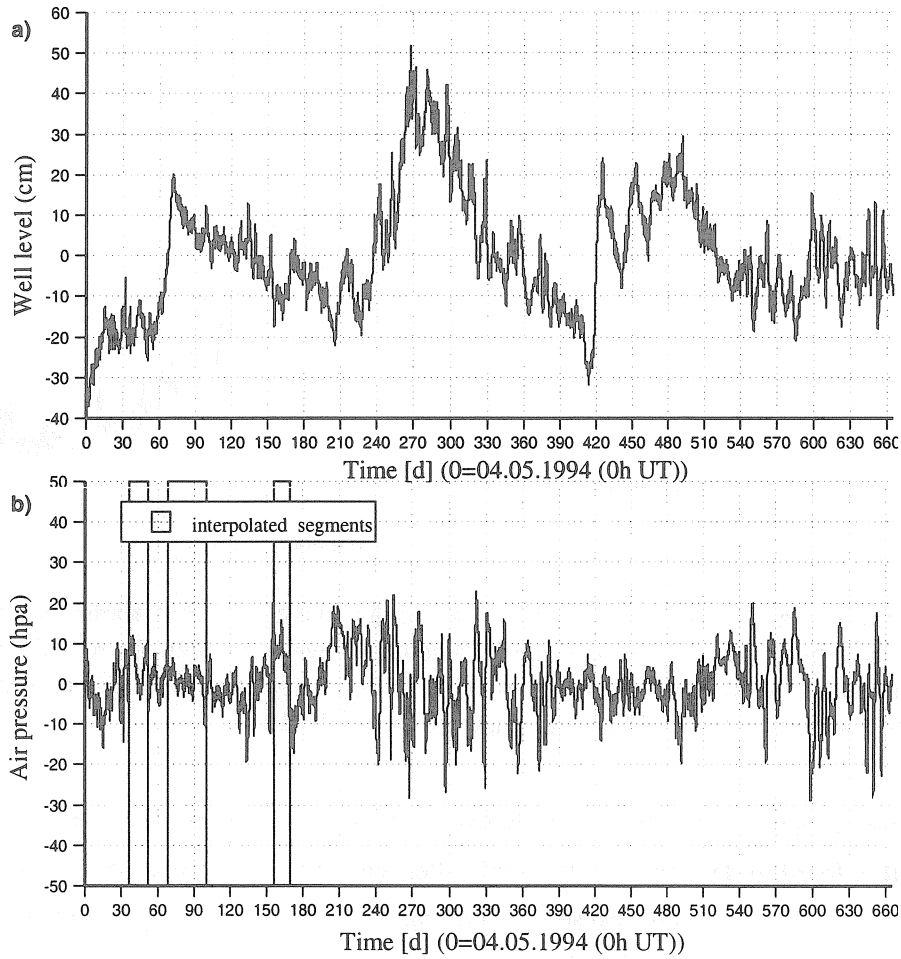

Figure 4: Water level (a) variations relative to 39.75 m depth below the upper end of the borehole (up: level rise) and (b) interpolated air pressure variations at Soultz relative to 993.6 hPa. The time spans marked with gray color show the sections, where data from the Research Center of Karlsruhe were used for air pressure interpolation.

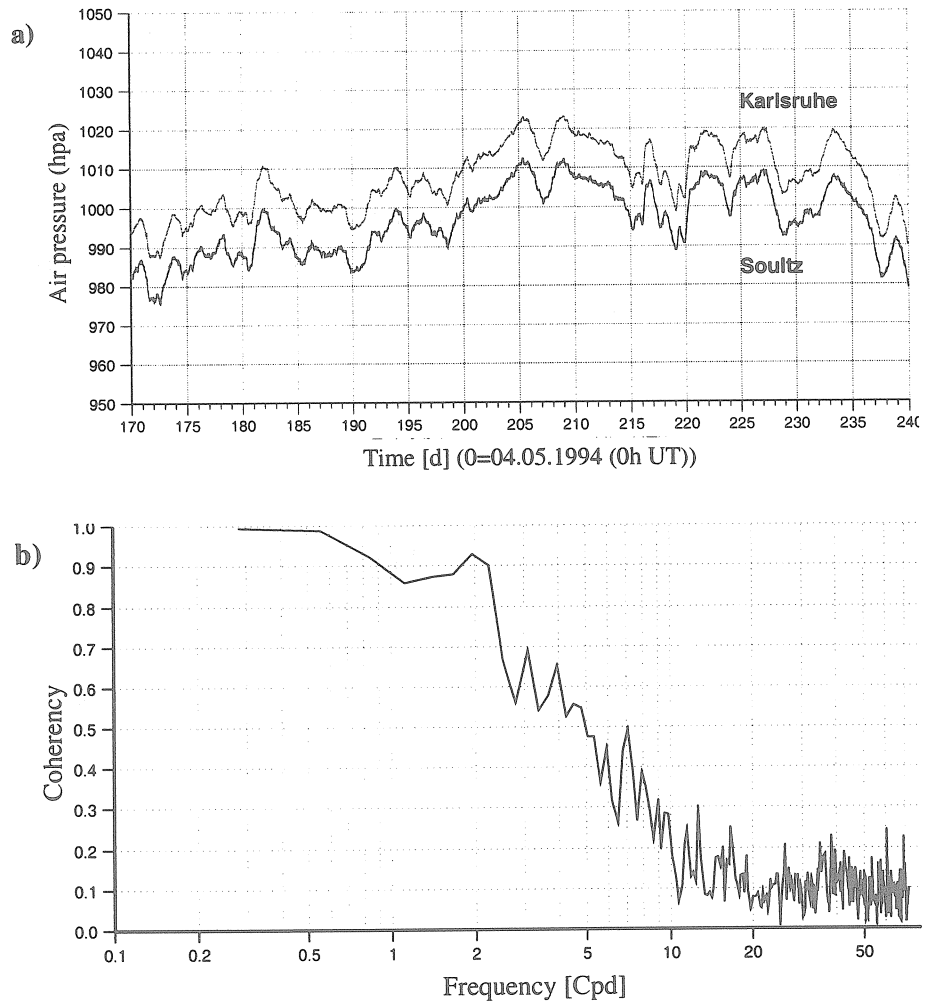

Figure 5: (a) Air pressure recordings in Soultz-sous-Forêts and Karlsruhe for an undisturbed 70 days time window. (b) Coherence function between air pressure recordings in Soultz-sous-Forêts and the Research Center Karlsruhe. It was calculated using 5 non-overlapping data segments at both stations with a total length of about 230 days.

Before resampling the data to hourly values, the level and air pressure data were low-pass filtered with a fourth order causal Butterworth filter with cut-off frequency of 10 cpd back and forth to eliminate the phase shift caused by filtering in one direction. Fig. 4 shows (a) the water level variations relative to 39.75 m depth below the upper end of the borehole and (b) the corresponding interpolated air pressure variations at Soultz relative to 993.6 hpa. The time spans marked with gray color show the sections, where data from the Research Center of Karlsruhe were used for air pressure interpolation. At first glance remarkable rapid changes in the order of 50 cm appear in the water level, which reflect hydraulic activities like drilling, hydraulic testing and stimulation at the main boreholes GPK-1 and GPK-2. These strong reactions indicate a hydraulic connection between the boreholes. The remaining variations are clearly anticorrelated with the air pressure variations, which is typical for a well open to the atmosphere, and reach amplitudes of 10-20 cm.

A closer look at the time series reveals that there are also tidal variations in the water level and air pressure. For day no. 150 to day no. 158 the detrended variation of the water level is displayed in Fig. 6 (a) with the theoretical tidal dilatation which is in phase with the areal strain and the tidal potential, and in Fig. 6 (b) together with the detrended airpressure. The diurnal and semi-diurnal tides in the well level observations as well as the anticorrelation with the air pressure are clearly visible.

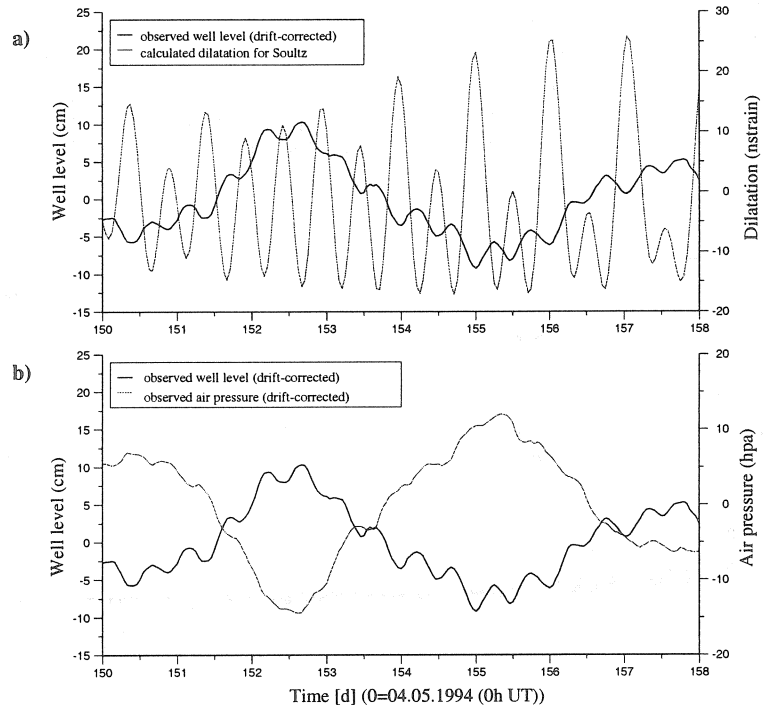

Figure 6: (a) Detrended well level variations (up: level rise) with the theoretical tidal dilatation (compression: negative) and (b) the same well level variations with the detrended air pressure. The diurnal and semidiurnal components of the tidal signal in the well level data (a) as well as the anticorrelation to the air pressure in (b) can be clearly observed.

The theoretical spectrum of the diurnal and semi-diurnal areal strain components is shown in Fig. 7 together with the spectral amplitude of the well level and the air pressure data. The well level spectrum clearly reflects the larger spectral lines of the theoretical dilatation, however with different relative amplitudes. The air pressure, on the other hand, does only show the thermal influence of the solar irradiance at the solar diurnal and semi-diurnal frequencies, i.e. the solar tidal lines S_1 and S_2. Because the well level is anticorrelated with the air pressure its influence modifies the relative magnitudes of the K_1 and S_2 lines in the spectrum of the well level data compared to their strength in the spectrum of the theoretical dilatation. The complete spectra are shown in logaritmic scale in appendix A (Fig. 15). In the diurnal and semi-diurnal tidal band the five main components, named O_1, K_1, N_2, M_2, and S_2 make up 95% of the tidal potential. The quality of the data was, however, so high that smaller spectral lines could be clearly resolved.

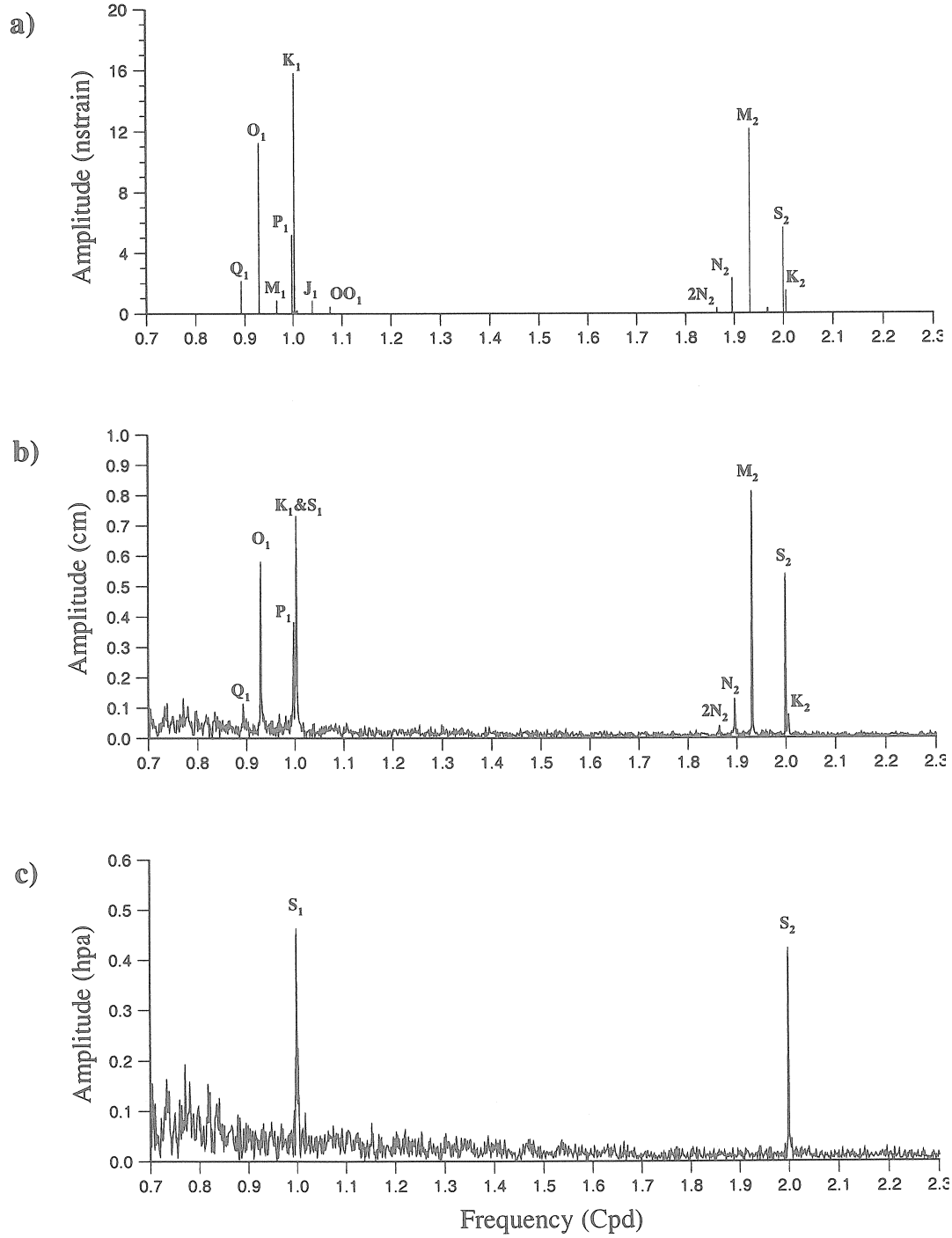

Figure 7: Spectra of the theoretical tidal areal strain (a), the observed well level (b) and air pressure (c) data in Soultz-sous-Forêts. The amplitude spectra have been calculated using the complete data sets with a total length of 665 days and a sampling rate of 10 minutes. Å double logarithmic plot of these amplitude spectra showing the complete frequency range is shown in appendix A (Fig. 15).

Hydraulic activities

During the recording of the water level data several hydraulic activities in the frame of the HDR project have been performed. In order to show the reactions of the level data in well 4550 more clearly we tried to eliminate the air pressure influence by a linear regression factor. The result is shown in Fig. 8. The grey colored segments indicate the periods of hydraulic activities which are briefly explained in the following list. For more details about the results of these and more recent hydraulic tests we refer to Gérard et al. (1997) and Jung et al. (1998). These authors also propose a conceptual model of induced circulations in the underground. More results on well level reactions of the different observation wells can be found in Dornstädter et al. (1998) and Gérard et al. (1997).

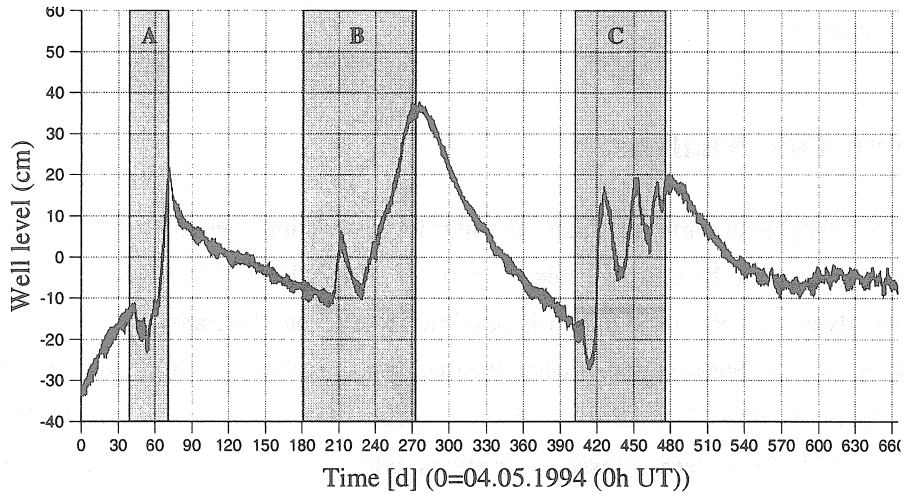

Figure 8: Well level variations relative to 39.75 m depth below the upper end of the borehole. A barometric efficiency value of -0.565 was used to reduce the air pressure influence in the well level data. The strong longperiodic variations are induced by the described massive hydraulic testing. The experiments in segments A, B and C are shortly explained in the text.

- A: Production test ($\approx$ 6.200 m^3) at the borehole GPK-1, as well as testing of injectivity at GPK-1 ($\approx$ 10.000 m^3 fluid injected).
- B: Drilling of new borehole GPK-2 to a final depth of 3876 m (Fig. 2). Partly with complete drilling fluid losses.
- C: Hydraulic stimulation of GPK-2 in summer 1995. During a massive stimulation of the accessible part of well GPK-2 (3200 m to 3650 m) about 28.000 m^3 fluids of different densities were injected with high pressure and injection rates of up to 56 l/s in order to establish a hydraulic connection to well GPK-1. Afterwards circulation experiments between the two deep boreholes GPK-1 and GPK-2 have been performed for more than 6 weeks with up to 77 tons per hour. The injected fluid volume at GPK-2 was about 50.000 m^3. About the same volume has been extracted at GPK-1.

D: Long term production test at GPK-2 with reinjection at GPK-1 from June to November 1997. At flow rates of 25 l/s a thermal power of 11 MW was reached. Tracer experiments showed that about 35% of the injected water was retrieved at the production well. Although 65% of the injected fluid was lost to the surrounding rock, injection and production rate could be completely balanced over a long time span. Only the events A, B, and C have influenced the considered well data.

The water level in well 4550 is strongly reacting to hydraulic impacts on the geothermal reservoir. After hydraulic testing periods the water level immediately starts to change to its original level. However, due to the fact that the time between the tests (A,B,C) was too short the well level could not reach its original value. After test period C a stable level was reached, which is not equal to the starting level.

Earth Tide Analysis

For the analysis of earth tide induced water level variations general earth tide analysis procedures and programs can be used. In this work we used ETERNA 3.21 (Wenzel, 1994). From an earth tide analysis of water level data it is possible to calculate the transfer function, namely the amplitude factors and phase shifts between the theoretical tidal strain components and the corresponding well level reaction. In addition to the tidal strain the water level changes in the well are strongly influenced by barometric pressure variations, which act as a load on the fluid column as well as a load on the surface. ETERNA offers the possibility of a simultaneous least squares fit of a tidal model and additional input channels, like e.g. air pressure recordings, to the observed data. These additional input data are considered in form of a linear regression model and yield a single frequency independent regression coefficient for each of them. Therefore results of the earth tide analysis of water level variations with air pressure data as additional input include a regression factor between the air pressure and the water level data called 'barometric efficiency' in case of boreholes open to the atmosphere (e.g. Endom and Kümpel, 1994). The possible spectral resolution increases with the length of the data series. For the tidal analysis 18 wavegroups, 10 in the diurnal, 6 in the semi-diurnal, as well as the third- and fourth-diurnal tidal wavegroups have been used. The long-period tidal components could not be evaluated because they are disturbed from numerous long-periodic events, like hydraulic testing and hydraulic stimulation of the reservoir. In order to use also these frequencies it would have been necessary to perform driftmodelling to eliminate the different events. The long period effects of hydraulic testing prevented a standard drift elimination. On the other hand the massive disturbances with low frequencies could be eliminated rather well by digital high-pass filtering prior to the earth-tide analysis. We used ETERNA high-pass filter no.6 with a cut-off frequency of 0.8 cpd. As a tidal potential the Tamura (1987)

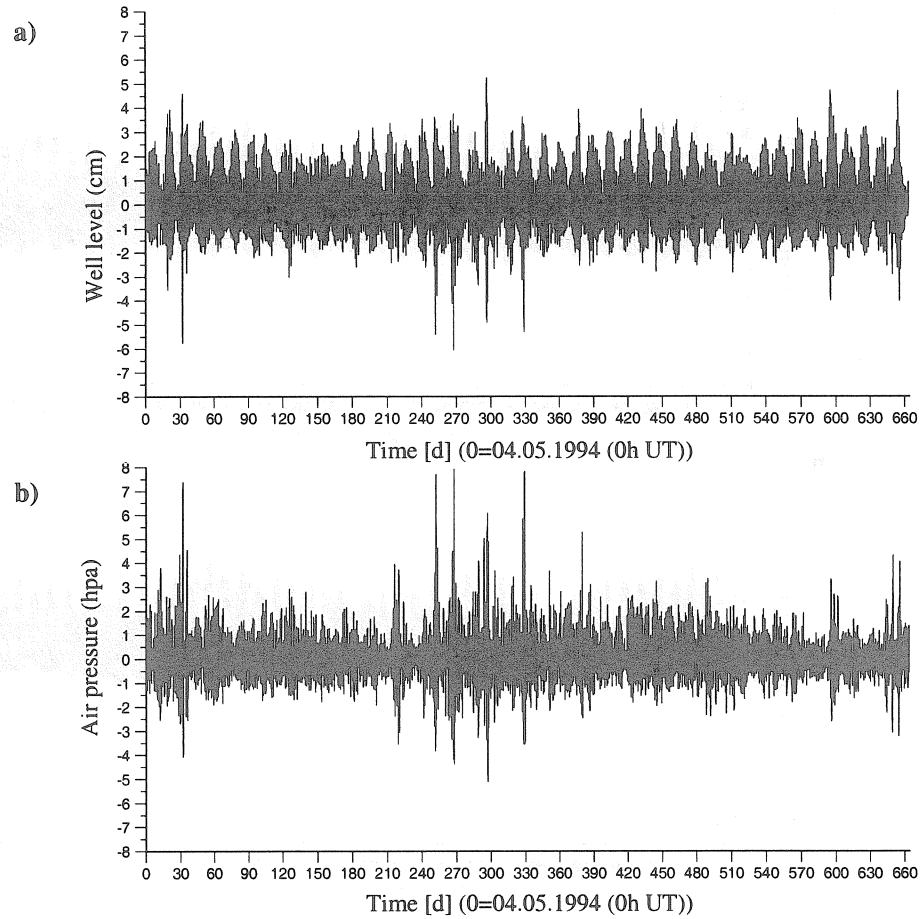

Figure 9: (a) High-pass filtered well level and (b) air pressure data. We used Filter no. 6 of ETERNA with a cut-off frequency of 0.8 cpd. In cases of strong air pressure variations the anti-correlated well level reaction is clearly visible. Sampling rate is 1 hour.

model with 1200 waves was chosen. In Fig. 9 the complete high-pass filtered well level and air pressure data are shown. The anticorrelation between the air pressure and well level is clearly visible. The ‚barometric efficiency' between the time series in Fig. 9 (a) and (b) is -0.565 ± 0.002. Using this value the high-pass filtered well level data have been reduced from the air pressure influence. The results are shown in Fig. 10 (b) and more detailed in a 90 days time window in Appendix B (Fig. 16). The theoretical dilatation at Soultz-sous-Forêts is shown for comparison in Fig. 10 (a).

The residual time series produced by ETERNA, the amplitude spectrum of the residuals and their histogram are shown in Fig. 11. The residuals displayed in Fig. 11 (a) in the same scale as in Fig. 10 (b) show higher values during periods of hydraulic activities. Between day number 120 to 240 and 570 to 665 the residuals are especially low, because during this period there was almost no noise due to hydraulic work. The distribution of the residual amplitudes in the histogram of the residuals is Gaussian, see Fig. 11 (c). In order to evaluate the misfit at different frequencies and

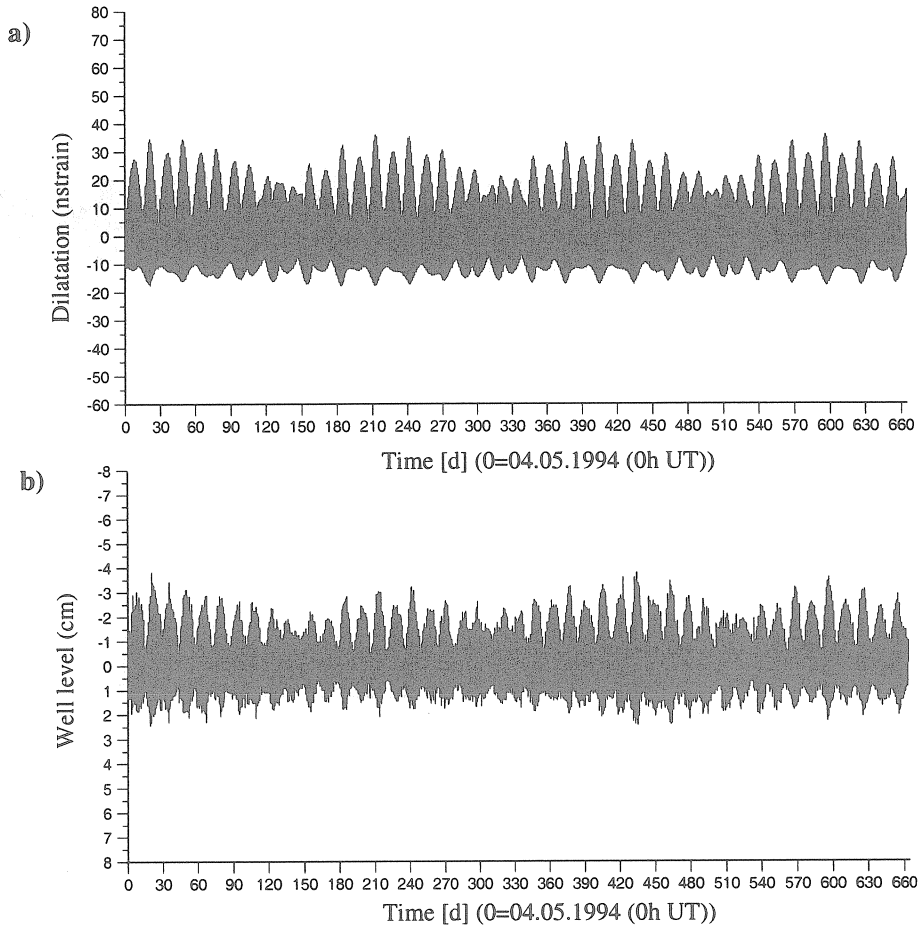

Figure 10: (a) Theoretical dilatation for the location Soultz-sous-Forêts. (b) High-pass filtered and air pressure reduced well level data. A zoomed section is shown in Appendix B (Fig. 16).

wave groups the spectrum of the residuals is shown in Fig. 11 (b). Higher values are located at the diurnal, semi-diurnal and third-diurnal frequencies. This situation is very common because the solar tides can be meteorologically disturbed and therefore not modelled well enough by ETERNA. In Fig. 12 (a) and (b) the results obtained by tidal analysis with ETERNA are displayed graphically. In Appendix C they are shown in tabular form (Tab. 6). Except for S_1 and ψ_1 the amplitude factors are within the range of 0.4 to 0.8 mm/nstrain and do not show a specific frequency dependence. In case of the phase differences this effect cannot be excluded. This may partly be due to ocean tide corrections which have not been applied yet. S_1 is clearly meteorologically disturbed and the special role of ψ_1 in connection with the NDFW will be discussed later.

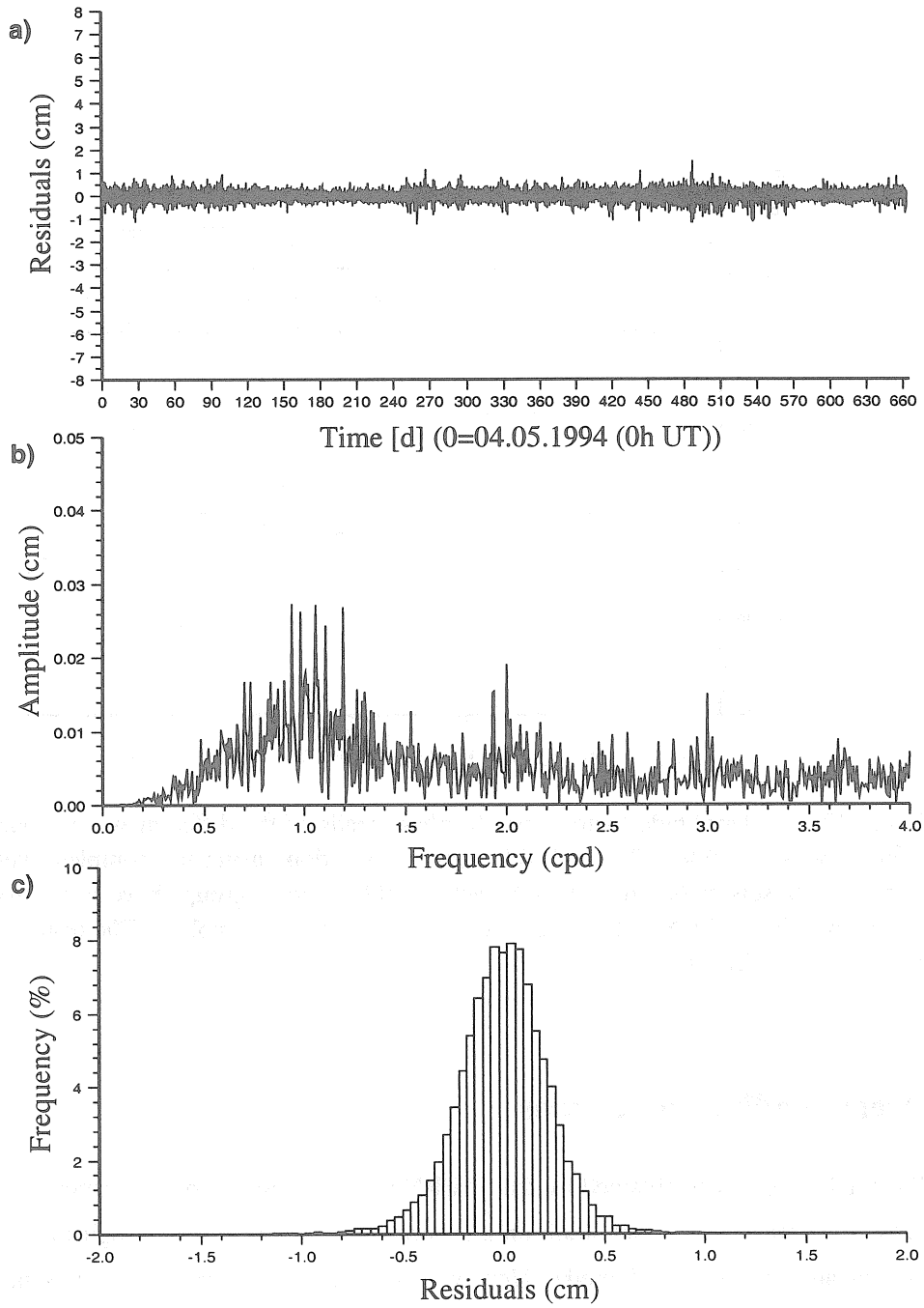

Figure 11: Residuals of the earth tide analysis (a), amplitude spectrum of the residuals (b) and histogram of the residuals (c). The earth tide analysis was done using the complete well level and air pressure data sets of 665 days length each.

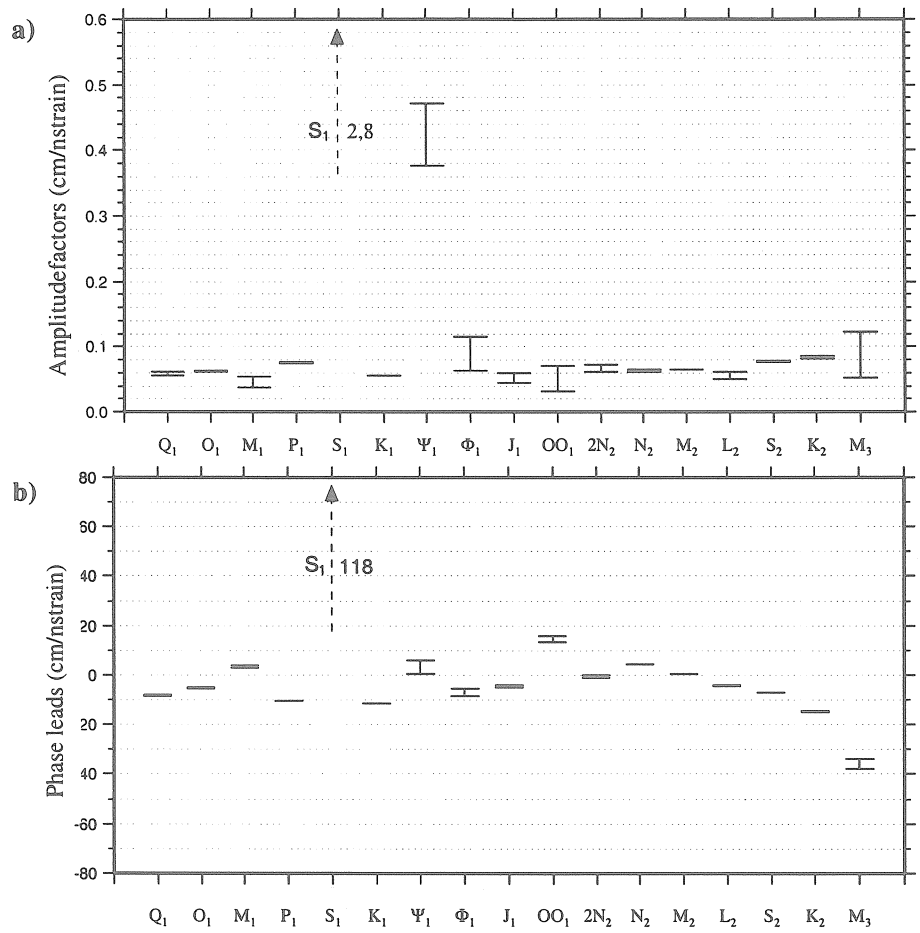

Figure 12: (a) Amplitude factors and (b) phase leads of the different wave groups with respect to the areal strain tide. The earth tide analysis was done using the complete well level and air pressure data sets of 665 days length each. Eighteen wave groups have been used in the fitting procedure with ETERNA. There is no ocean load correction applied. The results are also shown in Appendix C (Tab. 6).

Ocean loading corrections

The tidal admittances obtained by the ETERNA routines represent the response of the well level to the theoretical areal tidal strain on a spherically symmetric seismologically constrained non-rotating and oceanless earth model. However, these theoretical strains misrepresent the tidal strains acting on the aquifer for three reasons.

The first are deviations from the above theory due to local and regional lateral heterogeneities (geology, topography and cavity effects (e.g. Harrison, 1985)). We assume in the following that due to the spatial averaging of these effects by the effective volume of the aquifer the total effect is small compared to effects a linear extensometer or a borehole strainmeter would suffer. The second reason is the frequency dependence of the transfer function in the diurnal band, which

is exploited below to retrieve parameters of the NDFW. We assume that the aquifer response to tidal strain is frequency independent through the diurnal tidal band and that the use of a single barometric regression factor (Table 6) suffices to keep our NDFW analysis free of barometric pressure effects. Neuberg and Zürn (1986) have shown that even large local modifications of the strain field do not affect the estimation of the NDFW parameters to first order. The reason is that the strain tensors of all tides within one band (in this case the diurnals) are proportional to each other. The third problem arises from the contribution of ocean loading strains to the input signal at the location of the aquifer. We used the NLOADF program of Agnew (1997) to compute the ocean load strain components at the location of the borehole for the older ocean tide models of Schwiderski (1980) and for 2 modern models based on the TOPEX/ POSEIDON mission: TPXO.2 (e.g. Egbert et al., 1994) and CSR 3.0 (Eanes and Bettadpur, 1995). These three models include tidal maps for the tides O_1, P_1 and K_1. Areal strain is simply the sum of the two horizontal strains $\varepsilon_{\theta\theta}$ and $\varepsilon_{\lambda\lambda}$ computed by NLOADF. The results of these computations are presented in Table 4. For the minor, but important tides ψ_1 and ϕ_1 near the resonance we took the usual two approaches: completely neglecting the corrections for these two tides or scaling the amplitudes to K_1 using the relative theoretical ones and assigning the phase of K_1.

Tide	Component		Schwiderski	CSR 3.0	TPXO.2
O_1	$\varepsilon_{\theta\theta}$	Amplitude	0.1941	0.1972	0.1838
		Phase	171.1	167.8	166.9
	$\varepsilon_{\phi\phi}$	Amplitude	0.2302	0.2763	0.2176
		Phase	55.1	53.5	43.8
P_1	$\varepsilon_{\theta\theta}$	Amplitude	0.1280	0.1394	0.0762
		Phase	52.8	61.4	47.4
	$\varepsilon_{\phi\phi}$	Amplitude	0.0859	0.0906	0.1180
		Phase	17.7	22.1	46.5
K_1	$\varepsilon_{\theta\theta}$	Amplitude	0.4170	0.4391	0.3497
		Phase	51.7	54.9	48.0
	$\varepsilon_{\phi\phi}$	Amplitude	0.2507	0.2652	0.3466
		Phase	18.6	17.4	33.4

Table 4: Results of ocean load computations for Soultz-sous-Forêts for three models of the ocean tides. Units for strain components are 10^{-9}, phases in degress with respect to the tidal potential, lags negative.

The observed well level tides can be expressed as the product of the aquifer transfer function and the volumetric strain acting on the aquifer. The volumetric strain in a near-surface situation and for isotropically elastic rocks is proportional to the areal strain. Under these assumptions we are allowed to work with the areal strains. The proportionality factor between areal and volumetric strain is then included in the transfer function. The areal strain at a site has two contributions, when local geological and topographic effects are small and also included in the transfer function.

The first is the tide of the solid earth (body tide) including the resonance due to the NDFW, the second is the ocean loading tide. Since the model tides used in the tidal analysis with ETERNA did not include the NDFW effect, this resonance is included in the apparent transfer function of the aquifer. It is assumed that the transfer function has no contribution from the resonance near ψ_1 for O_1. The correction of the observed admittances for ocean loading are carried out by taking the observed admittances for each tide and subtracting the complex ratios of ocean loading tide to theoretical tide multiplied by the observed admittance for O_1. This method is only valid, if the ocean loading tide is small compared to the theoretical body tide. In our case these ratios are in the order of 0.024 to 0.042 for the tides O_1, P_1 and K_1 (and ψ_1, ϕ_1), respectively.

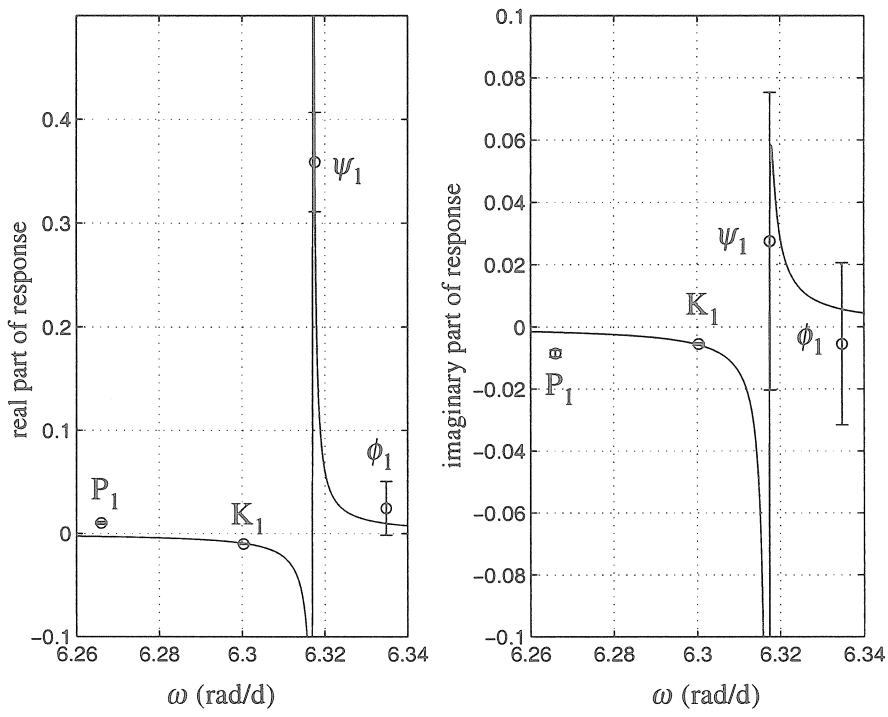

Figure 13: Real and imaginary parts of the NDFW resonance function versus angular frequency ω. Solid curves represent solution for the parameters found with CSR3.0 ocean load corrections for the 5 tides P_1, K_1, ψ_1, ϕ_1, and O_1. The corresponding parameters are: T(FCN)=376.84 sidereal days, Q=-13708.9, A=-0.00210-i0.00124 in units of $(10^{-9}$cm(rad/day)^2. The open circles represent the ocean corrected tidal admittances for P_1, K_1, ψ_1 and ϕ_1, respectively. The model curves are forced to fit O_1 due to the analysis method. The error bars represent formal uncertainties from tidal analysis without calibration errors and errors in the ocean load corrections. All tides are fit by the model within these errors except P_1.

NDFW Analysis

Since about 1985 tidal gravity measurements of high quality are being used to retrieve the parameters of the NDFW (Zürn, 1997). Only very few data from other types of measurements of earth tides were used for this purpose (e.g. Sato, 1991; Polzer et al., 1996). In gravity only about 16 % of the signal are due to the response of the earth to the tidal forcing, most of the observed gravity variation is due to the direct tidal forces on the sensor mass itself. In contrast, in strain observations the earth's response makes up 100 % of the signal, therefore the use of strain tides is promising. However, this advantage of a factor of 6 is (probably more than) compensated by the higher noise level in strain data (e.g. Polzer et al., 1996). Since the formal signal-to-noise ratios for our well level record are 135 and 8.8 for the tides K_1 and ψ_1, respectively, we decided to try a NDFW analysis with these results in order to see, how well such measurements perform. One has to keep in mind that the present data from our "volumetric strainmeter" are heavily disturbed by the hydraulic testing.

After correction for ocean loading we subjected the tidal results to the same NDFW-analysis method as used and described by Polzer et al. (1996). Table 5 and Fig. 14 present the results for the following cases: no ocean loading correction, correction using Schwiderski's model, CSR 3.0 and TPXO.2 for three and five tides as described above. For all of these solutions the variance reduction with respect to the corrected data is about 63 %. Clearly the resonance is a significant feature of our well level tides.

Ocean model -	Number -	T_{FCN} sid. days	ΔT sid. days	Q_{FCN} -	A_{real} see caption	A_{imag} see caption
none	0	374.41	0.110	-13776.4	-0.00162	-0.00119
SCH	5	376.96	0.129	-13130.5	-0.00212	-0.00128
	3	376.91	0.128	-13310.8	-0.00212	-0.00129
CSR 3.0	5	376.84	0.130	-13708.9	-0.00210	-0.00124
	3	376.80	0.129	-13901.3	-0.00210	-0.00124
TPXO.2	5	376.92	0.133	-12579.8	-0.00211	-0.00133
	3	376.88	0.132	-12752.9	-0.00211	-0.00133

Table 5: NDFW-parameters obtained for different ocean loading corrections. First column indicates the ocean tide model used, the second column gives the number of tides corrected (see text). Columns 3 through 7 present the period of the FCN, its formal standard deviation, Q, real and imaginary part of the resonance strength. The units for the strength components are 10^{-9}cm(rad/day)^2.

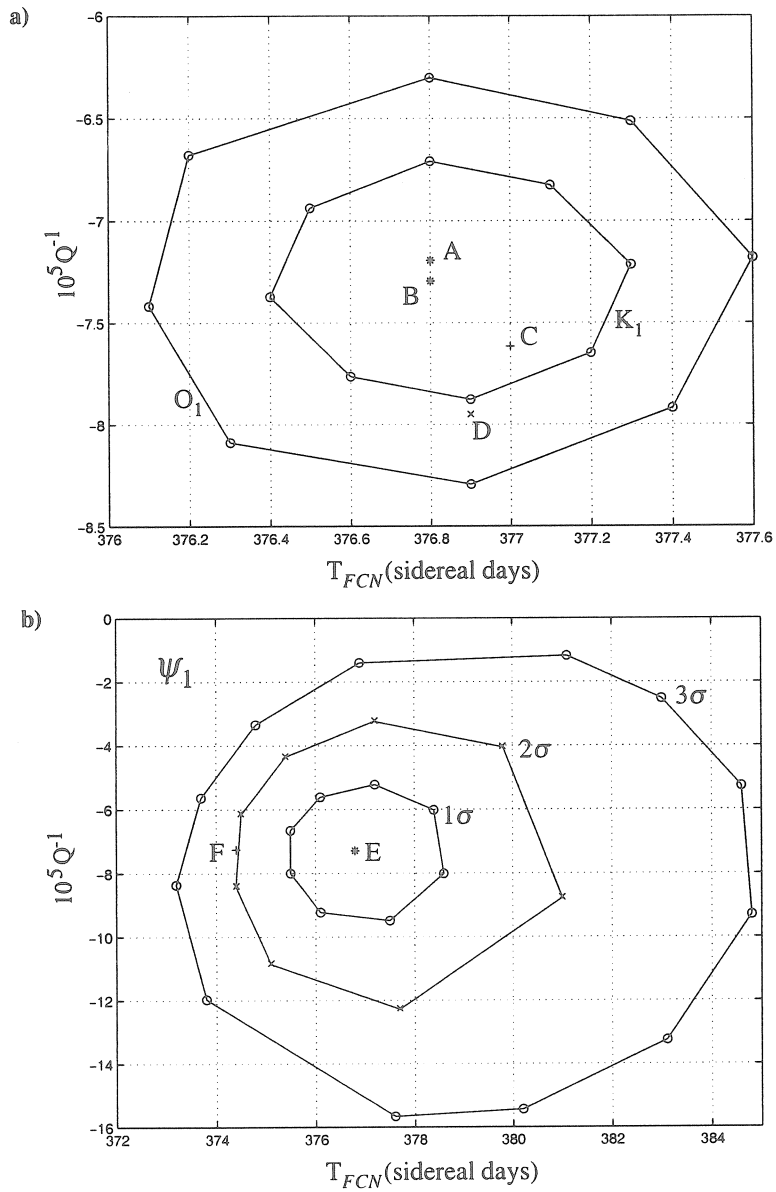

Figure 14: Sensitivity analysis: different solutions for NDFW parameters in the $Q^{-1} - T$-plane. (a) The asterisks represent the solutions using the CSR3.0 ocean tide model (B: corrections for ψ_1 and ϕ_1 scaled to K_1, A: no corrections for these two tides). C represents the solution using the Schwiderski ocean model, and D the solution using the TPXO.2 ocean model, both with the small tides ψ_1 and ϕ_1 scaled to K_1. The other symbols represent solutions where the tidal admittances for O_1 (outer ring) and K_1 (inner ring) were disturbed with phasors of length 1σ standard deviation as given by ETERNA and 8 different phases. Note that disturbing O_1 affects all admittances used. (b) Solutions for ψ_1 tidal admittances disturbed by 3σ (outer ring), 2σ (intermediate ring) and 1σ (inner ring) as given by ETERNA and different phases. E represents the solution for the CSR3.0 ocean tide model and small tides scaled to K_1. F was obtained with no ocean tide correction at all.

Inspection of the results in Table 5 also clearly shows, that the solution is very stable against small modifications of the input data. The main features of our results which do not agree with those from VLBI (Gwinn et al., 1986) and high quality gravity tide data (e.g. Neuberg et al., 1987; Defraigne et al., 1994) are: Q is negative and the free period T_{FCN} of the free core nutation is too low by more than 50 sidereal days. The problem of negative Q is extensively discussed by Florsch and Hinderer (2000). We think the low eigenperiod is a more serious problem, however, since the Q found here is very high in magnitude and cannot easily be distinguished from infinity by our method of analysis. Among others Polzer et al. (1996) also have found high negative Q and a low eigenperiod (by about 24 sidereal days). In Fig. 13 the reduced tidal admittances for the case of CSR 3.0 and 5 corrected tides are interpreted by the resonance model for the solution. The formal uncertainties are also given as error bars. Within those all the data are fit by the model except those for P_1: the real part of the model is too low and the imaginary part is too high. This pattern does not change significantly for any of the solutions in Figure 14. Since the effect of the differences in the ocean loading correction and the effect of the noise level in the tidal results (see below) is much smaller than the overall shift in eigenperiod we must suspect either a serious systematic disturbance in the data or a violation of our assumptions.

Errors

In the previous section we demonstrated that the effects of the ocean loading corrections and modifications thereof are not sufficient to explain the devious results. The formal uncertainties ΔT from the linearized least squares solutions given for T_{FCN} in Table 5 are underestimating the random errors for the NDFW-parameters for two reasons: correlations between pairs of parameters (e.g. Zürn and Rydelek, 1991) and neglect of errors in the tidal admittances (e.g. Polzer et al., 1996). We followed a procedure used by the latter authors to study the effect of the noise level in the tidal data. We disturbed the complex tidal admittance for one tide by adding successively phasors of lengths 1σ (O_1, K_1 and ψ_1) and 2σ (ψ_1) and 3σ (ψ_1 and P_1) with phases evenly distributed over 360^o. Subsequently we solved for NDFW-parameters in each case. The results in the $T_{FCN} - Q_{FCN}^{-1}$ plane are shown in Fig. 14. Not shown are the results for disturbing P_1 by 3σ, because all these disturbed solutions are located well within the ring of solutions when K_1 was disturbed by 1σ. As already mentioned above, the general pattern of Fig. 13 did not change significantly. The maximum deviations were obtained by disturbing ψ_1, not a surprising result and consistent with the findings of Polzer et al. (1996). However, in the worst case treated here the change in free period was 8 sidereal days, far short of the discrepancy to the accepted values. The ringlike patterns for the different experiments show again that the solution is very stable.

From all these results we are forced to conclude, that systematic errors hidden in the tidal

observations or in our assumptions must cause the deviations from accepted values for the NDFW-parameters: a free period of 432 sidereal days and a high and positive Q. We see in Fig. 13 that the tide P_1 does not fit the resonance model at all, but from the analysis above it appears, that this tide can hardly be made responsible for the deviations.

One systematic effect is possibly caused by S_1 strains near the surface. This becomes obvious on inspection of Table 6 in Appendix C. S_1 appears rather strongly in the tidal results although the borehole is cased until a depth of 1500 m. Apparently thermal effects exist in the data which can only be produced near the surface. Among others Friederich and Wilhelm (1985) have shown that thermoelastic strains have much larger penetration depths than the temperature. Another possible source of systematic errors could be the leakage of energy to the tides (especially ψ_1 of course) used in the analysis of Riede et al. (1997) from the hydraulic testing, although this is not obvious from the high-pass filtered record. Along the same lines one possibility is a temporal change of the aquifer properties and in consequence the tidal admittances caused by the hydraulic fracturing, the effect we were looking for in the first place. From monthly analyses during the record it appears that the magnitudes of the admittances for both M_2 and O_1 increased after the hydraulic stimulation (Test C) by about 10 % (Zaske, 1997). If this is a real feature in our data, energy at the major tides should show up in the residuals, because the tidal analysis by ETERNA cannot account for such effects. Indeed, inspection of the residual spectrum (Fig.11 b) shows a peak at the frequency of M_2 and several peaks between 0.9 and 1.2 cpd (including O_1) besides the harmonics of the solar day, which often show up in such spectra for similar reasons (Polzer et al., 1996).

In order to investigate this conjecture we performed a tidal analysis and subsequently estimation of NDFW-parameters for two modified versions of the data set. In the first case we took only the data before the test-phase C, i.e. before 390 days in Fig. 8, and in the second case we took the full record but multiplied the data with the factor 0.9 after day number 420 to account for the suspected change in the aquifer by the hydraulic stimulation. Indeed in the second case the M_2-peak in the spectrum of the residuals disappeared in the noise, together with the one for S_2. The overall noise level was slightly lower than for our unmodified record. However, in both cases the lines in the diurnal band of the residual spectrum remained at the same level and at the same frequencies, which by the way do not coincide with major tides with the exception of one close to O_1. The resulting NDFW-parameters also did not show any changes in the expected direction towards the accepted values. The modification of the data set helped possibly to understand M_2 better, but not the NDFW-results.

Conclusions

The well level data set from Soultz-sous-Forets clearly shows the NDFW- resonance in the diurnal tides. However, the parameters retrieved from the tidal admittances deviate from the values

expected from the previous results obtained with VLBI (Gwinn et al., 1986) and gravity tide data (e.g. Neuberg et al., 1987; Defraigne et al., 1994). The quality factor Q is negative but very high, a result sometimes obtained with gravimeters as well (Polzer et al., 1996; Florsch and Hinderer, 2000). More serious is the 50 sidereal day offset for T_{FCN}. Large offsets in the opposite direction have also been obtained sometimes with superconducting gravimeters (e.g. Imanishi and Segawa, 1998; Crossley et al., 1998). We suspect some systematic error in the observations or a violation in our assumptions to be the reason for this shift rather than the level of random noise in the data. One possibility tested was a possible modulation of the tidal admittances during the record due to hydraulic stimulation of the aquifer. A test in this direction did not produce conclusive results. One remaining possibility is the leakage of spectral energy from the three major hydraulic tests during our registration period. It would be very interesting, to leave such a "volumetric strainmeter" alone for a number of years to find its true usefulness for studies of the NDFW-resonance in the tidal strains applied to the aquifer.

Acknowledgement

We wish to thank Jürgen Dornstädter from GTC Kappelmeyer GmbH for the well level and air pressure recordings in Soultz-sous-Forêts and helpful discussions. Additionally we thank the Research Center of Karlsruhe for making the air pressure data available to us.

Appendix A

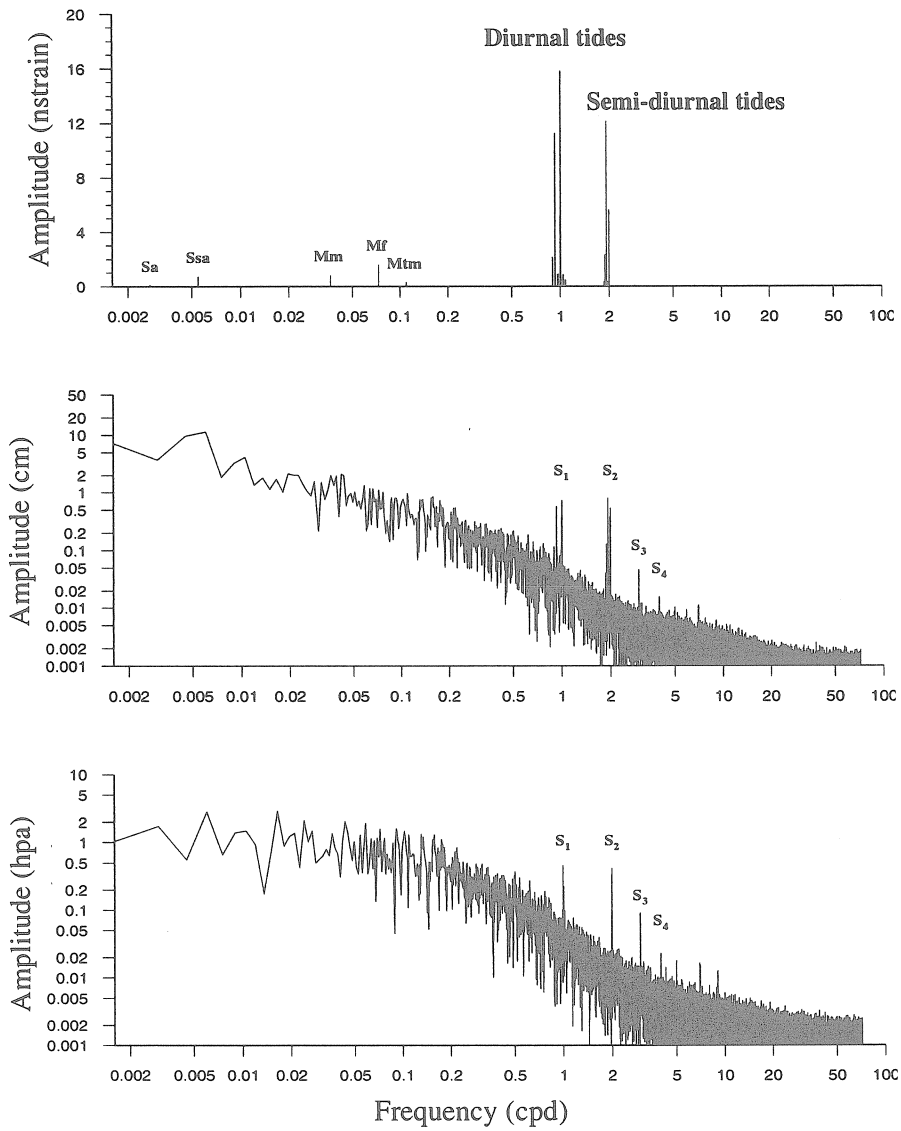

Figure 15: Spectrum of the theoretical tidal areal strain (a), as well as the amplitude spectra of the observed well level (b) and air pressure (c) data in Soultz-sous-Forêts . The amplitude spectra have been calculated using the complete data sets with a total length of 665 days and a sampling rate of 10 minutes.

Appendix B

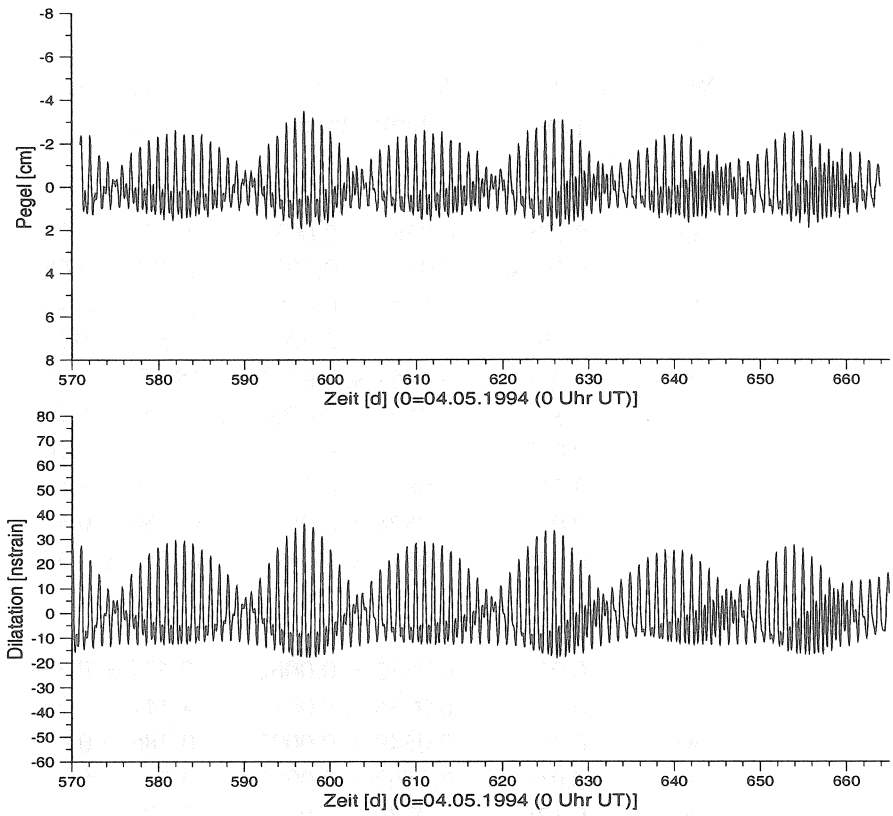

Figure 16: (a) High-pass filtered and air pressure reduced well level data and (b) theoretical tidal dilatation calculated for Soultz-sous-Forêts using the Tamura potential. The air pressure reduction was done using a barometric efficiency of 0.575, determined by the earth tide analysis.

Appendix C

Wave	Amplitude [cm]	Amplitude factor [cm/nstrain]	Phase leads [°]
Q_1	0.126	0.0586 ± 0.0036	-8.178 ± 0.204
O_1	0.703	0.0625 ± 0.0007	-5.183 ± 0.038
M_1	0.040	0.0449 ± 0.0084	3.279 ± 0.483
P_1	0.396	0.0757 ± 0.0011	-10.513 ± 0.065
S_1	0.351	2.8353 ± 0.0721	118.456 ± 3.961
K_1	0.877	0.0554 ± 0.0004	-11.354 ± 0.024
ψ_1	0.052	0.4237 ± 0.0479	2.991 ± 2.742
ϕ_1	0.020	0.0895 ± 0.0260	-6.998 ± 1.493
J_1	0.046	0.0524 ± 0.0073	-4.350 ± 0.417
OO_1	0.025	0.0517 ± 0.0197	14.552 ± 1.131
$2N_2$	0.025	0.0672 ± 0.0062	-0.427 ± 0.354
N_2	0.148	0.0635 ± 0.0013	4.444 ± 0.073
M_2	0.789	0.0649 ± 0.0002	0.386 ± 0.014
L_2	0.019	0.0562 ± 0.0061	-4.235 ± 0.352
S_2	0.436	0.0771 ± 0.0005	-7.030 ± 0.031
K_2	0.129	0.0837 ± 0.0024	-14.569 ± 0.136
M_3	0.005	0.0876 ± 0.0349	-35.906 ± 1.998
M_4	0.004	20.0347 ± 7.7556	0.237 ± 444.350

Mean error	:	0.225 cm
Air pressure regression coefficient	:	-0.565 ± 0.002

Table 6: Results of the earth tide analysis with respect to the areal strain using the complete dataset with a total length of 665 days. Phase leads have positive sign. 18 wave groups have been considered for the least squares fit. Air pressure was considered as an additional input channel. No ocean tide correction has been applied yet, compare Fig 12.

References

Agnew, D. C. (1997). NLOADF: A program for computing ocean-tide loading. *J. Geophys. Res.*, 102:5109–5110.

Baria, R., Baumgärtner, J., and Gêrard, A. (1995). *Stimulations- und Zirkulationsexperimente im HDR Versuchsfeld Soultz-sous-Forêts -Stand der Forschungsarbeiten Ende 1995.* Socomine, Soultz-sous-Forêts, France.

Baumgärtner, J., Gêrard, A., and Baria, R. (1996). Energiegewinnung aus heißem Tiefengestein. das europäische projekt in Soultz-sous-Forêts. *Geothermische Energie*, 15:1–8.

Crossley, D. J., Xu, S., and van Dam, T. (1998). Comprehensive Analysis of 2 years of SG Data from Table Mountain, Colorado. 13th Int. Symp. Earth Tides, edited by B. Ducarme and P. Paquet, Royal Observatory of Belgium, Brussels, pages 659–668.

Defraigne, P., Dehant, V., and Hinderer, J. (1994). Stacking gravity tide measurements and nutation observations in order to determine the complex eigenfrequency of the nearly diurnal free wobble. *J. Geophys. Res.*, 99:9203–9213.

Dornstädter, J., Fabritius, A., and Zaske, J. (1998). Long term circulation experiment at the HDR-site Soultz-sous-Forêts: Hydraulic impact on the surrounding rocks. 4th International HDR Forum, Strasbourg, September 28-30, 1998.

Eanes, R. J. and Bettadpur, S. (1995). The CSR 3.0 global ocean tide model. *Center for Space Research, Techn. Mem.,CSR-TM-95-06.*

Egbert, G. D., Bennett, D. A. F., and Foreman, M. G. G. (1994). TOPEX/POSEIDON tides estimated using a global inverse model. *J. Geophys. Res.*, 99:24821–24852.

Endom, J. and Kümpel, H.-J. (1994). Analysis of Natural Well Level Fluctuations in the KTB-Vorbohrung– Poroelastic Aquifer Parameters and Single Fracture Models. *Scientific Drilling*, 4:147–162.

Evans, K., Mousa, J., and Simpson, D. (1991). Estimating aquifer properties from analysis of forced fluctuations in well level: an example from the nubian formation near Aswan, Egypt, 2: Poroelastic properties. *J. Geophys. Res.*, 96:12139–12160.

Florsch, N. and Hinderer, J. (2000). Bayesian estimation of the free core nutation parameters from the analysis of precise tidal gravity data. *Phys. Earth Planet. Inter.*, 117:21–35.

Friederich, W. and Wilhelm, H. (1985). Solar radiational effects on earth tide measurements. 10th Int. Symp. Earth Tides, edited by V. Vieira, Madrid, pages 865–879.

Gérard, A., Baumgärtner, J., Baria, R., and Jung, R. (1997). An attempt towards a conceptual model derived from 1993-1996 hydraulic operations at Soultz. NEDO International Geothermal Symposium, 11–12 March 1997, Sendai, Japan.

Gwinn, C., Herring, T. A., and Shapiro, I. I. (1986). Geodesy by radio interferometry: Studies of the forced nutations of the earth. 2. interpretation. *J. Geophys. Res.*, 91:4755–4765.

Harrison, J. C. (1985). *Earth Tides*. Benchmark Papers in Geology Series, 419 pp., Van Nostrand Reinhold, New York.

Hsieh, P., Bredehoeft, J., and Farr, J. (1987). Determination of aquifer transmissivity from earth tides analysis. *Water Resources Res.*, 23:1824–1832.

Imanishi, Y. and Segawa, J. (1998). Earth tides and residuals observed by a superconducting gravimeter at Kakioka. 13th Int. Symp. Earth Tides, edited by B. Ducarme and P. Paquet, Royal Observatory of Belgium, Brussels, pages 575–582.

Jung, R., Baumgärtner, J., Rummel, F., Tenzer, H., and Tran-Vieth, T. (1998). Erfolgreicher Langzeit-Zirkulationstest im europäischen HDR-Versuchsfeld Soultz-sous-Forêts. *Geothermische Energie*, 22/23:1–8.

Mohr, S. and Frey, S. (1991). *Bestimmung hydraulischer Gesteinseigenschaften aus gezeitenbedingten Druckschwankungen in der Tiefbohrung GPK-1, Soultz-sous-Forêts, (Elsaß)*. Diploma thesis, Faculty of Physics, University of Karlsruhe, Germany.

Neuberg, J., Hinderer, J., and Zürn, W. (1987). Stacking gravity tide observations in Central Europe for the retrieval of the complex eigenfrequency of the Nearly Diurnal Free Wobble. *Geophys. J.R. astron. Soc.*, 91:853–868.

Neuberg, J. and Zürn, W. (1986). Investigation of the Nearly Diurnal Resonance Using Gravity, Tilt and Strain data simultaneously. Proc. 10th Int. Symp. Earth Tides, Madrid 1985 (R. Vieira, Ed.), Cons. Sup. Invest. Cient., Madrid, 305 - 311, page 1986.

Polzer, G., Zürn, W., and Wenzel, H.-G. (1996). NDFW Analysis of Gravity, Strain and Tilt Data from BFO. *Bull. Inf. Marées Terrestres*, 125:9514–9544.

Riede, M., Zürn, W., and Widmer, R. (1997). Application of multiple tapers in tidal analysis. Proc. 13th Int. Symp. Earth Tides, edited by B. Ducarme and P. Paquet, Royal Observatory of Belgium, Brussels, pages 367 – 376.

Rojstacer, S. and Agnew, D. (1989). The influence of formation material properties on the response of water levels in wells to earth tides and atmospheric loading. *J. Geophys. Res.*, 94:12403–12411.

Sato, T. (1991). Fluid Core Resonance Measured by Quartz Tube Extensometers at Esashi Earth Tide Station. 11th Int. Symp. Earth Tides, edited by J. Kakkuri, Schweizerbart, Stuttgart., pages 573–582.

Schwiderski, E. W. (1980). On charting global ocean tides. *Rev. Geophys. Space Phys.*, 18:243–268.

Tamura, Y. (1987). A Harmonic Development of the Tide-Generating Potential. *Bull. Inf. Marées Terrestres*, 99:6813–6855.

van der Kamp, G. and Gale, J. E. (1983). Theory of earth tides and barometric effects in porous formations with compressible grains. *Water Resources Research*, 19:538–544.

Wenzel, H.-G. (1994). Earth tide analysis package ETERNA 3.0. *Bull. Inf. Marées Terrestres*, 118:8719–8721.

Zaske, J. (1997). *Einfluß eines Langzeitinjektionstests auf die Gezeitenantwort eines Bohrlochpegels am HDR-Standort Soultz-sous-Forêts*. Diploma thesis, Faculty of Physics, University of Karlsruhe, 150 pp., Germany.

Zürn, W. (1997). *The Nearly-Diurnal Free-Wobble Resonance.* In: Tidal Phenomena, Lecture Notes in Earth Sciences, 66: 95-109, edited by H. Wilhelm, W. Zürn and H.-G. Wenzel, Springer, Heidelberg.

Zürn, W. and Rydelek, P. A. (1991). Investigation of the "Nearly Diurnal Free Wobble" - resonance in individual tidal records. 11th Int. Symp. Earth Tides, edited by J. Kakkuri, Schweizerbart, Stuttgart., pages 521 – 530.

A PRELIMINARY DISCUSSION ON TIDAL GRAVITY ANOMALIES AND TERRESTIAL HEAT FLOW IN LANZAROTE (CANARY ISLANDS)

José Arnoso[(1)], José Fernández[(1)], Ricardo Vieira[(1)] and Michel Van Ruymbeke[(2)]

[(1)]Instituto de Astronomía y Geodesia (CSIC-UCM), Universidad Complutense de Madrid. Facultad de Matemáticas. 28040-Madrid. Spain.

[(2)]Observatoire Royal de Belgique, Avenue Circulaire 3, 1080 Bruxelles. Belgium.

ABSTRACT

Since 1987, gravity tide observations have been conducted on the island of Lanzarote, with different gravimeters at different locations. Very anomalous values of heat flow data have also been collected in what is known as the Timanfaya National Park, in the southwestern part of the island. Results for gravity tide anomalies, after correction of the indirect oceanic effect using different global ocean models, complemented with regional and local charts, reveals that cosine component of the final residue vector depends on the ocean model considered. For station CV, if we take into account the porosity effects of the lava rock, the final residue goes to values close to or greater than zero. For station T, the values of the cosine component are equally large for O_1 and M_2 tidal waves and of negative sign. Nevertheless, although our result reveals important differences between stations, it cannot be extended for a global gravity residue-heat flow correlation.

1. INTRODUCTION

One of the most frequently measured parameters, related to the thickness and the age of the crust, is heat flow. Observations have been made to allow us to study its relationship with other geodynamic phenomena. For this reason it has been studied its connection, among other geodynamic phenomena, to gravimetric tide, in particular with the residual vectors corresponding to different waves of the harmonic development of the gravimetric tide potential. Clear discrepancies appear in the results of these investigations. Several of the investigations carried out to date show that a correlation exists between heat flow values and the component of the observed gravity tide residual which is in-phase with the body tide (cosine component) for several waves of the gravity tide potential (Melchior et al., 1983; Yanshin et al., 1986; Melchior et al., 1986; Jeligovskii et al., 1988; Robinson, 1989, 1991, 1993; Melchior et al., 1991; and Melchior, 1995). The correlations appear more clearly between the main lunar wave M_2 and the

heat flow value. The cosine component of the M_2 wave residual (Yanshin et al., 1986) presents positive and negative anomalies in excess of an average value, in absolute terms, of 1 μGal (10^{-8} m s^{-2}). Those anomalies are associated, respectively, with areas of a thin crust, high heat flow values and recent basaltic-type volcanic activity, and with stable structures that have a deeper Mohorovicic discontinuity and a lower heat flow. Robinson (1989, 1991) associates the correlation found in his studies to features in the upper crust, suggesting a measurable upper crustal tidal response.

In contrast to the above results, Rydelek et al. (1991) do not find in their statistical studies a significant correlation between the values of the earth heat flow and the cosine component of the gravimetric tide waves residuals; and they impute the loss of significance to the level of errors in both observations. Also, Fernández et al. (1992) fail to find this relation in the results obtained for Lanzarote, an island with an average crustal thickness of 11.5 km (Banda et al., 1981) and recent, basaltic-type volcanic activity. The average heat flow value on the island is 109 mW m^{-2}, and there are anomalous zones where values of up to 130 W m^{-2} were measured, according to the estimates available when the study was performed. However, the M_2 wave residual was practically zero.

Robinson (1993) makes several comments on the results presented by Rydelek et al. (1991), highlighting that the relations between the gravity tide component and heat flow shown by the graphs, plotted using a global distribution of data, reveals a clear tendency for the M_2 harmonic. He writes that this tendency cannot be explained by theory, but the correlation is too obvious to ignore. His study reveals a clear and interesting need to carry out gravity tide measurements in the same areas in which the heat flow determinations are carried out, as an essential element in this investigation. According to Robinson (1993), it is necessary to select both zones where the distribution of radioactive elements is known to be the predominant cause of the heat flow variations, as well as zones where the circulation of groundwater is the predominant cause.

Melchior (1995) puts forward a new interpretation of the correlation found between the heat flow values and the tide residues by first reviewing and reanalyzing the original tide data of 300 stations (Melchior, 1994a,b). This review takes into account the objections raised by Rydelek et al. (1991), removing what the latter regard as important sources of error, essentially the instrument calibration errors. Melchior (1995) proposes a correlation between the tidal gravity residuals and the age of the tectonic provinces as an alternative to correlation with the heat flow: negative residuals in areas older than 800 m.y. (-0.21±0.10 μGal) and positive residuals in areas younger than 250 m.y. (0.36±0.12 μGal). According to his results, the existence of such a correlation is confirmed with the same degree of probability as in his previous studies.

In the framework of the research previously described, we discuss in this paper the last updated results obtained on the island of Lanzarote, including new heat flow determinations (Díez-Gil et al., 1992; Albert et al., 1994) and results from a new gravity tide station (Vieira et

al., 1995) located right above one of the main heat flow anomalies. To supplement this work, a summary of the geodynamic framework of the Canary Islands can be found in Fernández et al. (1992).

2. HEAT FLOW OBSERVATIONS

The heat flow observation studies performed on the island of Lanzarote and described in Fernández et al. (1992) until beginning on the 90s, include the geothermal drilling Lanzarote-1 (Sánchez Guzmán et al., 1986). This drilling was carried out between Montaña Rajada and Tremesana in Timanfaya National Park (Figure 1). The obtained heat flow value of 109 mWm^{-2} can be considered as an average value for the whole island.

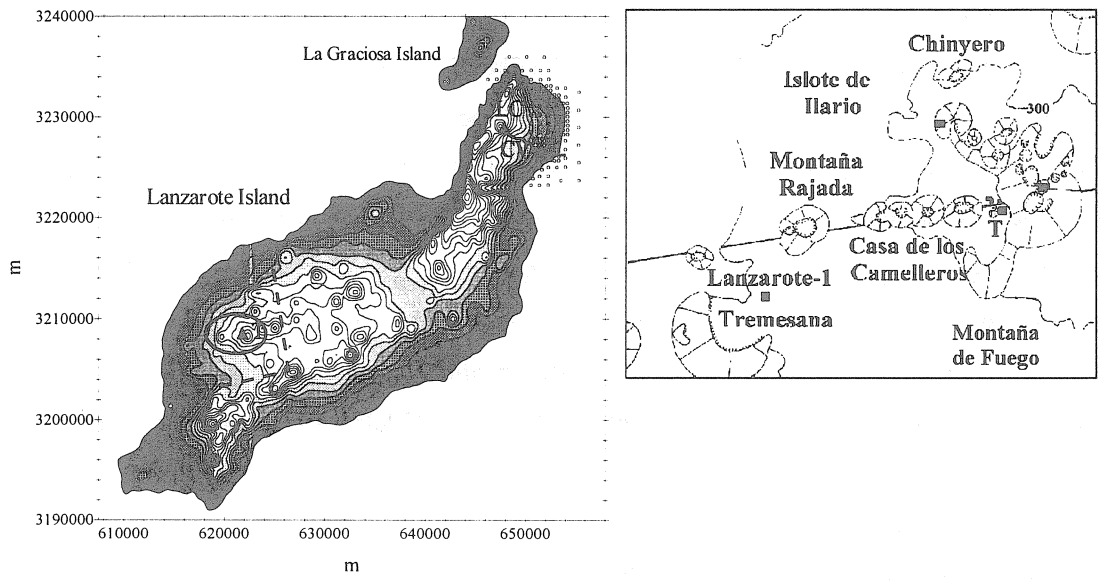

Figure 1. *Location of Cueva de los Verdes (CV) and Timanfaya (T) stations in Lanzarote Island. At top of the figure is shown the center of the land (filled circles) and sea (open circles) polygons of CLML local ocean model. The land polygons are bounded by the old coastline before the eruption of La Corona volcano (LC). The course of the lava tunnel from the volcano to the coast line is also indicated. The surface of the Parque Nacional de Timanfaya is marked with the dashed line. The axis coordinates are UTM, in meters. The right side of the figure is the circled area around station T, showing the location of the geothermal anomaly areas (see text for details).*

Timanfaya National Park (Figure 1) contains areas with marked shallow thermal anomalies, most of that have surface temperatures in excess of 100°C. They are linked to the debris of the 1730-1736 eruption in Timanfaya National Park. Timanfaya is an example of a HDR (Hot Dry Rock) geothermal field with very high surface temperatures (610°C at 13 m depth) although the existence of fumaroles does not indicate the fluid that transports the energy from sources of heat habitually linked to magmatic debris in shallow chambers. Diez-Gil et al. (1987) put forward a

convective geophysical model that justifies the shallow thermal anomalies and permits heat flow evaluations because of the non-proportionality between heat flow and temperature gradient in convective heat transfer. They use a model of heat transfer by convection of gases in posteruptive systems. The convection model is valid for a range of conditions that include those measured in the Montañas de Fuego. Díez-Gil et al. (1992) and Albert et al. (1994) note that the data available at present suggests that the source of heat in this area of the island is a magmatic intrusion, hypothetically cylindrical, with a radius of 200±100 m, located at 4±1 Km depth and with a surface temperature of 850±100°C (Araña et al., 1984; Díez-Gil et al., 1986). Their studies have revealed that the geothermal anomalies are very localized geographically. The heat is provided by the convection of hot gases and the flow of heat is very dispersed in the surface anomalies. In this convective system, a flow of 8 Kg/m² a day, supposing a heat flow of q=130 W/m², would suffice to justify the thermal anomalies observed on the surface (Araña et al.1984). It would also justify the fact that the geothermal field is a typical hot dry rock field. A research project of the European Union's JOULE program was conducted in this area, and the results (Díez-Gil et al.,1992, Albert et al.,1994) experimentally confirmed the convective flow of gases and the main results of this model. It was found that main geothermal anomalies are located at (see Figure 1): Islote de Hilario (1 anomaly area), La Casa de los Camelleros (4 anomaly areas), and Montaña de Fuego central crater (3 anomaly areas). The overall heat flow released in each anomalous area studied has been quantified, obtaining values of 789 W/m^2 for Casa de los Camelleros area, 560 W/m^2 for Islote de Hilario area, and 600 W/m^2 for the Restaurant Furnace.

3. TIDAL GRAVITY OBSERVATIONS

Continuous tidal gravity observation have been conducted in two different locations of the Geodynamics Laboratory of Lanzarote (LGL). Since 1987 at Cueva de los Verdes station (CV in Figure 1) and from 1993 to 1997 at station Parque Nacional de Timanfaya (T in Figure 1). The first station is located inside the lava tunnel of La Corona volcano (LC in Figure 1) and the second one is located right above the largest heat flow anomaly in the zone (for more details see: Vieira et al.,1991a; Vieira et al., 1991b, Fernández et al., 1992, Fernández et al., 1994, Vieira et al., 1995). Two gravimeters LaCoste & Romberg model G, numbers 336 and 434, both with an electrostatic feedback system (Van Ruymbeke, 1985), have been used in this study. Both of them have been normalized on the Brussels tidal factors.

The data set analyzed concerns to a period of observation from May 1987 to March 1997 for station CV and from February 1993 to August 1996 for station T. The tidal analysis has been performed using the programs NSV (Venedikov et al., 1997) and ETERNA (Wenzel, 1996) for comparison and the differences between the results obtained with the two programs are less than 0.1 %. The results of the tidal harmonic analysis for O_1 and M_2 tidal waves from the two

stations are shown in Table 1.

Table 1. *Observed amplitude A, tidal parameters δ, α and the amplitude and phase of the tidal residue vector (B,β) of O_1 and M_2 in CV (Latitude: 29°.16. Longitude: -13°.44. Elevation 37 m. Distance to the sea: 1.6 Km) and T (Latitude: 28°.99. Longitude: -13°.75. Elevation: 381 m. Distance to the sea: 6 Km) stations. The results are evaluated by the least squares harmonic analysis method. The potential used is Tamura and modelisation is according to Molodensky for body tides. Amplitudes are given in microgal and phases, in degree, are local.*

	O_1					M_2				
	A	δ	α	B	β	A	δ	α	B	β
CV	30.57	1.1571	-1.603	0.86	-94.6	58.24	1.0176	2.267	8.52	164.3
	±0.02	±0.0007	±0.036			±0.02	±0.0004	±0.022		
T	29.74	1.1298	-1.452	1.09	-136.2	56.66	0.9869	2.074	10.19	168.4
	±0.05	±0.0019	±0.097			±0.03	±0.0006	±0.034		

3.1 Gravity ocean loading and attraction computations

The ocean loading and attraction effects at both stations have been computed using different ocean models, SCHW80 (Schwiderski, 1980), TPXO2 (Egbert et al., 1994) and FES95.2 (Le Provost et al., 1994). To complement these global ocean models, we have included also a regional model of the Canary Islands and a local model, named CLML, which covers the Northeastern part of Lanzarote Island (Arnoso, 1996). The Farrell procedure (Farrell, 1972) with the Guttemberg-Bullen model has been adopted for these computations (see results in Table 2 for O_1 and M_2 waves).

Table 2. *Amplitude and phase of the ocean load and attraction vector (L,λ) computed based on SCHW80, TPXO2 and FES95.2 ocean tide models for the waves O_1 and M_2 at the CV and T stations. Amplitudes are given in microgal and phases, in degree, are local. A 50% of sea-water density in the land polygons of CLML model has been considered.*

	CV				T			
	O_1		M_2		O_1		M_2	
	L	λ	L	λ	L	λ	L	λ
SCHW80	0.7	−95.7	8.8	168.6	0.7	−93.1	8.7	170.6
TPXO2	0.6	−102.3	9.5	167.7	0.6	−99.7	9.4	169.6
FES95.2	0.6	−91.3	8.3	165.6	0.6	−88.5	8.2	167.6

The CLML local model includes new polygons, smaller than used in the global and regional ocean models and closer to station CV. It is composed by a total of 121 polygons, 65 of which are located on the Northeastern coast of Lanzarote, up to 2600 m offshore. The other 56 polygons cover the interior of the Malpaís de La Corona, inland, marking the former coastline (Bravo, T., 1964) existing before the eruption of La Corona volcano (see Figure 1). The eruption, which took place in the Holocene, gave rise to a volcanic tunnel of approximately 6 km long, which stretches from the volcano to the coast and runs for at least 2 km under the sea.

Thus, the design of CLML model permits a more thorough modeling of the loading component of the oceanic effect.

In the vicinity of station CV several ocean tide gauges have been set up, inside the volcanic tunnel in some small natural lakes scattered along it. The ocean tides observed in the lakes (see Table 3 for results of the harmonic analysis for O_1 and M_2 tidal waves), show sea tide elevations up to 1 m at the inner point furthest from the coastline. For that reason, considering also the porosity of the lava, we assume that the water penetrates to the interior of most of the Malpaís de la Corona zone (Arnoso, 1996). For a better adaptation to the current coastline profile and for covering the former coastline, the polygons of the local model are of three different grid sizes: the largest polygons measure approximately 1700×1700 m and the smallest ones 425×425 m. Figure 1 shows the spatial distribution of the polygons and also indicates the location of the volcanic tunnel and the station CV. In the land zone of CLML model, formed by highly porous lava, we have assigned a different water density value than in the sea polygons. In this way we can reproduce the load effect of the water mixed in the porous rock. In other words, the quantity of the water in the polygons has been varied from a percentage of 10% to 100% such that an increase in the said quantity results in another increase in the value of the gravity ocean loading effect calculated. The final value of the gravity loading effect that we have determined for station CV, is the value that results from assigning 50% of water to the land polygons of the local chart. The polygons located within a radius of 300 m around the station point have been discarded for computations. The gravity loading contribution of CLML model has practically no effect at station T, which is some 30 km far from station CV.

Table 3. *Observed amplitude (A) and phase shift (α) of the ocean tide at the three lakes (Small Lake: Latitude: 29°.1566, Longitude: -13°.4279. Large Lake: Latitude: 29°.1572, Longitude: -13°.4308. Cave of the Lakes: Latitude: 29°.1586, Longitude: -13°.4368) of the lava tunnel (Arnoso, 1996). Amplitudes are given in cm of elevation and phases, in degree, are given with respect to the local tidal potential.*

	Small Lake		Large Lake		Cave of the Lakes	
	A	α	A	α	A	α
O_1	4.45	66.0	4.39	59.5	3.68	50.0
	±0.02	±0.3	±0.03	±0.4	±0.06	±0.9
M_2	64.86	-24.3	64.67	-32.7	52.42	-46.5
	±0.05	±0.1	±0.10	±0.1	±0.09	±0.1

4. TIDAL GRAVITY RESIDUES

Following the notation used by Melchior and De Becker (1983), we have computed the tidal gravity residuals $\mathbb{X}(X,\chi)$ for O_1 and M_2 tidal waves in the form $\mathbb{X} = \mathbb{B} - \mathbb{L}$, where $\mathbb{B}(B,\beta)$ is the observed residual and $\mathbb{L}(L,\lambda)$ the computed oceanic effect. Tidal gravity residuals for the two stations and the three ocean models considered, which have been corrected using the regional and local maps mentioned above, are listed in Table 4. We see that practically there is no

difference in the results for the O_1 wave, for the three ocean models, at both stations. For the M_2 wave, the results show differences between the models, being for the FES95.2 model the lowest value in amplitude at station CV. At station T, the lowest value is obtained with TPXO2 model. In addition, for both waves, the tidal gravity anomalies seem to be higher in station T than for station CV, except for M_2 for the TPXO2 ocean model.

Table 4. *Tidal gravity residue vector (X,χ) calculated with several ocean models for the waves O_1 and M_2 at stations CV and T. Amplitudes are given in microgal and phases in degree. A 50% of sea-water density in the land polygons of CLML model has been considered.*

	CV				T			
	O_1		M_2		O_1		M_2	
	X	χ	X	χ	X	χ	X	χ
SCHW80	0.2	−89.8	0.7	53.2	0.8	−175.8	1.5	155.8
TPXO2	0.3	−77.7	1.1	14.6	0.7	−166.6	0.8	154.4
FES95.2	0.2	−104.4	0.3	124.0	0.8	−169.1	2.0	171.7

Table 5 lists the Xcosχ and Xsinχ components of vector X. The Xcosχ (in-phase) component is sensitive to the Earth response whereas Xsinχ (out-of-phase) component gives us information of the instrumental noise or unmodelled effects (Melchior, 1995). If we compare these results with the ones presented by Fernández et al. (1992) at station CV, we obtain that for M_2 wave, the magnitude of Xcosχ is 1.4 times larger and the magnitude of Xsinχ is 1.3 times less. These differences should be attributed to a more precise determination of the station's coordinates, the observed residual vector B obtained with a longer series of tidal gravity data and to the oceanic effect computations with the new local models included. For O_1 wave, the results are practically the same as presented by Fernández et al. (1992) for both Xcosχ and Xsinχ components.

Table 5. *Xcosχ (in-phase) and Xsinχ (out-of-phase) components of the vector X (Table 4) for the waves O_1 and M_2 at stations CV and T. The values are given in microgal.*

		O_1		M_2	
		CV	T	CV	T
SCHW80	X cos χ	0.00	-0.80	0.42	-1.37
	X sin χ	-0.20	-0.06	0.56	0.61
		O_1		M_2	
		CV	T	CV	T
TPXO2	X cos χ	0.06	-0.68	1.06	-0.72
	X sin χ	-0.29	-0.16	0.28	0.35
		O_1		M_2	
		CV	T	CV	T
FES95.2	X cos χ	-0.05	-0.79	-0.17	-1.98
	X sin χ	-0.19	-0.15	0.25	0.29

Following Melchior (1995), the Xsinχ component has significant absolute amplitude if it is higher than 0.20 μGal. In our case for the O_1 wave, in station CV, we obtain values in the limit of significance for all three ocean models but in station T this value is clearly not significant. For the M_2 wave, we obtain close to significant level at both stations, reaching the highest value of some 0.6 μGal with SCHW80 model at both stations. Finally, for all ocean models the values of Xsinχ component are slightly higher in station T than in station CV.

For the O_1 wave, the Xcosχ component is negligible at station CV but at station T is of around 0.8 μGal for all ocean models. Nevertheless, for M2 wave we observe important differences in magnitude of the Xcosχ component in both stations. The highest values are obtained at station T, except with TPXO2 model at station CV.

Furthermore, the in-phase component of the final residue vector at station T is still in excess of the Xsinχ component and of negative sign, contrary to the one that should be associated, according to previous studies (e.g., Yanshin et al. (1986), Melchior (1995)) to the high heat flow value in the zone, and even to the island's assumed mean heat flow density, in addition to the type of recent basaltic volcanism on the island, which must be associated to positive anomalies. Also, if we consider the thickness of the lithosphere in the zone (Chapman and Pollack, 1977), the values of the residuals from observations on the island of Lanzarote should be positive. Following the results given by Melchior (1995) for M_2 tidal wave, who is using 174 new and revised stations, he gives a correlation coefficient k=0.691, with a linear regression

$$X \cos \chi = 0.0201(H-57)-0.063 \pm 0.0013$$

with Xcosχ in μGal and H in mWm^{-2}. If we consider the heat flow values assumed for Lanzarote (Fernández et al., 1992), 109 mWm^{-2} at CV, this relationship will give us the following estimated value (X cos χ) = 0.98 μGal, which is quite different from the values shown in Table 5 (except the value corresponding to the TPXO2 model for station CV).

For the wave O_1, the correlation coefficient between the tidal residual and the heat flow given by Melchior (1991), using a total of 56 stations, is k=0.708, with a linear regression

$$X \cos \chi = 0.0109(H-58.4) \pm 0.0015$$

with Xcosχ in μGal and H in mWm^{-2}. Taking into account the heat flow values given above, we obtain the following estimated value for station CV (X cos χ) = 0.55 μGal, which again are different from the values shown in Table 5.

On other side, if we consider the anomalous high heat flow close to station T (798 Wm^{-2}) we

obtain an extraordinarily large tide anomaly according to Melchior's relations. However, this value would not represent regional crustal and upper mantle conditions.

All this leads us to conclude that the anomalies observed in Lanzarote in the $X\cos\chi$ component corresponding to the final residue vector of the O_1 and M_2 tidal waves are not associated with very broad features (Melchior, 1995), but instead could be the result of more local characteristics of the crust or lithosphere.

5. CONCLUSIONS

In this paper, we have studied the tidal gravity anomalies in Lanzarote Island obtained with the data observed at two recording gravimetric stations. We have used available heat flow data, with very anomalous values in Timanfaya National Park (southwestern part of the island).

The indirect oceanic effect has been corrected suitably using global ocean charts complemented with regional and local ones, including a newly-determined local chart (Arnoso, 1996) in the CV station's zone. The cosine component of the final residue vector of the M_2 wave in station CV is practically zero, except for the TPXO2 ocean model. For station T, located above the main heat flow anomaly of the island, Casa de los Camelleros, this same component has a negative sign of some microGal (Table 5).

The study very clearly shows that the major heat flow anomalies in the Timanfaya National Park, with station T being located above the major anomaly, are very local, and therefore would not have the same effect predicted by the results of other authors (Melchior, 1995). The final residue values for M_2 in CV and T stations are quite different depending on the ocean models but in station T, we obtain the largest value for both O_1 and M_2 tidal waves. Nevertheless, it should be noted that results from Lanzarote by itself is not sufficient to challenge the gravity residue-heat flow correlation.

Finally, the results of this study make note again, as mentioned by Robinson (1993) and Melchior (1995), the existing necessity of theoretical studies and observations of the highest quality to answer the different questions regarding the significance of the tidal gravity anomaly-heat flow trends.

ACKNOWLEDGMENTS.

We are grateful to J. L. Díez and J. Albert for making available to us the heat flow data determined within the framework of the EU project JOULE-JOUG-OOO-ES (JR). We are also grateful for the support given by the staff of the Casa de los Volcanes and Timanfaya National Park, in particular Orlando Hernández. The research has been supported by projects AMB97-0706 and AMB96-0498-C04-04 of CICYT and European Centre for Geodynamics and Seismology (Council of Europe).

REFERENCES

Albert, J.F.; Díez-Gil, J:L; Valentin, M.A.; Torres, F. (1994): Evaluación de las anomalies geotérmicas de Lanzarote. In: Serie Casa de los Volcanes, nº 3, Sc. Ed.: A. García, A. Felpeto. Ed. Cabildo Insular de Lanzarote. pp. 41-60.

Araña, V.; Díez-Gil, J.L.; Ortiz, R.; Yuguero, J. (1984): Convection of geothermal fluids in the Timanfaya volcanic area (Lanzarote, Canary Islands). Bull. Volcanol., 47, pp. 667-677.

Arnoso, J. (1996): Modelización y evaluación de los efectos indirectos sobre las mareas terrestres en la área de las Islas Canarias. Ph. D., Univ. Complutense de Madrid, 148 p..

Banda, E.; Dañobeitia, J.J.; Suriñach, E.; and Ansorge, J. (1981): Features of crustal structure under the Canary Islands. Earth and Planetary Science Letters, 55, 11-24.

Bravo, T. (1964): El volcán y el malpaís de la Corona. La Cueva de los Verdes y los Jameos. Publ. del Cabildo Insular de Lanzarote. 30 p.

Chapman, D.S.; and Pollack H.N. (1977): Reogional geotherms and lithospheric thickness. Geology, 5, 265-268.

Díez-Gil, J.L.; Yuguero, J.; Ortiz, R.; Araña, V. (1986): Termometrías y modelos matemáticos para el estudio de gradientes térmicos superficiales en Lanzarote (Islas Canarias) Anales de Física, serie B, 82, pp. 91-101.

Díez-Gil, J.L.; Araña, V.; Ortiz, R.; Yuguero, J. (1987): Stationary convection model for heat transport by means of geothermal fluids in post eruptive systems. Geothermics, 15, pp.77-87.

Díez-Gil, J.L.; Albert, J.F.; Torres, F.; Valentín, A. (1992): Shallow H.D.R. geothermal field in Lanzarote (Canary Islands). Potential evaluation and heat extraction tests. Final Report. Proyecto JOUG.0004.ES(JR).

Egbert, G.D:, Bennett, A.F. and Foreman, M. (1994): TOPEX/POSEIDON tides estimated using a global inverse model. Journal of Geophysical Research, vol. 90, C12, pp. 24821-24852.

Farrel, W.E. (1972): Deformation of the Earth by surface loads. Review of Geophysics and Space Physics, vol. 10, pp. 761-797.

Fernández, J., R. Vieira, J. L. Díez, C. Toro (1992): Investigations on crustal thickness, heat flow and gravity tide relationship in Lanzarote island. Physics of the Earth and Planetary Interiors, 74, 199-208.

Fernández, J., R. Vieira, A.P. Venedikov, J.L. Díez (1994): Vigilancia de riesgo volcánico en Canarias. Isla de Lanzarote. Física de la Tierra, vol. 5, 77-88.

Jeligovski, V.A.; Melchior, P.; Sadovskii, A.H. (1988): Anomalies de marées, flux thermique et séismicité. Probl. Seismol. Informatiki, Moscou, Naouka 21, pp. 32-37.

Le Provost, C., Genco, M.L., Lyard, F., Vincent, P. and Canceil, P. (1994): Spectroscopoy

of the world ocean tides from a finite element hydrodinamic model. Journal of Geophysical Research, vol. 99, pp. 24777-24797.

Melchior, P.; De Becker, M. (1983): A discussion of world-wide measurements of tidal gravity respect to oceanic interactions, lithosphere hetereogeneities, Earth's flattening and inertial forces. Physics of the Earth and Planetary Interiors, vol. 31, pp. 27-53.

Melchior, P.; Ducarme, B.; De Becker, M. (1986): Corrélation entre le flux de chaleur et les déformations radiales de marée terrestre in Afrique. INQUA, Dakar Symposium, "Changements globaux in Afrique"; pp. 305-308.

Melchior, P.; Ducarme, B. (1991): Tidal gravity anomalies and tectonics. In: J. Kakkuri (Editor) Proc. 11th Inter. Symp. Earth Tides. Helsinki,1989, pp. 445-454.

Melchior, P. (1991): Tidal gravity anomalies and tectonics. Proc. 11th Int. Symp. Earth Tides. Helsinki, 1989, pp. 445-454.

Melchior, P. (1994a): Checking and correcting the tidal gravity parameters of the ICET data bank. Bulletin d'Informations Marees Terrestres, vol. 119, pp. 8889-8936.

Melchior, P. (1994b): A new data bank for tidal gravity measurements (DB92). Physics of the Earth and Planetary Interiors, vol. 82, pp. 125-155.

Melchior, P. (1995): A continuing discussion about the correlation of tidal gravity anomalies and heat flow densities. Physics of the Earth and Planetary Interiors, vol. 67, pp. 231-256.

Robinson, E.S. (1989): Tidal gravity, heat flow, and the upper crust. Physics of the Earth and Planetary Interiors, vol. 56, pp. 181-185.

Robinson, E.S. (1991): Correlation of tidal gravity and heat flow in eastern North America. Physics of the Earth and Planetary Interiors, vol. 67, pp. 231-236.

Robinson, E.S. (1993): On tidal gravity, heat flow and lateral heterogeneities-comment. Physics of the Earth and Planetary Interiors, vol. 76, pp. 343-346.

Rydelek, P.A.; Zürn, W.; and Hinderer, J. (1991): On tidal gravity, heat flow and lateral hetereogeneities. Physics of the Earth and Planetary Interiors, vol. 68, pp. 215-229.

Sánchez Guzmán, J.; Abad, J. (1986): Sondeo Geotérmico Lanzarote-1. Significado geológico y geotérmico. Anales de Física, serie B, 82, pp. 102-109.

Schwiderski, E. W. (1980): On charting global ocean tides. Reviews of Geophysics and Space Physics, vol. 18, pp. 243-268.

Van Ruymbeke, M. (1985): Transformation of nine LaCoste-Romberg gravimeters in feedback system. Bulletin d'Informations Marees Terrestres, vol. 93, pp. 6202-6228.

Venedikov, A. P., Vieira, R., de Toro, C., Arnoso, J. (1997): A new program developed in Madrid for tidal data processing. Bulletin d'Informations Marees Terrestres, vol. 126, pp. 9669-9704, Bruxelles.

Vieira, R.; Fernández, J.; Toro, C.; Camacho, A.G. (1991a): Structural and oceanic effects in the gravimetric tides observations in Lanzarote (Canary Islands). In: J. Kakkuri (Editor),

Proc. 11th Int. Symp. Earth Tides. Helsinki, 1989, pp. 217-230.

Vieira, R.; Van Ruymbeke, M.; Fernández, J.; Arnoso, J.; and Toro, C. (1991b): The Lanzarote underground laboratory. Cahiers du Centre Européen de Géodynamique et de Séismologie.Vol 4, pp. 71-86.

Vieira, R., M. Van Ruymbeke, J. Arnoso, N. D'Oreye, J. Fernández, C. Toro (1995): Comparative study of the tidal gravity parameters observed in Timanfaya, Jameos del Agua and Cueva de los Verdes stations at Lanzarote island. Proc. XII Int. Symp. Earth Tides (H.T. Hsu Ed.), pp. 41-52. Science Press. Beijing, New York.

Wenzel, H.-G. (1996): The nanogal software: Earth tide data processing package ETERNA 3.30. Bulletin d'Informations Marees Terrestres, vol. 124, pp. 9425-9439, Bruxelles.

Yanshin, A.L.; Melchior, P.; Keilis-Borok, V.I.; De Becker, M.; Ducarme, B.; Sadovsky, A.M. (1986): Global distribution of tidal anomalies and an attempt of its geotectonic interpretation.In: R. Vieira (Editor) Proc. 10th Int. Symp. Earth Tides, Madrid-1985, Consejo Superior Investigaciones Científicas, pp. 731-755.

Results of tidal gravity observations in Tenerife, Canary Islands

José Arnoso, José Fernández, Ricardo Vieira, Emilio J. Vélez and Angel P. Venedikov*

Instituto de Astronomía y Geodesia (CSIC-UCM). Universidad Complutense de Madrid. Facultad de Matemáticas. 28040 Madrid. Spain.

*Geophysical Institute. Acad. G. Bonchev steer block 3, Sofia 1113. Bulgaria

Abstract

Tidal gravity observations have been carried out in Tenerife (Canary Islands) at the base of the Teide volcano, more than two thousand meters above the sea level. The measurements have been done using a Lacoste&Romberg-G gravimeter (number 665), with electronic feedback during a period of six months. The results show, after a suitable correction of the ocean loading and attraction effects, a good adjustment with the body tide response. The environment conditions of the station produced also instrumental effects during the observation period leading to disturbances in the long term signal.

1. Introduction

A new tidal gravity station called Teide-Parador (TP) has been established in Tenerife Island (Figure 1). The observations has been carried out between December 1998 and June 1999, using the gravimeter Lacoste&Romberg, model G, number 665 (LCR665) equipped with electronic feedback (Van Ruymbeke, 1985).

The objective of this study was to determine the tidal gravity model at TP station in order to continue with the National Network of Earth Tide's profile and the geodynamics investigations in Canary Islands (Vieira, 1978; Vieira et al., 1991; Fernández et al., 1992; Vieira et al., 1995; Arnoso et. al., 1999). Among other objectives, these investigations allow us to validate global and local ocean models and also to establish a methodology to study indirect effects that disturb the Earth tide observations.

2. Tidal gravity station and data observed

The TP station is located at Tenerife Island (Canaries), in the *National Park Las Cañadas del Teide*. The gravimeter was installed in a room (isolated from others through various corridors) of the main

building of the *Parador Nacional de las Cañadas del Teide*, 2150 m above the sea level and 18 Km far from the nearest coast-line (see Figure 1).

The gravimeter was fixed to a platform, in contact directly with the ground, which allows ensuring the position of minimum sensitivity of the gravimeter to tilt. The difference between the position of the two spirit levels at the beginning and at the end of the period of observation (6 months) was of 0.2% for the transversal and of 4.6% for the longitudinal one. The calibrations performed, with the gravimeter's screw, during the period of observation lead to maximum differences of 0.4% between them.

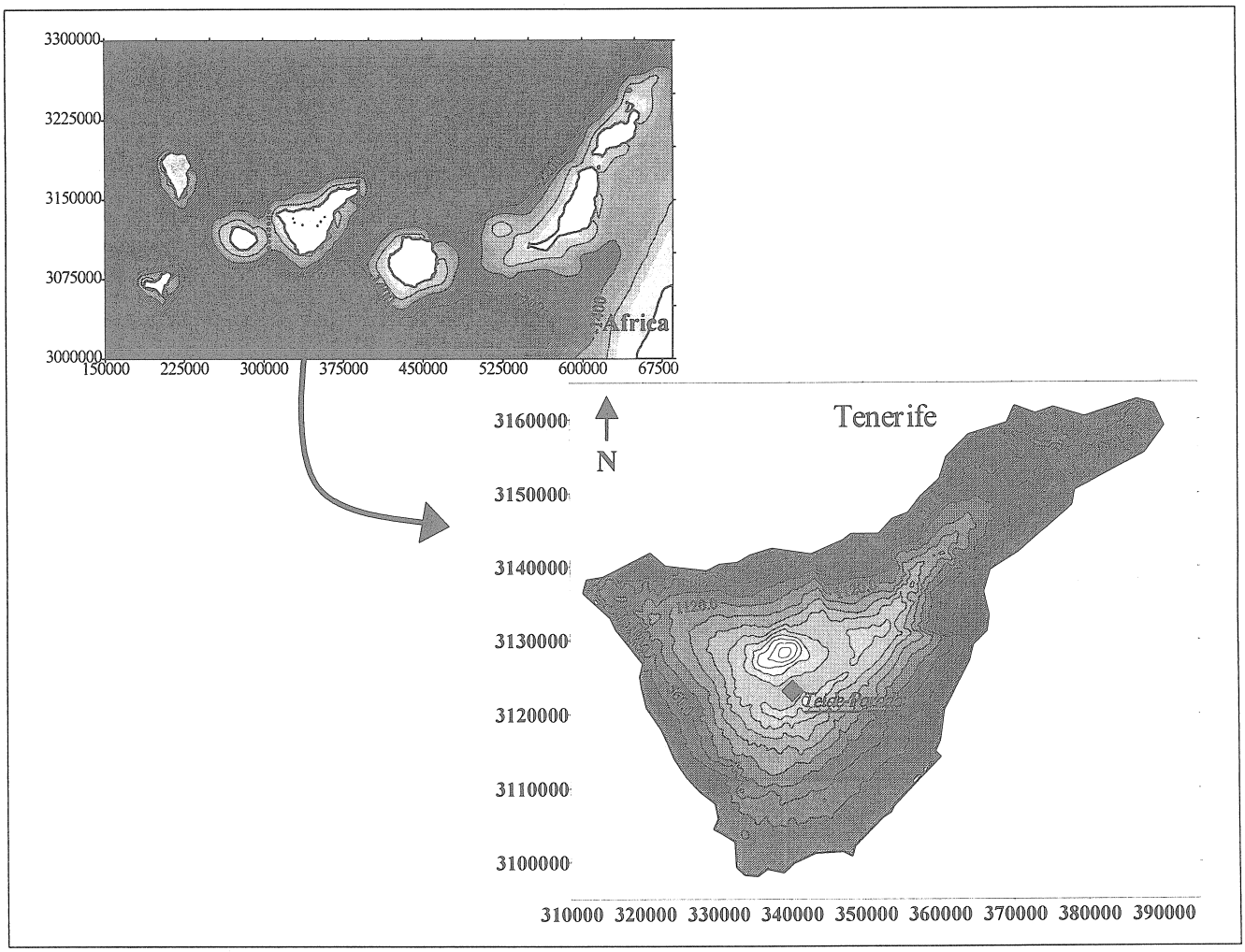

Figure 1. Location of the tidal gravity station *Teide-Parador* at the National Park Las Cañadas del Teide in Tenerife, Canary Islands. Coordinates are UTM, in meters.

Atmospheric pressure and air temperature were observed in the room. All the sensors were connected to a data acquisition system Microdas (Van Ruymbeke et al., 1997). The data collected were stored in the hard disk of a portable computer with a storage period of 1 minute.

During the period of observation the instruments were connected to the power supply of the main building, which consists of two diesel generators. The gravimeter was also equipped with a battery,

which permits a maximum period of 6 hours of autonomy. Four cut of supply were produced during observations. The largest one, due to a snow thunderstorm that isolated the main building and the area of the National Park, produced a blocking in the gravimeter and an interruption of 12 days in the recording, until the operator can access to the station.

The observed tidal gravity data are plotted in Figure 2. For a better viewing a lineal component of the instrumental drift has been removed. Same figure shows the air temperature and pressure variations recorded in the room.

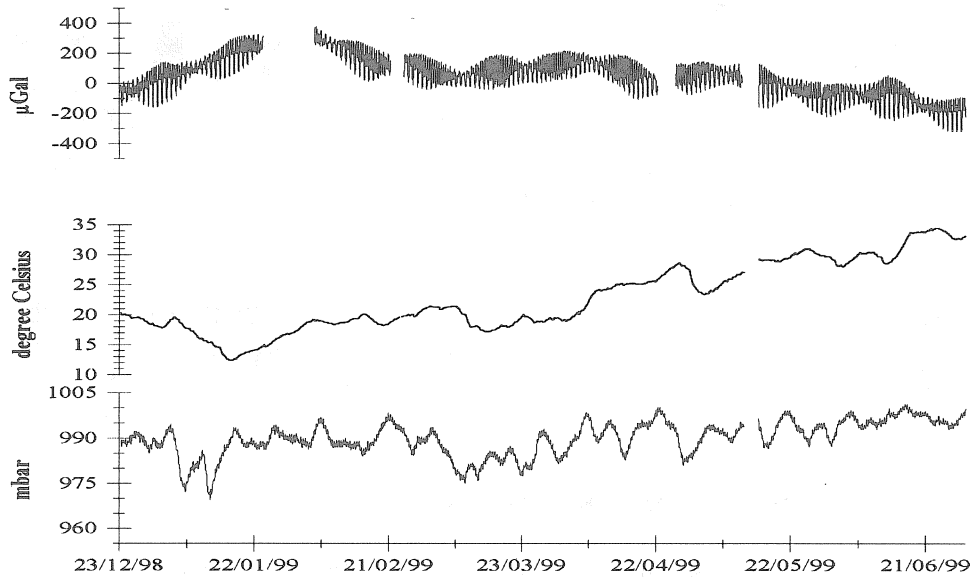

Figure 2. From top to bottom: raw data observed from LCR665, air pressure and temperature variations in TP station. A linear component of the instrumental drift has been removed in the gravity data.

3. Tidal analysis and indirect oceanic effect

After correcting of spikes, jumps and other disturbances in the signal observed, we obtain the local tidal model. The tidal analysis has been done with the NSV program (Venedikov et. al, 1997), based on the least squares harmonic analysis method of Venedikov (1966). The adjusted tidal parameters δ and κ, for the main diurnal and semidiurnal tidal waves, are shown in Table 1. These results show important discrepancies with respect to the theoretical amplitude factor. We observe amplitude factors closer to 1.16 for the diurnal band than for the semidiurnal band. The relationship M2/O1, which is of some 0.862, suggests more significant differences in the semidiurnal tidal band.

After a suitable correction of the indirect oceanic effect, taking into account global ocean charts (Schwiderski, 1980) together with regional ocean models of the Canaries (Arnoso, 1996), the results obtained seems more consistent with the body tide and the ratio M2/01 becomes 0.991 (see δ^c and κ^c values in Table 1).

Figure 3 is a graphic representation of the observed and corrected amplitude factors and phase shifts listed in Table 1. We can see at the graphics more clearly the influence of the ocean tide effect

in the observed values of δ and κ. The amplitude factors present more differences in the semidiurnal band, being these differences of almost three times larger than for the diurnal band, except for K1 due to problems of temperature stabilization in the room (see temperature variation in Figure 2). The phase shift also seems more homogeneous after ocean tide correction, being the largest differences found again in the semidiurnal tidal band (N2 and S2 tidal waves).

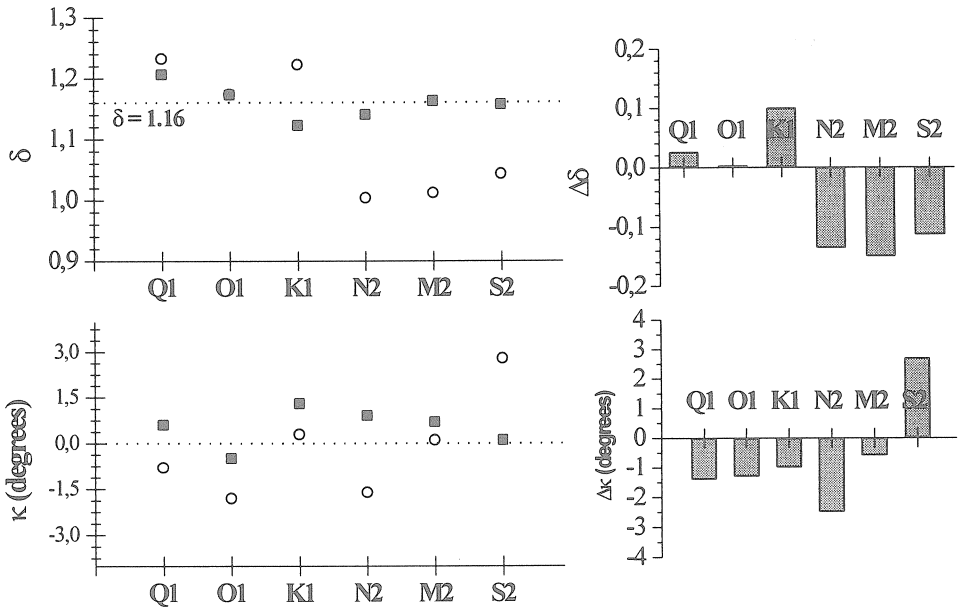

Figure 3. *(Left-up):* Observed amplitude factor (open circles) and corrected form ocean tide effect (filled squares) for the main diurnal and semidiurnal tidal waves. The dotted line shows the theoretical value of 1.16. *(Right-up):* Bar diagram showing the differences between observed and corrected amplitude factors. *(Left-down):* Observed phase shift (open circles) and corrected from ocean tide effect (filled squares) for the main diurnal and semidiurnal tidal waves. *(Right-down):* Bar diagram showing the differences between observed and corrected phase shifts.

Table 1. Observed amplitude (A) and tidal parameters (δ, κ) for station TP (coordinates 28°13' N, 16°37' W), according to Molodenski model. Tidal potential is Tamura (1987). δ^c and κ^c are the tidal parameters corrected from ocean loading. Amplitudes are in μGal and phases, in degrees, are local.

Wave	A	δ	κ	δ^c	κ^c
Q1	6.10	1.2322	-0.8	1.2061	0.6
O1	30.37	1.1738	-1.8	1.1728	-0.5
K1	40.85	1.1226	0.3	1.1223	1.3
N2	11.20	1.0038	-1.6	1.1398	0.9
M2	58.97	1.0117	0.1	1.1622	0.7
S2	28.28	1.0429	2.8	1.1567	0.1

To assess the sensitivity and the behaviour of the gravimeter during the period of observation we perform an analysis of the tidal parameters δ and κ each 30 days, taking data intervals of 30 days without overlapping. Figure 4 shows the results of this analysis, where we can see that the variation

of those parameters keeps practically constant during all the period. Even, the variation of δ reflects the semidiurnal discrepancy with regards to the diurnal tidal band mentioned above. The phase shift variation keeps slightly unstable, especially for S2 component due to probably unmodelled effects of the air pressure.

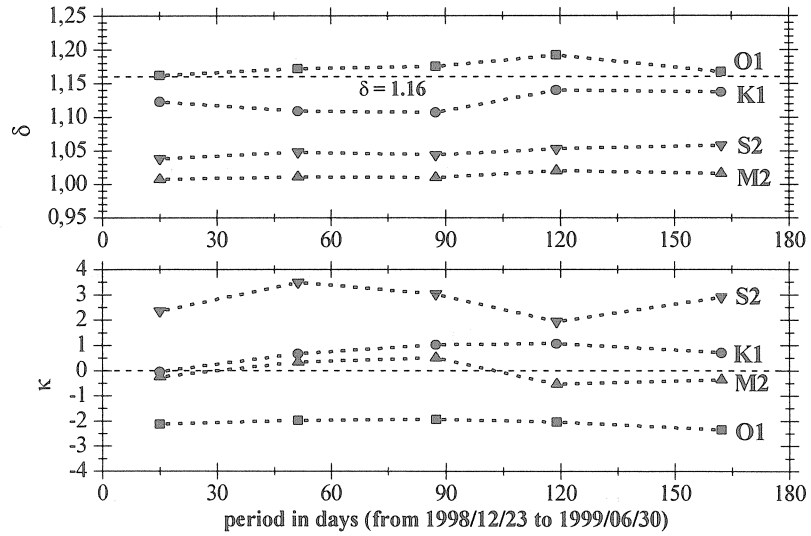

Figure 4. Time variation of δ and κ factors at intervals of 30 days without overlapping. The phase shifts (local) are given in degrees.

4. Air pressure and temperature effects

Is well know that the gravity data is influenced by atmospheric pressure variations. A tentative evaluation of this effect has been done with the local air pressure data recorded at the station (see in Figure 5 the anti-correlation effect of the air pressure in the detided gravity data). Using the ETERNA program (Wenzel, 1996) we compute a single linear regression coefficient of –0.27 ± 0.04 μGal/mbar.

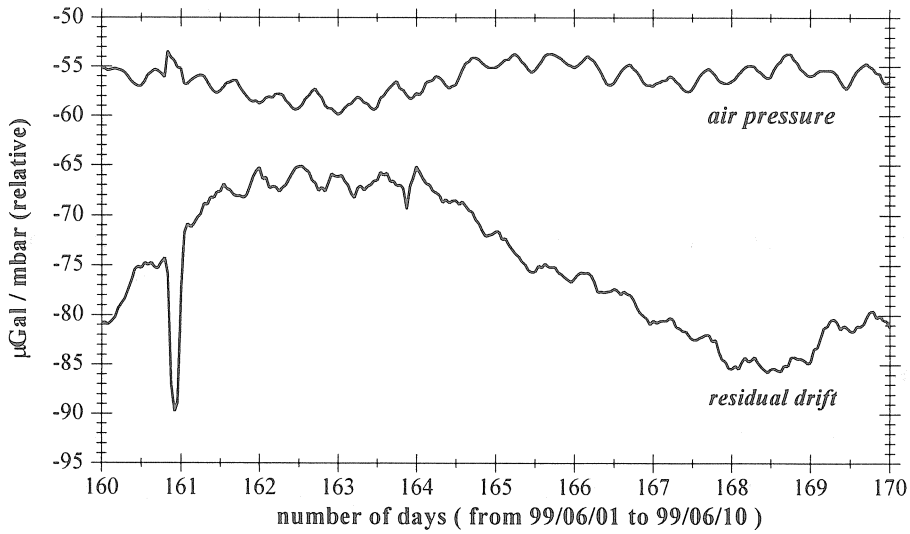

Figure 5. (up) Variation of local air pressure and (down) gravity residuals (after subtracting the local tidal model) during a period of observation selected at TP station.

Looking at figure 2 seems that a correlation between air temperature variations and gravity signal exists. This effect is more clearly visible in figure 6 when we detide the gravity data. Although is quite variable, sometimes the amplitude of the gravity residual is of some 115 μGal for periods of 1 month. However, other perturbations that appear in the temperature record do not correspond to the detided gravity curve. Similar long term gravity-temperature correlation has been detected by Arnoso (1996) in the gravity tide measurements in Lanzarote Island and by El Wahabi et al. (1997), with two Lacoste&Romberg gravimeters installed in the area of Mount Etna (Sicily). Like these authors, we suspect that temperature effect is not the total reason of the apparent gravity change detected in the long term signal but air humidity, which is directly correlated to temperature variation, or other geophysical phenomenon (e.g. soil moisture, water table level, rainfall or some instrumental effect) of long term variation that we cannot correlate up to now due to unavailability of data.

Using the program NSV (Venedikov et al., 1997) we do not detect any influence of the temperature in the tidal bands for periods of less than one day. However, if we perform a direct analysis of data with DD program (Arnoso et al., 1997), we obtain a linear regression coefficient of −3.2 μGal/0.1°C for periods of 15 days.

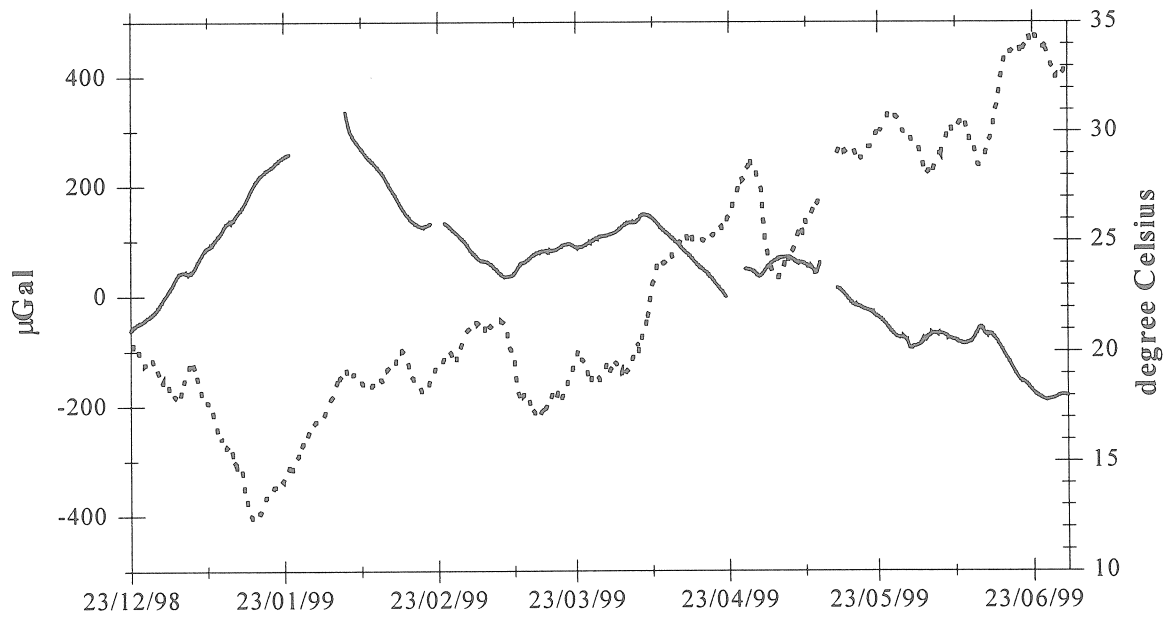

Figure 6. Gravity residual (solid line) after removing the tidal signal from the observed data shown in Figure 2 and air temperature variations (dotted line) recorded in TP station.

5. Conclusions

After six months of continuous gravity observations at Teide-Parador station we have obtained the tidal gravity model. Tidal parameters of the model present a considerable perturbation in the semidiurnal frequency band. After correcting the ocean tide loading and attraction effects, with global ocean charts supplemented with regional models of the Canaries Archipelago, we reduce

considerably such deficiency. Nevertheless, we appreciate thermal influences in the amplitude factor of K1 wave due to stabilization of temperature inside of the room as well as air pressure effects in the phase of S2 wave.

A noticeable temperature effect has been found in the long term drift gravity signal, which produces large apparent gravity changes with sometimes reaches a magnitude of some 115 μGal per month. Up to now we have not a solution for this problem, although we suspect of an instrumental effect induced by the variation of meteorological parameters (e.g. air humidity). Nevertheless, we cannot state other hypothesis whereas we do not dispose of more geophysical data subject to long period variations, e.g. rainfall or water table level, that we can correlate with the long term gravity signal. Further studies to search for other related geodynamical phenomena and observations will be done in future.

ACKNOWLEDGEMENTS

We are grateful to Head and Staff of Parador Nacional de las Cañadas del Teide. Special thanks to Mr. Enrique Caso Alonso for his help in maintenance of the tidal station. This research has been supported by projects AMB96-0498-C04-04 and AMB97-0706 of Spanish CICYT.

REFERENCES

Arnoso, J. (1996): "Modelización y evaluación de efectos oceánicos indirectos sobre las mareas terrestres en el área de las islas Canarias". *Tesis Doctoral. Universidad Complutense de Madrid.*

Arnoso, J., de Toro, C., Venedikov, A. P. and Vieira, R. (1997): "On the estimation of the precision of the tidal data". *Bulletin d'Informations des Marees Terrestres,* 127, 9757-9767.

Arnoso, J. Fernández, J., Vieira, R. and Van Ruymbeke, M. (1999): "A preliminary discussion on tidal gravity anomalies and terrestial heat flow in Lanzarote (Canary Islands)". *Bulletin d'Informations des Marees Terrestres*, (in press).

El Wahabi, A., Ducarme, B., Van Ruymbeke, M., d'Oreye, N. and Somerhausen, A. (1997): "Continuous gravity observations at Mount Etna (Sicily) and correlations temperature/gravimetric records". *Cahiers du Centre Européen de Gëodynamique et de Séismologie,* 14, 105-119.

Fernández, J. Vieira, R., Díez, J. L. and Toro, C. (1992): "Investigations on crustal thickness, heat flow and gravity tide relationship in Lanzarote island. Physics of the earth and Planetary Interiors, 74, 199-208.

Schwiderski, E.W. (1980): "On charting global ocean tides". *Reviews of Geophysics and Space Physics,* 18, 243-268.

Tamura, Y. (1987): "A Harmonic development of the Tide-generating Potential". *Bulletin d'Informations des Marees Terrestres,* 99, 6813-6855.

Van Ruymbeke, M. (1985): Transformation of nine LaCoste-Romberg gravimeters in feedback system. *Bulletin d'Informations Marees Terrestres*, 93, 6202-6228.

Van Ruymbeke, M., Beauducel, Fr. and Somerhausen, A. (1997): The Environmental Data Acquisition System (EDAS) developed at the Royal Observatory of Belgium. *Cahiers du Centre Européen de Gëodynamique et de Séismologie,* 14, 163, 174

Venedikov, A. P. (1966): "Une méthode pour l'analyse des marées terrestres â partir d'enregistrements de longueur arbitraire". *Observatoire Royal de Belgique. Série Geophysique,* 71, 437-459.

Venedikov, A. P., Vieira, R., de Toro, C. and Arnoso, J. (1997): "A new program developed in Madrid for tidal data processing". *Bulletin d'Informations des Marees Terrestres,* 126, 9669-9704.

Vieira, R. (1978): " Mareas Terrestres". *Urania*, 289/290, 93-117.

Vieira, R., Van Ruymbeke, M., Arnoso, J., D'Oreye, N., Fernández, J., and de Toro, C. (1995): " Comparative study of the tidal gravity parameters observed in Timanfaya, Jameos del Agua and Cueva de los Verdes stations at Lanzarote island". *Earth Tides XII Intern. Symp.*, 41-52. Science press. Beijing, New York.

Vieira, R., Van Ruymbeke, M., Fernández, J., Arnoso, J., and de Toro, C. (1991): "The Lanzarote Underground Laboratory". *Cahiers du Centre Europeen de Geodynamique et de Geismologie*, 4, 71-86.

Wenzel, H.-G. (1996): The nanogal software: Earth tide data processing package ETERNA 3.30, *Bulletin d'Informations Marees Terrestres*, 124, 9425-9439

First Results of the GGP Data Bank At ICET

B.Ducarme*, L.Vandercoilden
Royal Observatory of Belgium, Brussels

Abstract
The original one minute sampled data are carefully checked and preprocessed using the Tsoft software(Vauterin, 1998), in order to detect any anomaly. The most delicate part of the task consists in the detection of eventual sensitivity changes between the calibrations. The data are then decimated to the standard hourly interval before tidal analysis.
We present here some general comments on the station noise, pressure coefficient and tidal results obtained using the ETERNA analysis software(Wenzel, 1996) for 14 GGP stations.

1. Procedure

The contributors to the GGP data bank are sending monthly files with the raw gravity and pressure data decimated to one minute interval. The data format is the PRETERNA exchange format with a special header giving all required informations for data processing. A example of such a header is given in table 1.
Figure 1 is an illustration of the preprocessing procedure using Tsoft(Vauterin, 1998) based on a remove-restore technique. From top to bottom we find successively:

- the raw calibrated (1) gravity and (2) atmospheric pressure data together with (3) a tidal prediction computed using the best available tidal model. It should be noted that the instrumental phase lag has not to be applied at that level but only when performing the final analysis.
- (4) the raw residuals obtained by the operation (1) - (3) - β.(2), where β is a pressure coefficient close to -3nms^{-2}/hPa. This coefficient can be more accurately determined using ETERNA software(Wenzel, 1996).
- The raw residuals are affected by different anomalies. Some perturbations have a geophysical origin such as the teleseisms or a human one such as liquid helium refilling. The corresponding part of the data is interpolated in the residuals by a manual curve fitting. The spikes can be either automatically detected and removed or hand corrected. The jumps or tares represent a more serious problem as nobody knows if apparent jumps are not effectively compensated by a slow drift process afterwards. The drift itself is perhaps an accumulation of elementary jumps obscured by the noise. It is one of the main interest of the new dual sphere cryogenic instruments to help in discriminating instrumental jumps from rapid gravity changes due for example to heavy rainfall.
- In (5), the corrected gravity residuals curve, one should notice the change of scale. The remaining long term fluctuations are at the level of 30nms^{-2} with short term fluctuations of only a few nms^{-2} . The linearly interpolated portions are clearly seen on the graph.
- The final step is the restore procedure by the algorithm (6) = (5) + (3) + β.(2) where the original information is completely safeguarded.

• Chercheur Qualifié au Fonds National Belge de la Recherche Scientifique

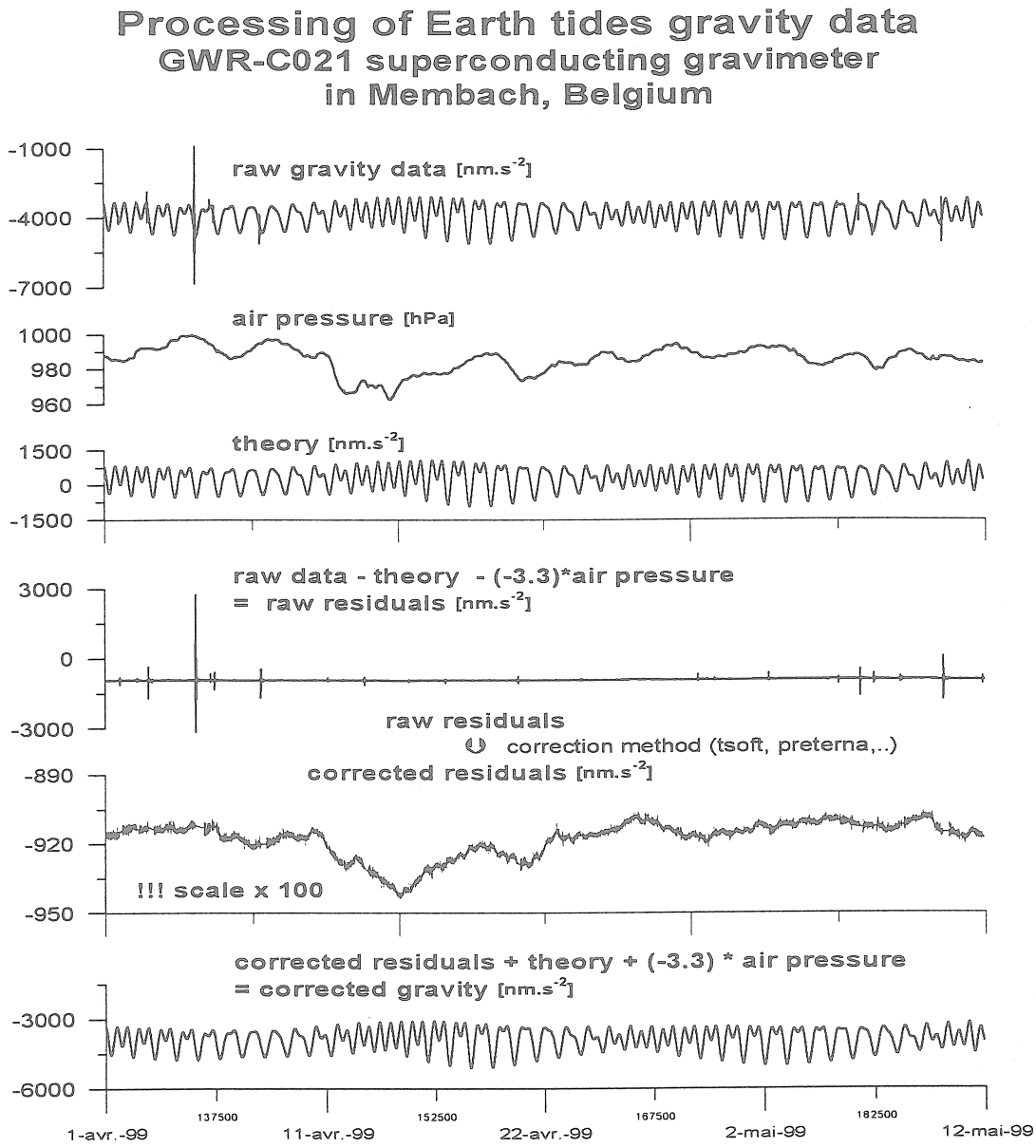

The corrected gravity signal is used to analyse Earth tides. The residuals are used to study the other physical phenomena

Figure 1
Reduction Procedure for Tidal Gravity Data
(Courtesy of M.Hendrickx, June 1999)

With the remove-restore procedure the tidal model is not affecting directly the final data (6). However Tsoft requires a good tidal model of the station in order to eliminate as completely as possible the tidal signal from the residues. For a new unknown station the best way is to perform a tidal analysis of the incoming data after a first quick preprocessing. Later on a final preprocessing will be done with the updated tidal model.
Tsoft is providing an option performing a multilinear regression on short time intervals between the tidal gravity signal, a theoretical tidal model and its time derivative. By shifting the interval one can see slight variations of sensitivity and/or instrumental time lag.

For tidal analysis the data will be decimated to the standard one hour interval by applying antialiasing filters implemented in Tsoft. This procedure is not compulsory as ETERNA allows to use directly a one minute data sampling. However the high frequency spectral content of the tidal potential is limited to the quater-diurnal waves and a low pass filtering of the gravity and pressure signals with a two hours Nyquist frequency will not degrade the tidal information.

Tidal Analysis

Besides ETERNA software one can apply the NSV tidal analysis program(Venedikov & al., 1997). The NSV procedure offers several possibilities of rejecting bad portions of the data, based on an internal quality check on the basic filtering interval, normally 48h. It is a weighing procedure based on the same principle which gives the best results for cryogenic instruments. Both analysis methods allow a direct regression with auxiliary channels. NSV is able to separately compute the external influence in the diurnal, semi-diurnal and ter-diurnal bands. So it is possible to find directly thermal perturbations affecting mainly the diurnal band.

In this paper we restrict ourselves to a straightforward ETERNA analysis using only the pressure channel as auxiliary input.

We shall first consider, in table 2, the standard deviation on the unit weight which is computed during the least square adjustment and the pressure regression coefficient β given with its internal error.

Then, in table 3, we shall consider the observed and modelled tidal factors for two main waves, O1 in the diurnal band and M2 in the semi-diurnal one. Both waves come from lunar origin and are thus practically free of the thermal perturbations of solar origin.

The tidal analysis determines the observed tidal vector $\mathbb{A}(A,\alpha_o)$.

The phase difference α_o is computed with respect to the local astronomical tide.

We also define the observed amplitude factor

$$\delta_o = A/ A_{th}$$

where A_{th} represents the theoretical amplitude of the wave derived from a tidal potential development.

We can compare the observed quantities with a model based on a body tides computation using a non hydrostatic inelastic Earth transfer function(Dehant, Defraigne, 1998) and an oceanic loading computations derived from the Schwiderski cotidal maps(Schwiderski, 1980). For each wave the final result is a simple addition of vectors for which the zero phase corresponds to the phase of the corresponding local astronomical tide. Lags are considered as negative.

We obtain a body tides vector $\mathbb{R}(R,0)$, with an amplitude

$$R = \delta_{th}. A_{th}$$

where δ_{th} is an amplitude factor given by the Earth response model. The corresponding phase lag is negligible. When the tidal loading effect is weak we obtain values of δ_{th} close to 1.154 for O1 and 1.163 for M2.

The computation of the tidal loading for the world ocean gives us a load vector $\mathbb{L}(L,\lambda)$ where L is the amplitude and λ the phase difference.

The modelled tidal wave $\mathbb{M}(A_m, ,\alpha_m)$ is given by

$$\mathbb{M} = \mathbb{R} + \mathbb{L}$$

We define the modelled amplitude factor as

$$\delta_m = M/ A_{th}$$

and the modelled phase difference as α_m.

In order to compare the observations with the model we define two additional quantities:

An amplitude ratio

$$\Delta\delta = \delta_o/\delta_m$$

and a phase error

$$\Delta\alpha = \alpha_o - \alpha_m$$

The first quantity gives information concerning the calibration of the gravimeter and the second one concerning its instrumental phase lag. It is due to the fact that the tidal loading vectors of O1 and M2 are not correlated as the diurnal and semi-diurnal tides amphidromic systems are completely independent. For example in Western Europe the tidal loading for O1 is very weak but it reaches 5% of the M2 amplitude.
Thus an amplitude ratio systematically too high or too low on both waves points to the fact that there is a calibration error for that station. However if we observe a systematic regional distribution we have to think about other sources such as lateral heterogeneities.
In a similar way a negative phase error in the ratio of one to two between O1 and M2 is an indication of a instrumental time lag improperly corrected. For example time lag of 30s will produce a phase lag of approximately $0^\circ.125$ on O1 and $0^\circ.25$ on M2. It corresponds to the lag of the output TIDES of the GWR instruments(Van Camp, 1998).

3. Discussion of the results

In table 2 the stations are identified using a four digit station number derived from the ICET data bank as well as their name and a two letters identifier which is their GGP code. In table 3 we give only the GGP code. When it is possible we give also the results obtained with older series recorded before the beginning of the GGP campaign.
The standard deviation on the unit weight is a measure of the noise of the station and of the instrument itself. In most of the stations it is below $2nms^{-2}$. The instruments of older generation are generally noisier than the more recent ones. It is especially the case in Wetzell, Strasbourg (first series) and Brasimone. The instruments in Wettzell and Strasbourg have been replaced. In Brasimone it is a gravimeter with smaller diameter especially designed for a metrology experiment.
Very often short series of less than one year have lower internal errors than long ones. In the table this fact is well illustrated by Membach. One should expect that the very low errors found in Strasbourg will increase slightly.
As expected the pressure coefficient is close to $-3nms^{-2}/hPa$. Its mean value is $-3.3nms^{-2}/hPa$. The lowest absolute value is found in Brasimone with $-2.93nms^{-2}/hPa$. It should be noted that Brasimone is located in the mountains.
In table 3 we grouped the instruments geographically. A separation line delimits the continents. The very low amplitude of the oceanic tidal loading on O1 in Europe is quite obvious with values of the amplitude factors close to 1.15 and very small phase differences. For M2 the amplitude ratios are systematically close to 0.995 even when their value is close to unity for O1. It is a regional pattern probably due to systematic errors in the tidal loading evaluation. This effect is specially obvious in Brussels which is the closest station to the sea. For the station Wetzell however we can suspect a calibration problem as the O1 ratio 0.995 is too low also. Increasing the calibration factor by half a percent will increase the ratio for M2 up to 0.998, value closer to Brasimone or Strasbourg.
For what concerns the phase lags, a time lag correction close to 30s should be applied on the old Strasbourg series when compared to the new one which has a phase in advance of 0.15° on O1 and 0.29° on M2 with respect to the old one. The station did not report any time lag for the first series. Brasimone has a large negative phase difference $\Delta\alpha$ compared to the model only for M2 and not for O1. It is thus not due to an instrumental phase lag. The result of Wetzell is surprising with a large phase advance $\Delta\alpha$ for the second series.

Outside of Europe calibration and instrumental lags seem to be well constrained with the exception of Matsushiro where the calibration seems weak. However Schwiderski cotidal maps are not so precise for Japan. Cantley is very interesting with larger discrepancies in amplitude ratios for M2. It is clearly due to the large oceanic loading on the Eastern coast of Canada not properly accounted for in the Schwiderski oceanic model. There is also a slight difference in the calibration of the two series, not larger than 0.15%.

4.Conclusions

This preliminary intercomparison of the results obtained with the cryogenic gravimeters participating to the GGP project is very instructive.
Except in a few station equipped with instruments of the older generation the standard deviation of the unit weight is close to $1 nms^{-2}$. Values as low as $0.52 nms^{-2}$ can even be observed on short series.
The coefficient of the barometric pressure admittance has a mean value of $-3.3 nms^{-2}/hPa$.
The calibration of the instruments is coherent to better than half a percent and fits to the models within the same range of accuracy. It is confirmed that the weakest part of the models is the oceanic tides. Systematic regional effects do appear especially for M2 in Western Europe(Sun & al., 1998) where the model gives amplitude factors for M2 which are half a percent too large, although it is fitting well for O1. It is a well known fact that the oceanic loading is small on O1 while it reaches five per cent of the tidal amplitude on M2. A ten per cent error on the tidal loading computations using Schwiderski maps is not surprising. GGP is thus able to contribute significantly to the choice of the best oceanic tides models.
Effort are still required from the GGP participants to improve the calibration of the instruments in amplitude as well as in phase.

TABLE 1
Input format for the raw GGP data

```
GGP-ISDC WEB SITE: http://etggp.oma.be

DATA FORMAT:

Filename                  : MB971000.GGP
Station                   : Membach, Belgium
Instrument                : GWR C021
Phase Lag (s)             :    38.6000
N Latitude (deg)          :    50.6093
E Longitude (deg)         :     6.0066
Height (m)                :   250.0000
Gravity Cal (nm.s-2/V)    :   774.7000
Pressure Cal (hPa/V)      :   133.3220
Author                    : olivier.francis@oma.be
yyyymmdd hhmmss gravity(V) pressure(V)
C**********************************
77777777              .000      .000
19970930 001600 -5.320152  7.516307
19970930 001700 -5.316351  7.516029
19970930 001800 -5.312263  7.515787
19970930 001900 -5.308268  7.515928
```

TABLE 2

STATION	NAME	EPOCH	STD on unit weight nms^{-2}	β(.nms^{-2}/hPa) (RMS)
0200	Brussels(BE)	82/04-99/02	1.780	-3.479 ±0.005
0243	Membach(MB)	95/08-96/07	0.616	-3.558 ±0.012
		96/08-98/10	1.057	-3.229 ±0.010
0306	Strasbourg(ST)	87/07-96/06	2.265	-3.129 ±0.010
		97/03-9710	0.499	-3.435 ±0.013
0515	Brasimone(BR)	95/08-98/01	2.728	-2.929 ±0.041
0698	Wien(VI)	97/07-98/04	0.820	-3.415 ±0.013
0731	Wetzell(WE)	96/07-98/08	2.660	-3.408 ±0.032
		98/02-98/08	1.071	-3.294 ±.0.030
0765	Potsdam(PO)	92/06-96/03	0.917	-3.338 ±0.006
		92/06-98/10	0860	-3.314 ±0.004
0892	Metsahovi(ME)	94/08-96/01	0.759	-3.690 ±0.007
		97/07-98/03	0.896	-3.661 ±0.018
2647	Wuhan(WU)	97/12-98/12	0.836	-3.077 ±0.019
2834	Matsushiro(MA)	97/05-97/12	0.833	-3.404 ±0.013
2849	Esashi(ES)	97/07-98/04	1.501	-3.350 ±0.022
4204	Canberra(CB)	97/07-98/03	0.986	-3.002 ±0.017
6085	Boulder(BO)	95/04-97/12	1.149	-3.559 ±0.009
6824	Cantley(CA)	89/11-95/12	1.309	-3.147 ±0.009
		97/07-98/02	0.946	-3.394 ±0.013

TABLE 3

STATION	NAME	O1 Observed δ_o / α_o	O1 Modelled δ_m / α_m	O1 Ratio, Diff. $\Delta\delta$ / $\Delta\alpha$	M2 Observed δ_o / α_o	M2 Modelled δ_m / α_m	M2 Ratio, Diff. $\Delta\delta$ / $\Delta\alpha$
0200	BE	1.1533 0.06	1.1501 0.07	1.0028 -0.01	1.1839 2.71	1.1917 2.69	**0.9935** +0.02
0243	MB	1.1511 0.07	1.1498 0.06	1.0011 +0.01	1.1899 2.37	1.1945 2.38	0.9962 -0.01
0305	ST	1.1472 -0.07 1.1490 0.08	1.1495 0.03	0.9980 **-0.10** 0.9996 +0.05	1.1850 1.85 1.1865 2.14	1.1893 2.20	0.9964 **-0.35** 0.9976 -0.06
0515	BR	1.1460 0.06	1.1500 0.01	0.9965 +0.05	1.1780 1.16	1.1812 1.55	0.9973 **-0.39**
0698	VI	1.1479 0.10	1.1503 0.07	0.9979 +0.03	1.1810 1.08	1.1854 1.10	0.9962 -0.02
0731	WE	1.1442 0.11 1.1441 0.26	1.1501 0.07	**0.9948** +0.04 **0.9948** **+0.19**	1.1798 1.38 1.1793 1.71	1.1878 1.46	**0.9932** -0.08 **0.9928** **+0.25**
0765	PO	1.1500 0.19 1.1498 0.18	1.1500 0.11	1.0000 +0.08 0.9998 +0.07	1.1861 1.48 1.1860 1.47	1.1909 1.40	0.9960 +0.08 0.9959 +0.07
0892	ME	1.1532 0.25 1.1535 0.25	1.1503 0.22	1.0025 +0.03 1.0028 +0.03	1.1818 0.73 1.1806 0.69	1.1869 0.77	0.9957 -0.04 0.9947 -0.08
2647	WU	1.1794 -0.38	1.1773 -0.36	1.0018 -0.02	1.1759 -0.26	1.1719 -0.09	1.0034 -0.17
2834	MA	1.2037 0.69	1.2098 0.80	0.9950 -0.11	1.1902 0.59	1.1964 0.72	0.9948 -0.13
2849	ES	1.2214 1.37	1.2197 1.31	1.0014 +0.06	1.1924 1.77	1.1947 1.74	0.9980 +0.03
*4204	CB	1.1742 -0.73	1.1701 -0.64	1.0035 -0.09	1.1858 -2.51	1.1860 -2.36	0.9998 -0.15
6085	BO	1.1645 1.31	1.1632 1.16	1.0011 +0.15	1.1591 0.47	1.1582 0.56	1.0008 -0.09
6824	CA	1.1665 0.53 1.1649 0.54	1.1614 0.53	1.0044 +0.00 1.0030 +0.01	1.2043 -0.54 1.2026 -0.52	1.2104 -0.64	**0.9950** +0.10 **0.9936** +0.012

References

Schwiderski, E.W., 1980,
Ocean Tides, I, Global ocean tidal equations,
Marine Geodesy, 3, 161-217.

Sun, H.P., Ducarme B., Hinderer J., Hsu H.T., 1998
Intercomparison of tidal gravity measurements at stations Wuhan, Brussels and Strasbourg,
Proc. Thirteenth Int. Symp. On Earth Tides, Brussels, July 22-25 1997, Observatoire Royal de Belgique, Série Géophysique, 455- 462.

Van Camp, M., 1998,
Qualification d'un gravimètre cryogénique pour les périodes supérieures à cent secondes,
Dissertation doctorale, Louvain la Neuve, décembre 1998.

Vauterin, P., 1998,
Tsoft: graphical & interactive software for the analysis of Earth Tide data,
Proc. Thirteenth Int. Symp. On Earth Tides, Brussels, July 22-25 1997, Observatoire Royal de Belgique, Série Géophysique, 481- 486.

Venedikov, A.P., Vieira R., de Toro, C., Arnoso, J., 1998
A new program developed in Madrid for tidal data processing
Bull. Inf. Marées Terrestres, 126, 9669-9704.

Wenzel, H.G., 1996,
The nanogal software: data processing package ETERNA 3.3,
Bull. Inf. Marées Terrestres, 124, 9425-9439.

Long-Term Increase of Gravity at the Medicina Station (Northern Italy) Confirmed by Absolute and Superconducting Gravimetric Time Series

SCHWAHN, W.[1]; BAKER, T.[2]; R. FALK[1]; G. JEFFRIES[2]; A. LOTHHAMMER[1], B. RICHTER[1]; H. WILMES[1]; P. WOLF[1]

[1] Bundesamt für Kartographie und Geodäsie (BKG)
Richard-Strauss-Allee 11, D-60598 Frankfurt a.M., Germany

[2] Proudman Oceanographic Laboratory, Bidston Observatory (POL)
Birkenhead Merseyside L43 7RA, U.K.

Abstract

In the framework of the EC SELF II – Project continuous measurements of gravity variations began in October 1996 at the station Medicina, near Bologna, Northern Italy, using the superconducting gravimeter GWR SG C023. These relative measurements were supported by six episodic absolute gravity determinations with two gravimeters of the type AXIS FG5.
Based on the low scatter of both the SG as well as the absolute measurements (rms. approximately 15 nms^{-2}) the data sets have been merged to a combined gravity time series. This guaranties a high reliability in the whole gravity spectrum.

Reducing tides, air pressure and the polar motion effects from both series and additionally instrumental drifts (exponential type in the starting phase, linear drift 45 nms^{-2}/year) from the SG data, the following constituents could be identified:
- a "geophysical" linear trend of + 10 nms^{-2}/year increase in gravity which is in accordance to the subsidence rate of a few millimeters/year in the Po River Plain, and
- a "ramp-like" gravity change characterized by a sudden linear increase of about 63 nms^{-2} in four month from June 15, 1997 to October 15, 1997. During the same period (Sept. 26, 1997) two Central Italian earthquakes (both M = 6.0) happened in a distance of about 150 km; a causal connection is unlikely.

After the removal of the above noted functions a garland-like feature remains with sharp turning points in the last days of November / first days of December each year. To explain this remaining variation two approaches are possible:
- two significant periodic terms: an annual (amplitude approx. 10 nms^{-2}) and a semi-annual (amplitude appr. 4 nms^{-2}), maximum for both terms in last days of November / first days of December each year. In addition there are indications for a bi-annual wave.
- modified results (factor 2, phase shift 30 days) of computations by FUKUDA and SATO basing on Sea Surface Dynamical Height variations could approximate this feature in a qualitative manner.

Besides the mentioned terms additional phenomena could be seen in the data series:
- very occasional positive anomalies over few days in the order of 20 .. 25 nms^{-2},
- persistent trends over a few weeks up to months < 10 nms^{-2} with changing signs.

I. Introduction

One objectives of the EC SELF II-Project (SEa Level Fluctuation: geophysical interpretation and environmental impact) is to perform gravity measurements at the SLR/VLBI stations and

in the vicinity of the tide gauges in order to contribute to the vertical reference frame at centimeter level and to verify vertical crustal movements. To monitor the height and gravity variations at the Medicina site continuous GPS and SG measurements have been carried out in parallel.

II. Station description, occupations, measurements and data processing

The gravity measurements have been carried out on the campus of the „CNR Stazione Radioastronomica di Medicina" (near Bologna), see fig. 1. The gravity building (fig. 2) is located in the northern part of the campus, coordinates 11.646° E , 44.5219° N, in a distance of about 700 m to the permanent GPS-antenna close to the southern border of the campus. Fig. 3 shows the situation inside the building with the three pillars. The room is air-conditioned to 22° ±2°C.
It is typical for locations in the Po river plain that there are several small surface drain ditches which are partly filled with water. During heavy or longer rainfalls the draining pipe which crosses the gravity house in the western section at a depth of 0.5 m can be filled with tailback water.
The upper ground water level is monitored in an artesian (?) well near the GPS antenna. The level shows very sharp increases which may be attributed to infiltration of surface water. Precipitation data are not available at the station but could be obtained from the Meteostation Castel San Pietro Terme nearby (12 km). Local air pressure was registered by the gravimetric registration system itself.

The superconducting gravimeter GWR SG C023 (see fig. 4) has been installed by BKG on the pier AN in October 21-26, 1996 (1996, week 43). After ending the preceding experiment at the site "Table Mountain", Boulder, CO, USA, the instrument was shipped to Frankfurt a.M., Germany. Here the gravimeter has been cooled down again and maintained. After transportation to Medicina a complete new initialization including demagnetisation took place.
The following observables have been recorded with a 5.5 – 6.5 digits resolution and sampled at 10-sec intervals for the gravity signal, other channels at 2-min intervals: air pressure, X-Tilt and Y-Tilt compensation power, cold head temperatures, indoor temperatures at floor level and at 1.80 meter height as well as the outdoor temperature from Dec. 98 on.
In a daily sequence the registered data are transferred to BKG in Frankfurt am Main via Internet. Here a coarse data check is done to monitor the gravimeter signal as well as the other channels to be alert in case of instrumental malfunction. The 10-sec gravity data were filtered to a 1-min-data sampling, the air pressure data have been interpolated to the same time points. Theoretical tides on the base of empirical gravimeter factors up to M_m were computed and subtracted from the observations, an empirical regression factor for the air pressure was used to obtain corrected observations (residuals). The data were visualized in daily, weekly and monthly intervals.
The monthly 1-min-sampled data have been pre-screened with the software package „TSoft" (Vauterin, 1998),provided by P. VAUTERIN and M. VAN CAMP, Royal Observatory of Belgium. Important features of the software package allow the removal of spikes due to earthquakes or man-induced seismic events, the offset removal between the data blocks and the interpolation of data to fill gaps. The data channels are filtered to 10-min- and to hourly values, both transformed in ETERNA-format (see also results of tidal analysis).

Due to power line interruptions, malfunction of the air-conditioner, and a major disturbance in the feedback electronics of the leveling system after a lightning stroke, the data set is cut into several blocks. The gaps between the data blocks vary between a few hours and nearly one

month in the worst case in July 1997. The instrumental response is different depending on these disturbances. Decisive improvements were the installation of the uninterruptible power system in June 27, 1997 and of the emergency power generator in Oct. 28, 1997. In November 1997 a sudden tilt event interrupted the SG registration again. But in contrast to a similar effect in July 1997 no malfunction of the tilt feedback system could be monitored. All facts indicate that there was a sudden tilt of the pillar of half a millimeter / meter (3 arcmin) due to strong rainfall. Such events have been observed in June 98 and the first days of Dec. 98 too. In table 1 a short classification is given.

Helium refills	instrumental effect	Power failures	Disturbance / instrumental effect	Tilt resets	Instrumental effect
03.06. 1997	offset	03.03.1997		01.08.1997	Offset
05.11. 1997	offset	02 – 03.05. 1997		06.08. 1997	Offset
22.09. 1998	no offset	07 – 10.06. 1997		08.08.1997	offset?
27.07.1999	no offset	18 – 21.06. 1997		06.05.1998	no offset
		23.06. 1997		18.06.1998	no offset
		29.06. 1997		17.07.1998	no offset
		30.06. 1997		9.12.1998	no offset
		01.07.1997	Lightning, offset	12.04.1999	no off-set
		10.09. 1997	offset	11.06.1999	no offset
		11.09. 1997	no offset	21.06.1999	no offset
		26.09. 1997	Earthquake, offset	27.07.1999	no offset
		28.10. 1997	no offset	16.08.99	no offset
		28.01. 1998	offset		
		30.06.1998	no offset		

Table 1: Instrumental perturbations caused by helium refills, power failures and tilt resets

The coldhead has been changed on March 29,30 1999; no instrumental offset could be seen.

The calibration of the SG C023 has been carried out in two ways: (1) artificial accelerations using sinusoidal vertical movements generated by the Frankfurt calibration system (RICHTER, WILMES, NOWAK, (1995)) at the preceding installation (Boulder, CO, USA) and (2) using the parallel observations during the 6 absolute measurements of the FG5-101 and FG5-103 (HARNISCH, HARNISCH, NOWAK, RICHTER (1999), Proceed. IUGG Birmingham). Both independent methods yield values which coincide within 0.01 percent: -748.24 ± 0.13 resp. –748.14 ± 1.82 nms^{-2}/V.

At the neighboring pillars in the gravity house seven absolute measurements have been performed.. Two absolute gravimeters AXIS FG5 took part in the experiment: #101 (BKG), #103 (POL). The absolute gravimeters FG5-101 and FG5-103 delivered by AXIS Company (now Micro-g Inc.), Boulder, USA, in 1993 are in principle two identical systems. In 1997 both systems have been significantly improved by upgrade works at the successor company Micro-g. The replacement especially of the instrument power supply gave an essential improvement of the stability and repeatability of both systems. This was visualized in the measurement drop and set standard deviations. The so-called truncation analysis became an important tool to select the unperturbed part of the free fall measurement and displayed clearly the situation before and after the upgrade works.
The typical absolute gravity measurement in Medicina was carried out over one to two days. The hourly data collection („set") contains 150 single drop measurements for FG5-101,

respectively 200 for FG5-103. In a post-processing analysis the recorded absolute gravity measurements are corrected with the final parameters for polar motion and an air pressure reduction in agreement with the SG data processing. As the residuals of FG5 standard reprocessing software showed significant tidal effects, an improved tidal modeling procedure („ETGTAB") was incorporated into the reprocessing analysis. ETGTAB (WENZEL (1998)) allows to use different tidal potential developments and the use of observed parameters as well as of synthetic tidal parameters as described in (TIMMEN and WENZEL (1994)). In case of external disturbances e.g. by earthquakes etc. single sets have been cancelled in the reprocessing analysis.

State-of-the-art absolute gravimeters reach a repeatability of ± 15 nms^{-2} which allows the determination of small SG instrumental drift rates. In spite of the high precision reached, individual absolute gravimeters may show also small systematic differences which are above the significance level. Causes are construction principles, electronic components etc. When using different absolute gravimeters in a common experiment it thus necessary to determine offsets by inter-comparisons. The sequence of mutual inter-comparisons of both instruments was Wettzell November 1996, Bad Homburg September 1997, Wettzell September 1997. After the measurement in Medicina in the first days of October 1997, the FG5-103 took part in the 5th International Comparison of Absolute Gravimeters in Sèvres, November 1997 (ROBERTSON et al. (1999)).

II. Results

II.1 Tidal analysis and first assessment of long-term characteristics

The superconducting gravity data have been analyzed using the ETERNA 3.30 software package (WENZEL (1998)). Table 2 shows the adjusted tidal parameters - the semi-annual wave S_{sa} up to the ter-diurnal wave M_3 - determined from the data from 1996 10 25 to 1998 10 31, 10-min-sampling, i.e. two years corresponding to four periods of the S_{sa}-tide. In the diurnal and semi-diurnal band the maximum difference to the pre-calculated synthetic tidal parameters (TIMMEN and WENZEL (1994)) are smaller than 0.5 % for the amplitudes and less than 0.3 degrees in phase.
For the assessment of long-term behavior of the superconducting gravimeter the δ-factors and the accuracy of zonal tidal waves are of high importance. The prominent M_f wave, estimated with an accuracy of 1%, agrees within the error bars with the global $\delta = 1.16$ but differs from the above noted TIMMEN-WENZEL-model ($\delta = 1.1797$) up to three percent. The δ-factor for M_m needs a further investigation. Also the δ-value for S_{sa}, the semi-annual tide, is encouraging: Its larger standard deviation, which is in agreement with the results of TT70 018 at Potsdam (DITTFELD (1997)), points on an additional non-tidal "energy" in the same range – see chapter IV. The spectrum of the residuals after the removal of the tides is given in fig. 8.

II.2 Reduction due to air pressure

The regression with the continuous air pressure registration verifies an overall scalar factor of - 2.809 nms^{-2} / hPa which is close to the standard factor of - 3 nms^{-2} / hPa. The reliability of this correction may be seen in figures 5, 6 and 7. A detailed analysis shows short time intervals of a few days where abnormal weather situations cause disturbances in the order of a few 10 nms^{-2} in the gravity residual data series. As an example consider (fig. 7) the time section January 10 till 13, 1999 with a non-pressure, non-precipitation induced gravity variation of 23 nms^{-2}. As a possible source dynamic processes in the atmosphere should be kept in mind, which cannot be seen in the air pressure measurement at the Earth surface.

frequency from [cpd]	Range to [cpd]	wave	amplitude [nms^{-2}]	ampl. factor	std.dev.	phase lead [deg]	Std.dev. [deg]
0.004108	0.020884	Ssa	16.2521	1.15339	0.27693	-16.700	11.4096
0.020885	0.054747	Mm	17.4896	1.09328	0.02120	-0.7053	1.1193
0.054748	0.091348	Mf	34.9332	1.15342	0.00913	0.9697	0.4532
0.091349	0.501369	Mtm	6.6816	1.15221	0.03104	-1.1767	1.5396
0.501370	0.911390	Q1	68.2937	1.14819	0.00070	-0.1079	0.0351
0.911391	0.947991	O1	357.0444	1.14932	0.00014	0.1669	0.0070
0.947992	0.981854	M1	28.2484	1.15682	0.00127	-0.0495	0.0627
0.981855	0.998631	P1	165.8358	1.14747	0.00024	0.3581	0.0122
0.998632	1.001369	S1	3.7781	1.10575	0.01454	4.5448	0.7536
1.001370	1.004107	K1	495.7997	1.13529	0.00009	0.4191	0.0046
1.004108	1.006845	PSI1	4.3827	1.28210	0.01049	0.4477	0.4688
1.006846	1.023622	PHI1	7.4412	1.19891	0.00559	1.3457	0.2674
1.023623	1.057485	J1	28.2972	1.15840	0.00172	0.4321	0.0848
1.057486	1.470243	OO1	15.4197	1.15395	0.00394	0.6248	0.1953
1.470244	1.880264	2N2	13.5101	1.15645	0.00082	1.7133	0.0406
1.880265	1.914128	N2	85.9723	1.17535	0.00017	1.7163	0.0084
1.914129	1.950419	M2	450.9626	1.18107	0.00003	1.3220	0.0016
1.950420	1.984282	L2	12.7381	1.17953	0.00108	0.0384	0.0523
1.984283	2.002736	S2	209.9172	1.18114	0.00007	0.2553	0.0036
2.002737	2.451943	K2	57.0664	1.18165	0.00036	0.3690	0.0176
2.451944	2.993333	M3	5.7276	1.06961	0.00136	0.0370	0.0728

Table 2: Tidal analysis SG C023 Medicina (1996/10/25 – 1998/10/31), 10-min sampled data corrected for seismic events, outliers and instrumental offsets. The adjusted tidal parameters are for the tidal range from the semi-annual wave S_{sa} up to the ter-diurnal wave M_3. Zonal waves are shaded in gray.

II.3 Reduction due to polar motion effect

For the elimination of the polar motion effect we have the choice to
- use a general model factor of $\delta = 1.16$,
- determine an empirical δ -factor using the gravity time series under consideration.

In the analysis work done so far it was renounced to determine the empirical factor by regression because the annual term in polar motion and other annual periods e.g. annual tide S_a (SCHWAHN (1998)) or non-tidal contributions (see chapter IV.3.1) are superposed. Therefore, to follow a straightforward analysis procedure, the model value was applied.
In fig. 9, lower box, the smooth function displays the polar motion effect in gravity according to the model, the rough function presents the gravity variations recorded by the SG C023, reduced due to tides up to M_m, the air pressure variations and the ultra-longperiodic tides S_{sa} and S_a using for both also $\delta = 1.16$. In the empirical data the gravity variation caused by polar motion can be seen very clearly.
The connection between the blocks is realized by steps in such a manner that the short-term trends agree for the two consecutive blocks.

II.4 Gravity variations by absolute measurements

Analyzing the results from the inter-comparison in Bad Homburg, Wettzell and Paris it seems that there is a systematic offset between the two FG 5 gravimeters. The final result of the Bad Homburg inter-comparison provides a small offset in the order of 20 nms^{-2}. The inter-comparisons in Wettzell, September 1997 and in Paris November 1997 are not of the same reliability but confirm independently the offset value.

Date	Instrument	Gravity reduced to floor level	Set std. dev.	Drop std. dev.
		[µm/s²] [100 µGal]	[µm/s²] [100 µGal]	[µm/s²] [100 µGal]
June 16, 1996 (without set 22)	FG5-101	9.804.751,359	0,032	0,206
Nov. 25-28, 1996	FG5-103	9.804.751,397* *9.804.751,377*	0,051	0,372
June 27, 1997 (without set 13)	FG5-101	9.804.751,370	0,014	0,207
Oct. 04, 1997 (without set 25)	FG5-103	9.804.751,461 *9.804.751,441*	0,018	0,129
Mar. 30, 1998 (without sets 14,15)	FG5-101	9.804.751,441	0,015	0,163
Oct. 23, 1998	FG5-101	9.804.751,469	0,018	0,273
Feb. 26 – Mar 01, 1999 (without set 36)	FG5-101	9.804.751,449	0,019	0,197

*including offset-correction +0,063 µm/s² due to scaler counter

Table 3. Absolute gravity values (status 99/04/21) measured in Medicina in the years 1996 - 1998 by FG5-101 (BKG) and FG5-103 (POL). The values of the FG5-103 in the "system FG5-101" have been diminished by 20 nms^{-2} mainly according to the inter-comparison in Bad Homburg, September1997.

To yield a common level ("system FG5-101") for the absolute gravity values in Medicina, all results of the FG5-103 were reduced by 20 nms^{-2}. Fig. 10, lower box, presents these values in "system FG5-101". Two different clusters can be distinguished very clearly, before and after July/August/September 1997, separated by the threefold amount of the formal error bars of the absolute measurements. Each single cluster incorporates different instruments.

Due to their higher temporal resolution the observations with the SG (see fig. 10, upper box) enable the exact determination of the time interval in which the gravity increase occurs, whereas the magnitude of the gravity increase is obtained by absolute measurements. This requires the **combined consideration** of both data sets.

To merge the time series of absolute and superconducting gravimeters the parameters of the applied models have to be identical:
- reduction due to Earth tides: one set of parameters, see Table 4,
- reduction due to air pressure influence: one regression coefficient –2.809 nms^{-2} /hPa,
- reduction due to polar motion effect: gravimeter factor δ = 1.16 (see, e.g. WAHR (1985)).

Wave group number in Tamura tidal potential development		wave	amplitude factor	phase lead [deg]	frequency [cpd]	
from	to				from	to
1	1	M0S0	1.0000	0.0000	0.000000	0.000000
2	19	SA	1.1600	0.0000	0.000000	0.003425
20	34	SSA	1.1600	0.0000	0.004710	0.010951
35	90	MM	1.1238	-1.3613	0.025812	0.044652
91	152	MF	1.1782	4.8053	0.060132	0.080797
153	281	MTM	1.2239	9.2097	0.096423	0.249951
282	424	Q1	1.1485	-0.2410	0.721500	0.906315
425	482	O1	1.1494	0.2057	0.921941	0.940487
483	530	M1	1.1561	-0.1782	0.958085	0.974188
531	585	K1	1.1353	0.4921	0.989049	1.011099
586	626	J1	1.1498	0.1417	1.013689	1.044800
627	731	OO1	1.1669	0.8644	1.064841	1.216397
732	830	2N2	1.1620	1.8317	1.719381	1.872142
831	880	N2	1.1768	1.8345	1.888387	1.906462
881	936	M2	1.1818	1.3267	1.923766	1.942754
937	975	L2	1.1821	0.3380	1.958233	1.976926
976	1108	S2	1.1838	0.1304	1.991787	2.182843
1109	1190	M3	1.0750	0.3118	2.753244	3.081254
1191	1200	M4	0.2830	71.3475	3.791964	3.937897

Table 4: Compilation of the parameters for the tidal correction in both data series

III. Merging Absolute and SG C023 Gravity Data Sets

III.1 Estimation of the instrumental behavior of SG C023 using absolute measurements

III.1.1 Estimation of the exponential drift in the initial period using absolute measurements

After the re-initialization the SG typically shows an exponential drift behavior for one to three months. For the determination of this instrumental constituent the absolute values in Nov. 96 (FG5-103) and June 97 (FG5-101) serve as reference points. The resulting exponential function

$$y = -160 * \exp(-0.032 * t)$$

(t in days after the start of observations in Medicina, i.e. after Oct. 26th, 1996, y in nms^{-2}) is subtracted. The corrected values (Oct. 26, 1996 – June 30, 1997) meet the absolute values.

III.1.2 Estimation of the linear drift of SG C023 using absolute measurements

To determine the drift determination of SG C023 the time interval end of January 98 till March 99 has been used due to the facts that

- one consistent absolute gravity data series is available, measured by FG5-101
- **no offset occurred** in the SG time series (see table 1).

This time section is marked in fig. 10, upper box, in gray and zoomed in fig. 11, where upper box, shows the two time series. The SG C023 data series is centered to the level of the absolute measurement on March 30, 1998. Table 5 displays for each of the absolute measurements the corresponding readings and the differences. The differences, black vertical bars in fig. 11, upper box, have been used for the determination of the linear instrumental drift **relative** to the absolute ones, fig. 11, lower box. Using a linear least squares fit the result is 45 nms^{-2}/year. This linear instrumental drift agrees very well with the one determined at the site Boulder, during period 12/95 – 06/96 (HARNISCH, HARNISCH, RICHTER, SCHWAHN (1998)).

Time	SG 023 (see fig. 11, upper box) [nms^{-2}]	Absolute (see fig. 11, upper box) [nms^{-2}]	Difference S - Abs (lower box)[nms^{-2}]
30.Mar 1998	206	206	0
23. Oct 1998	250	234	16
26. Feb.- 01.Mar. 99	255	212	43
Instrumental drift CG 023 (Medicina), period 01/98 – 02/99: 45.2 nms^{-2}/year			

Table 5: Values for the instrumental drift determination for the SG C023.

Fig. 11, central part, and fig. 12, upper part, show the residual gravity time series after eliminating for the linear instrumental drift.

III.2 Offset elimination using absolute measurements

The observational period Oct. 1996 till end of Feb. 1999 is divided into three main blocks (see also fig. 12, upper box):

- Oct. 26, 1996 – June 30, 1997,
- July 31, 1997 – Nov. 30,1997,
- Dec. 09, 1997 – Feb. 28, 1999.

In each period the levels of readings of SG are more or less relative and not related to each other. Here again the absolute measurements provide the level for the single blocks. The first level has been fixed in the course of the determination of the exponential function, the third one during the determination of the linear instrumental drift, see fig. 11. In fig. 12, upper box, upper function, the level in the **second** period (July 31, 1997 – Nov. 30, 1997) has been chosen in such a way that the SG residuals meet the level of the absolute gravity value measured by FG5-103 in Oct. 4, 1997. A different approach to connect the blocks is realized by steps in such a manner that the short-term trends agree for the two consecutive blocks, see lower rough function in upper box in fig. 12.

The sharp increase in gravity during the time interval mid August 1997 till end of October 1997 is confirmed by the record of the SG. At this stage the absolute and superconducting gravity time series can be regarded as a **combined unified** data series.

IV. Determination of signals of geophysical and geodetic significance

IV.1 Increase in gravity: linear geophysical trend of about +10 nms^{-2} / year

The deviation of the absolute measurements from a constant level is confirmed and monitored by the continuous SG record. Therefore this deviation shows an additional contribution and is not an instrumental effect. The result of the least squares adjustment of the 4 absolute measurements Oct. 1997 till Feb./March 1999 to a linear function is given in fig. 12, lower box. As it was to be expected both results coincide – they are referred to the linear function of absolute values, the SCG-values are not independent and differ only in their temporal density – and reflect by their low scatter the temporal stability of the SG C023. This linear geophysical trend of 10 nms^{-2}/year is in agreement with the subsidence rate of a few mm / year in the Po River Plain.

IV.2. Increase in gravity in summer 1997: ramp function

Three parameters determine the ramp function: start and end times of the transition and the difference between the levels (ramp height).

The ramp height has been determined as follows: The geophysical trend, +10 nms^{-2} / year was subtracted from the whole time series of residuals (see fig. 13a, upper box), and results in the rough function, central box. Now two significant levels around – 40 nms^{-2} and + 20 nms^{-2}, e.g. a difference of about 60 nms^{-2} can be seen. The difference of the two clusters in absolute measurements amounts to 81 nms^{-2}, see lower part of fig. 10. Taking into account the geophysical trend (10 nms^{-2}/ year respectively 15 nms^{-2} for 1.5 years) yields a level difference of 66 nms^{-2}. The absolute value in Oct. 1998 slightly falsifies the cluster mean value due to a seasonal term (see chapter IV.3). Therefore **the ramp height is fixed to 63 nms^{-2}**.

The start time of the gravity increase can be localized to about two weeks. This relatively coarse definition in time is caused by a series of disturbances in June 1997, cf. table 1. Here the **June 15, 1997** is used. The transition time ends when the gravity variations reach in autumn 1997 the same level as in autumn 1998. It is at the date around **October 15, 1997.** The gravity increase goes on for 4 month, i.e. a linear gravity increase of approx. 15 nms^{-2}/month happened .
At the time of this sharp sudden increase in gravity the two large Central Italian earthquakes in September 16, 1997, magnitude 6.0, occurred in a distance of about 150 km – at present a note of interest only. A causal connection is unlikely.

IV.3 Proposed non-modeled constituents

In combination with the absolute measurements the long-term stability of the SG C023 also other long-period constituents than the ramp can be detected, see fig. 13a, central box. After subtracting the ramp function a "garland"-like feature becomes visible (see fig. 13a, lower box) with maxima in the last days of Nov. / first days of Dec. 1996, 1997 and 1998 and minima in June 1997 and 1998. The variation between the extremes ranges to 30 nms^{-2}. The astonishing feature displays the sharp change in gravity happening during less than two weeks from increasing gravity during Sept. / Oct. / Nov. and decreasing gravity in Dec. / Jan. / Feb. in each year. Two attempts are undertaken to explain the feature.

IV.3.1 Parameters for an annual and a semi-annual wave

There are always good reasons to assume a non-tidal annual wave in gravity: temperature influences, mass re-distributions from local up to global scale (ground water and soil moisture changes and irrigation, processes in oceans and atmosphere). Since the models are not well elaborated, often a formal description has been carried out. A first approximation (see fig. 13a, lower box, thin line) for an *annual* term leads to the parameters: amplitude: approximately 10 nms^{-2}, maximum: end. Nov./first days Dec.
The interesting point is the time of the maximum leading to the question: which geophysical process with annual period gives a maximum in gravity just at that time or is this a result of superposition of different processes?

The rough line in Fig. 13b, box in the top, presents the residual gravity variation after subtracting the upper annual term. A minor *semi-annual* undulation can be seen (smooth line). The parameters are: amplitude: approx. 4 nms^{-2}, maximum: end Nov./first days Dec and end May/first days of June.
Fig. 13b, central box, displays the residuals after the elimination of the semi-annual term. A few time intervals can be identified now, for which a common linear tendency prevail: autumn 1997 and autumn 1998, long-term coherent decrease January 98 till August 98. The approximation by a bi-annual term removes this long-term coherence and results in a scatter between margins ± 10 nms^{-2} for all residual gravity variations (the lower part of fig. 13b).
The disadvantage of the previously described model is that each term in the set of harmonics needs a geophysical / geodetic explanation.

IV.3.2 Parameters for a modified FUKUDA-SATO-model

A "garland"-like gravity variations for central and western European sites has been computed by FUKUDA and SATO (1997) on the basis of sea surface height variations based on SSDT. To adopt this model, some modifications are needed concerning the steric effect due to the thermal expansion of the water masses, SATO et al. (1999). Final results for the Medicina site mentioned are not yet available.
The "garland"-feature of the function given in fig. 3, (A) of FUKUDA and SATO (1997) has been digitized. The optimal fit of this function provides a scale factor and "phase". The parameters are: scale factor 2.0 , shift 30 days (from end Oct. to end of Nov.).
Again the residuals after subtracting this modified function remain under ± 10 nms^{-2}. Some coherent repetition pattern persist: Constant level from November to April, sinusoidal half-wave between May and October, see esp. the year 1998.
Due to the tentative modifications introduced above the explanation by the FUKUDA-SATO-model is slightly speculative. As noted above there are a few other candidates for an annual repetition in gravity variations – but this is the only model which can explain the abrupt change from increasing to decreasing gravity. Since this model generates large-scale gravity variations coherent over Central and Western Europe, the garland like function should also be visible in the SG records of other sites like Membach, Strasbourg, Vienna, and Wettzell.

IV.3.3 Precipitation effects

The relation to rainfall (fig. 15) in the residual gravity time series (see fig. 13b, lower box, or fig. 14, lower box) cannot be described by a single function: Sometimes a direct relation can be detected like in December 1996 for a 152 mm precipitation, where a response of approx. 20 nms^{-2} can be seen, or for a rainy period of a few days where a temporal anomaly can be

remarked. However but there are also cases where there are no correlations. Further investigations are needed.

Acknowledgement

We are very grateful for the very active cooperation with our Italian colleagues. Without this local support this gravity time series and the relation to other time series would never have been obtained. We are thankful to the staff of the Stazione Radioastronomica di Medicina, CNR. Especially to Dr. A. ORFEI who helped us in many critical situations and to an unknown member of the guard service who often re-started the compressor in the early morning.

In the framework of the SELF II – Project we are very thankful to Prof. S. ZERBINI, Settore di Geofisica, Dipartimento di Fisica, Universita Bologna, and her staff, especially Drs. M. NEGUSINI and I. GAVAGNI, for the continuous support in improving the observational conditions. They provided us with time series of rainfall and groundwater near the station. W.S. also thanks G. HARNISCH, BKG Potsdam, for the C-Shell-Procedures to process the gravity files and P. VAUTERIN and M. VAN CAMP (ROB) for their TSoft-Software to handle and display the different stages of the time series.

References

DITTFELD, H.-J. (1997): The long-periodic constituents in the SG TT70 record at Potsdam. Proceed. 13th Inter. Sympos. Earth Tides 1997, ed. B. Ducarme, P. Paquet, Brussels 1998, p. 599-605

FUKUDA, Y.; SATO, T. (1997): Gravity effects of sea level variation at the superconducting gravimeter sites, estimated from ERS-1 and TOPEX-Poseidon altimeter data. Proceed. IAG Sympos. No. 117: Gravity, Geoid and Marine Geodesy, ed. SAGAWA et al., Springer Berlin (1997), p. 107-114

HARNISCH, M., HARNISCH, G., RICHTER, B., SCHWAHN, W. (1998): Estimation of Polar Motion Effects from Time Series Recorded by Superconducting Gravimeters. Proceed. 13th Inter. Sympos. Earth Tides 1997, ed. B. Ducarme, P. Paquet, Brussels 1998, p. 513-521

RICHTER, B., WILMES, H., NOWAK, I. (1995): The Frankfurt calibration system for relative gravimeters. Metrologia 32 (1995)3, p. 217-223

ROBERTSSON, L., FRANCIS, O., VAN DAM, T., FALLER, J., RUESS, D., DELINTE, J.-M., VITUSHKIN, L., LIARD, J., GAGNON, C., GUO YOU GUANG, HUANG DA LUN, FANG YONG YUAN, XU JIN YI, JEFFRIES, G., HOPEWELL, H., EDGE, R., ROBINSON, I., KIBBLE, B., MAKINEN, J., HINDERER, J., AMALVICT, M., LUCK, B., WILMES, H., REHREN, F., SCHMIDT, K., SCHNULL, M., CERUTTI, G., GERMAK, A., ZABEK, Z., PACHUTA, A., ARNAUTOV, G., KALISH, E., STUS, Y., STIZZA, D.J., FREDERICH, J., CHARTIER, J.-M., MARSON, I. (1999): Results from the Fifth International Comparison of Absolute Gravimeters, ICAG'97. Metrologia 1999 (in press).

SATO, T.; FUKUDA, Y., AOYAMA, Y. (1999): On the annual gravity changes induced by SSH variability. 2nd GGP workshop, Muenzbach castle, Luxembourg 1999 (this volume)

SCHWAHN, W. (1998): Parameters for S_a and Polar Motion from gravimetric time series in Central Europe – a review. Proceed. 13th Inter. Sympos. Earth Tides 1997, ed. B. Ducarme, P. Paquet, Brussels 1998, p. 357-364

TIMMEN, L., H.-G. WENZEL (1994): Worldwide Synthetic Gravity Tide Parameters. International Association of Geodesy Symposia 113: 93 – 101.

VAUTERIN, P.,(1998): Tsoft: graphical & interactive software for the analysis of Earth Tide data. Proc. 13th Int. Symp. on Earth Tides, Brussels 1997. Observatoire Royal de Belgique, Série Géophysique, 481- 486.

WAHR, J. (1985): Deformation induced by Polar Motion. J. Geophys. Res. 90 B11 (1985), 9363-9368
WENZEL, H.-G. (1998): Earth Tide Data Processing Package ETERNA 3.30: The Nanogal Software. Proceed. 13th Intern. Sympos. Earth Tides 1997, ed. B. Ducarme, P. Paquet, Brussels 1998, p. 487 - 494

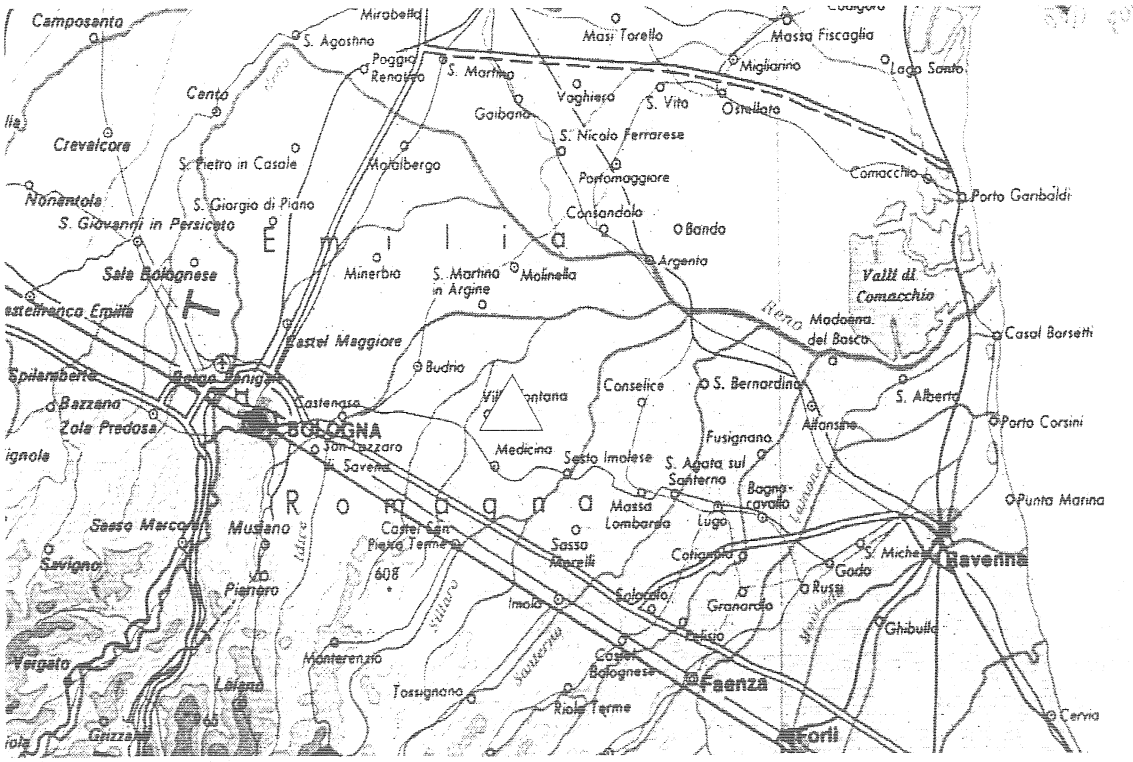

Fig. 1: Medicina site, sketch of the position of the CNR campus (white triangle) in the Upper Italian Po Valley, Region Emilia Romagna, east of Bologna, west of Porto Corsini, near Medicina and Villa Fontana

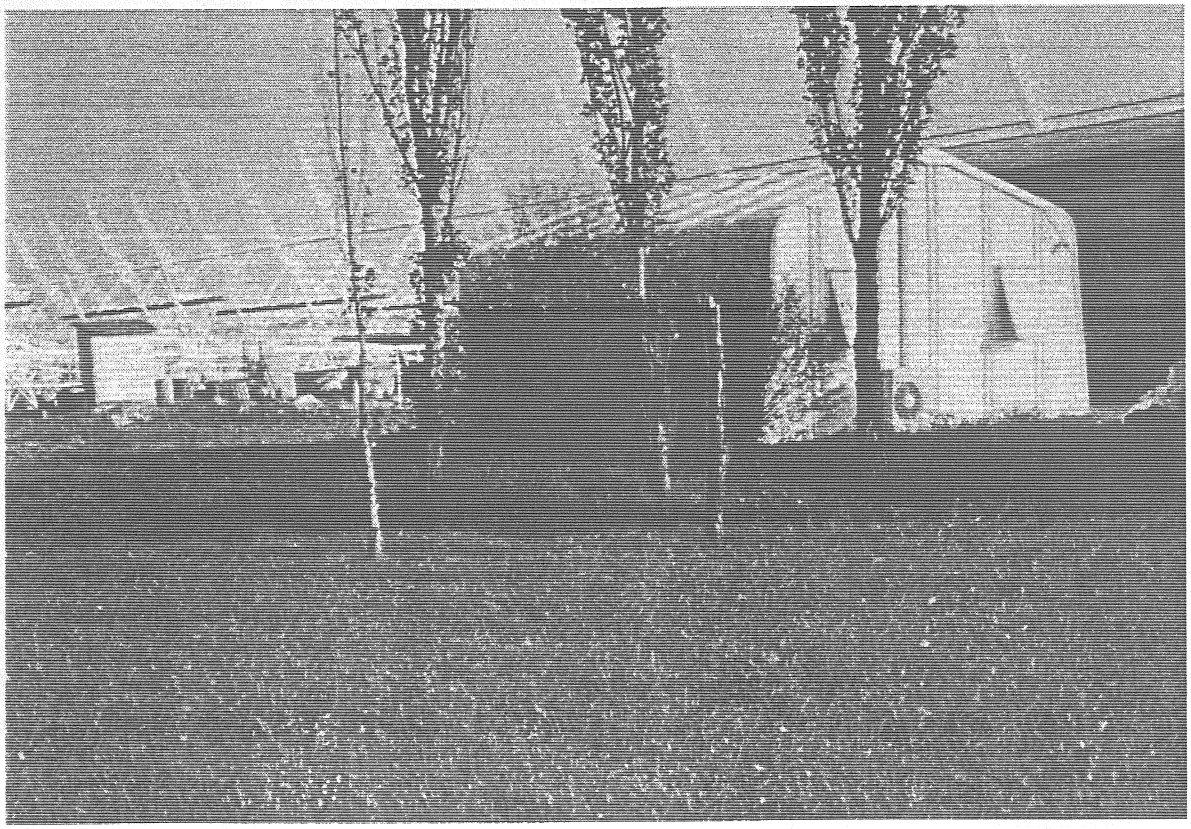

Fig. 2: Medicina site, the gravimetric observatory ("Capanna di ferro"), white, on the campus of the CNR Stazione Radioastronomica di Medicina. In the background the antenna of the "Croce del Nord".

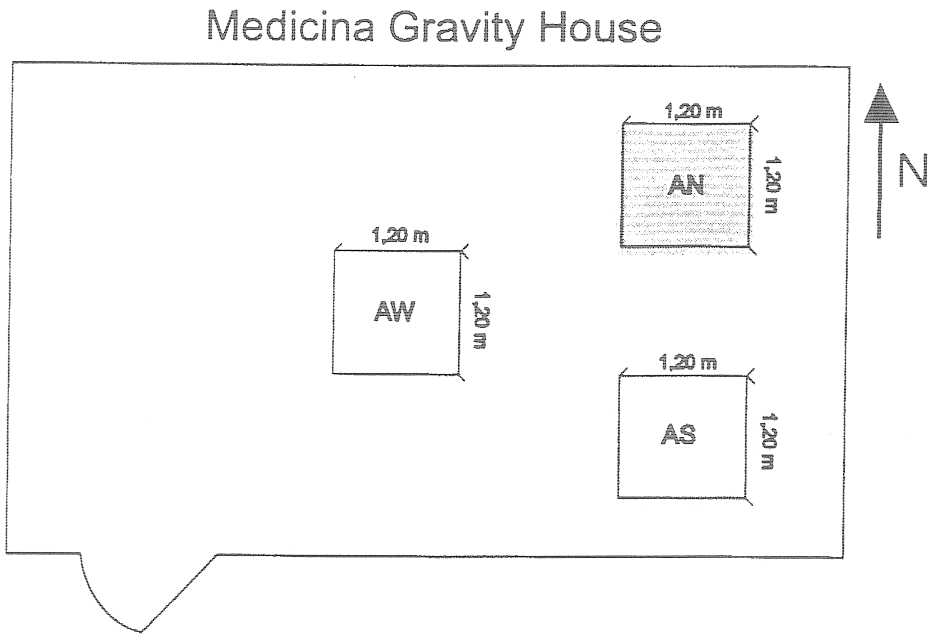

Fig. 3: Medicina site, sketch of the piers in the gravimetric house. On the northern pillar (in gray) the superconducting gravimeter SG C023 has been installed, whereas for absolute measurements with the AXIS FG5 instruments the southern and (seldom) the western pillar have been used.

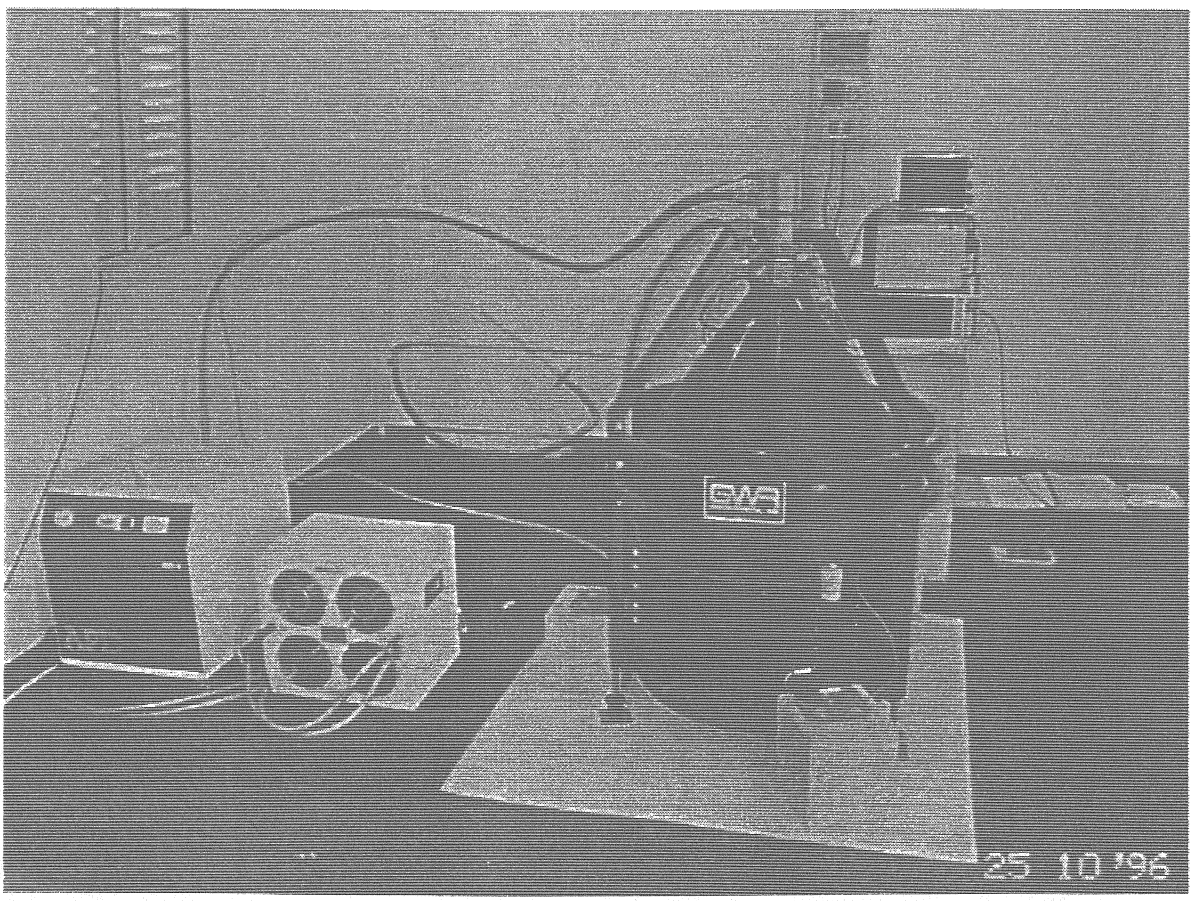

Fig. 4: Medicina site, the superconducting gravimeter SG C023 on the northern pillar in the gravimetric house, assembled ready to work! On the left the compressor and the coolpack, on the right the SG C023 .

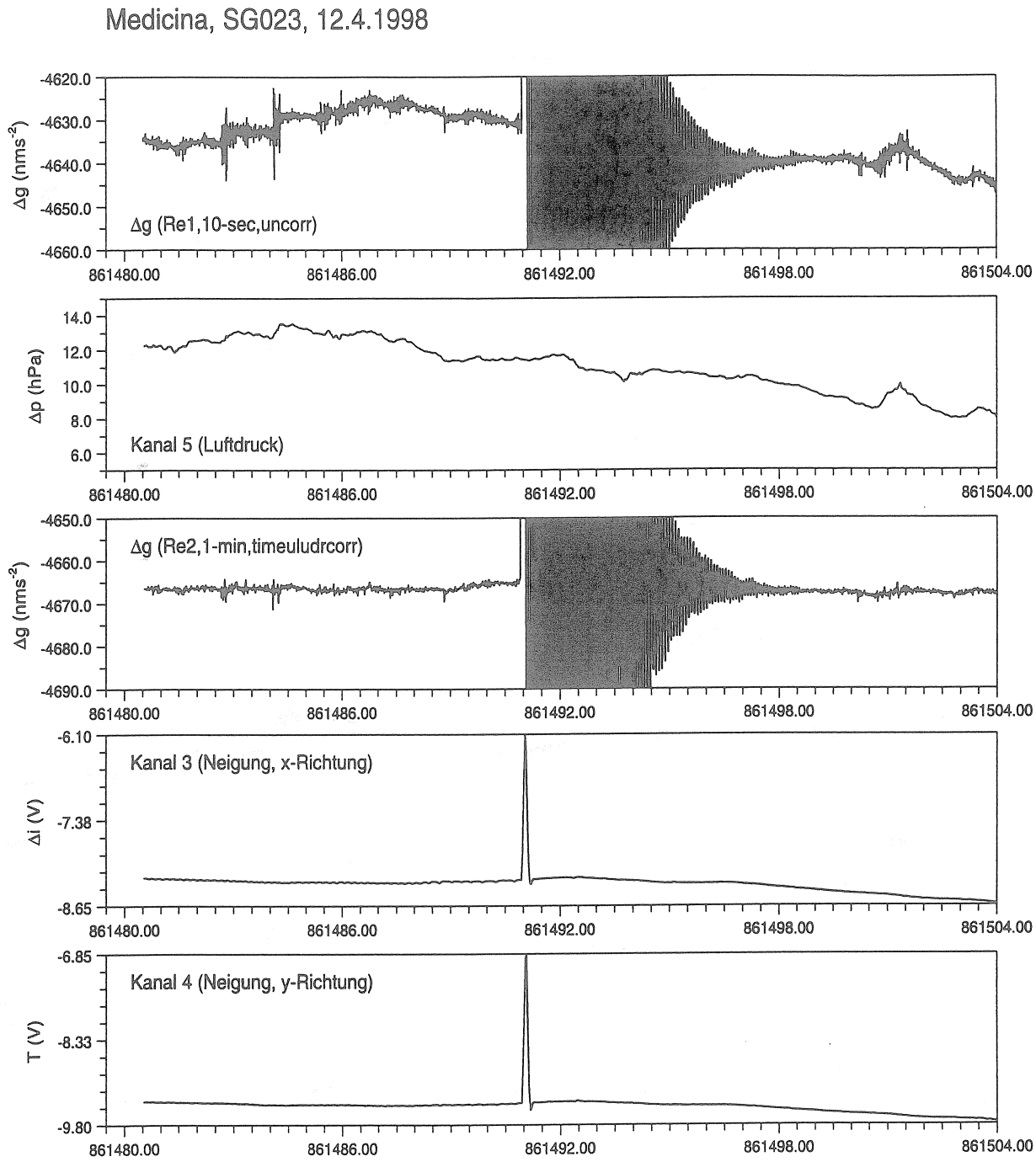

Fig. 5: Medicina site, sensor stability: Example of the high stability of the gravimetric signal against disturbances. Disturbance (inclination of the gravimeter due to saturation of the tilt feedback (?)) is caused by the earthquake at 10.55 UT, M = 5.5, southern border of Austria / Friuli and which provoces oscillations of sensor's sphere.
From top to bottom (horizontal range: 24 hours, vertical ranges: for gravity variations 40 nms^{-2} (4 microgal), for air pressure 10 hPa, for tilt compensation voltage approx. 2.75 V):
- gravity variation tides reduced, the sphere modes after the strong tilt 11^h UT for approx. 6 hours,
- air pressure variation, **opposite** sign,
- "restkurve" (air pressure influence corrected), note the same level before and after noon, note also the low scatter (appr. 2 nms^{-2}) despite the rough air pressure
- X-tilt
- Y-tilt.

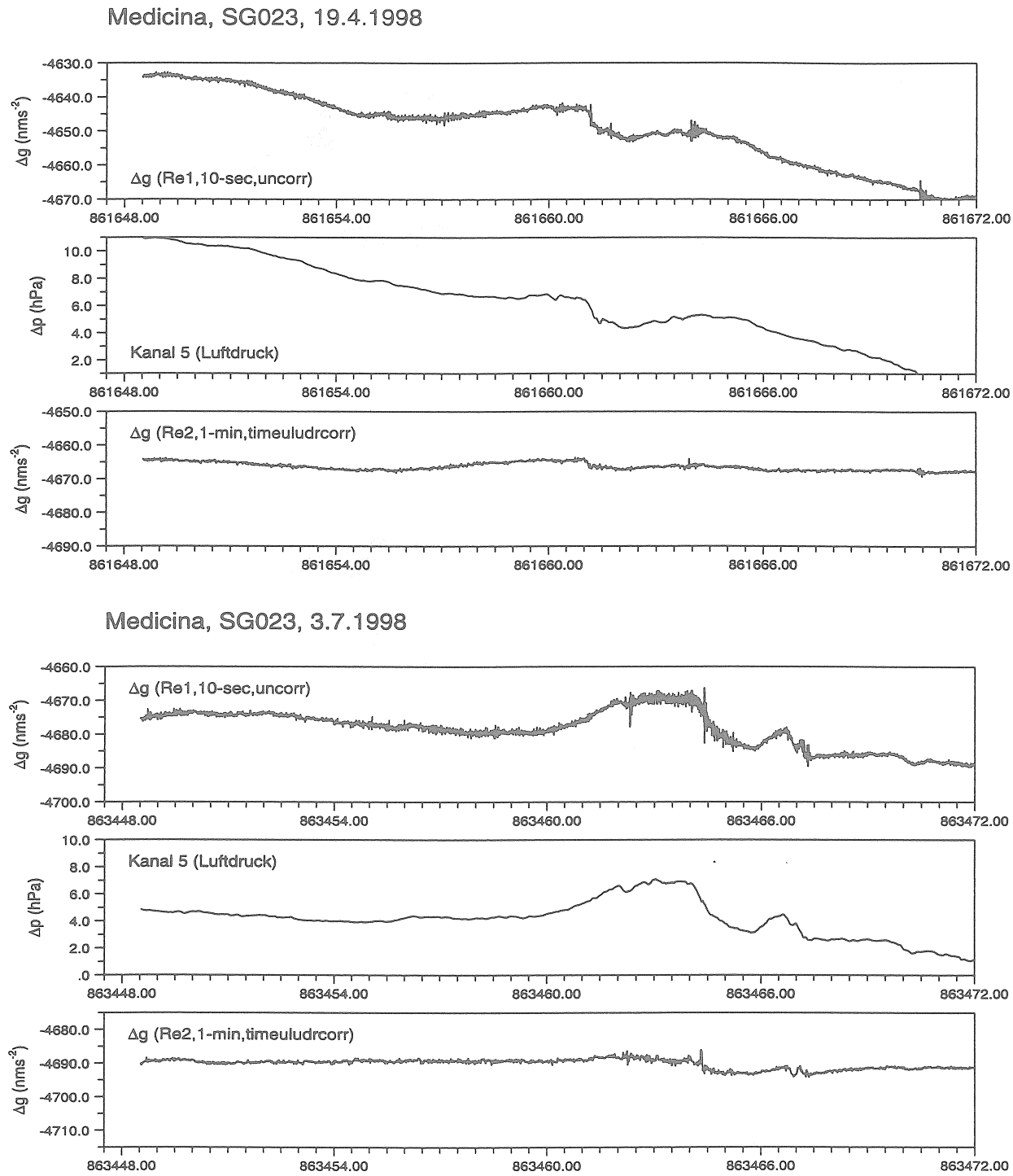

Fig. 6: Medicina site, correction of gravity variations from the influence of air pressure variations, almost complete elimination of the air pressure influence using the overall regression coefficient r = - 2.809 nms^{-2}/hPa. For each day from top to bottom:
- gravity variation without tides, 10-sec-sampling, total vertical range 40 nms^{-2},
- air pressure variation in hPa, 2-min-sampling, opposite sign, vertical range 10 hPa,
- gravity variations without tides and air pressure influences, 1-min-sampling, range 40 nms^{-2}.
In the course of April 19, 1998 an increase in the air pressure of about 11 hPa (middle box) takes place. The corresponding gravity decrease (upper box) is in the order of 35 nms^{-2}, i.e. 3.5 microgals. Every detail may be seen in both curves. The aim is a constant level in the third box of each day. Only a small extraordinary increase in connection with the passage of the cold front for 10^h till 13^h UT may be seen in the lower box. Also warm sections between colder air pressure regions are well documented, see July 3, 1998.
Please note for the third boxes: The internal precision seems to be better than 1 nms^{-2}.

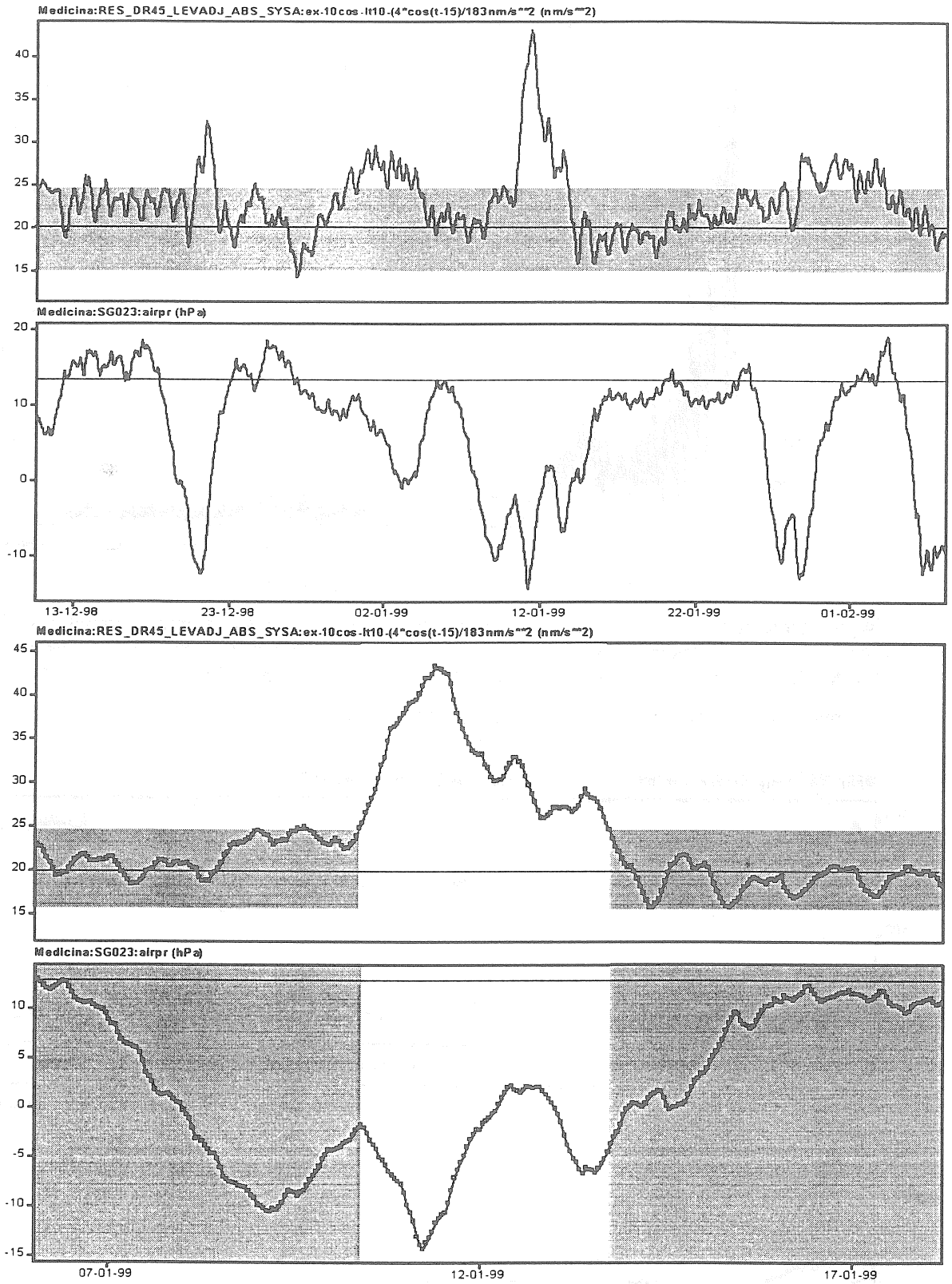

Fig.7: Medicina site, gravity variations after the standard reduction procedure due to tides and air pressure. An exceptional temporal gravity anomaly in the order of 20 ... 25 nms^{-2} for the time interval Jan. 10 -13, 1999 can be seen. The same anomaly was visible also in Wettzell, Germany, in a distance over 650 km (see the fig. 11 in the paper HARNISCH, HARNISCH, NOWAK, RICHTER, WOLF, this volume). The two upper figures show reduced gravity variations and air pressure for three months (Dec. 98 - Feb. 99), the lower figures shows a zoomed interval Jan 05 till Jan 19, 1999.

It can be seen very clearly that applying the regression coefficient r = -2.809 nms^{-2}/hPa the reduced gravity variations in general remain in the margin of 10 nms^{-2} (shaded area) even for strong air pressure variations up to 30 hPa with the only exception in the days of Jan 10 - Jan 13.

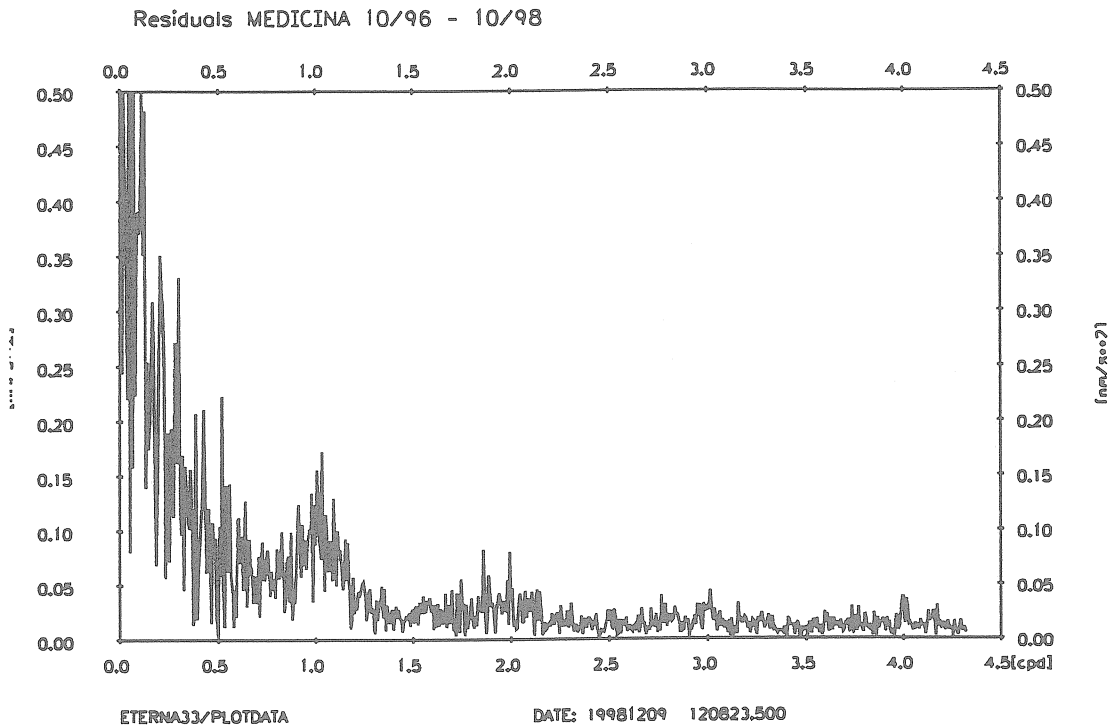

Fig. 8: Medicina site, time interval 11/96 -10/98: Spectrum of the residual gravity variations after elimination of the tides including the long-periodic ones, air pressure influence not yet removed. Besides the very low noise level for the period range of half-days and shorter a moderate low noise of 0.5 nms^{-2}, i.e. 0.05 microgal, can be seen in the range of up to a few weeks.

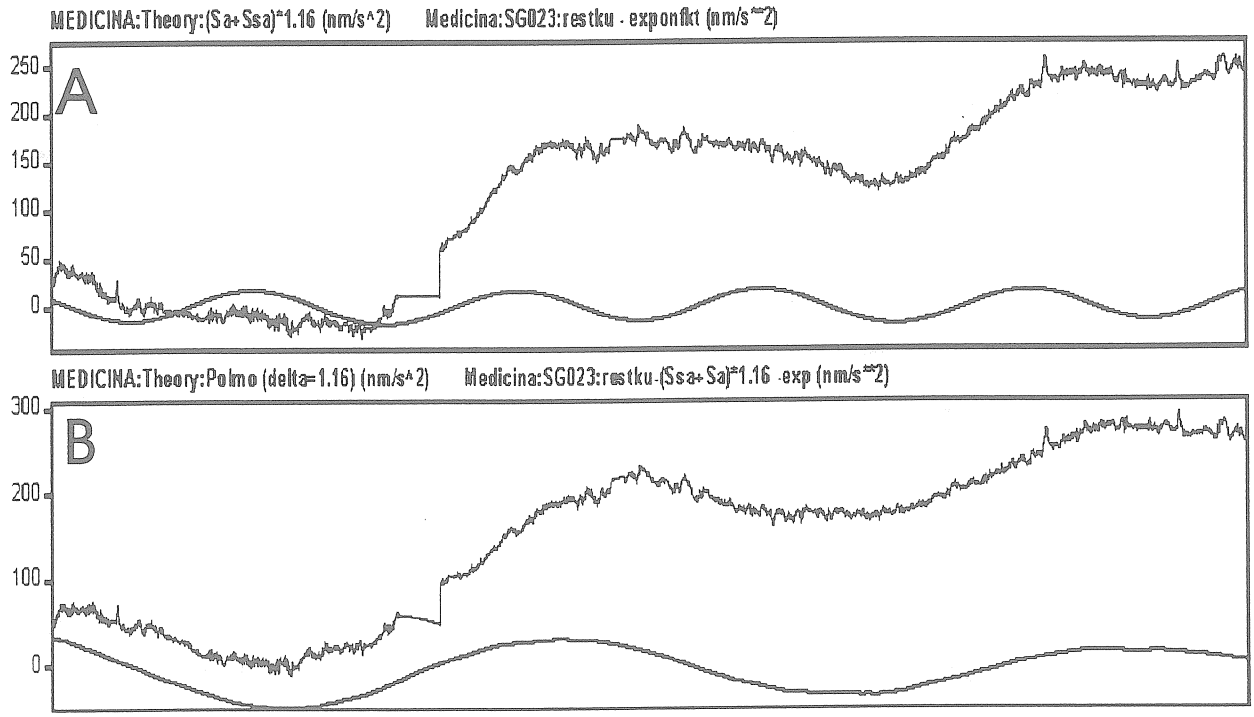

Fig. 9: Medicina site, gravity variations, stepwise elimination of well-modelled physical terms: (from top to bottom):

(A) - rough line: Measurements of SG C023 10/96 - 02/99 reduced for tides up to M_m and influence of air pressure (often called restkurve), also reduced for exponential Instrumental drift at the beginning,

- smooth line: model: ultralong-periodic zonal tides S_{sa} and S_a, delta-factor 1.16.

(B) - rough line: residuals reduced for S_{sa} and S_a,

- smooth line: model: gravity variation due to polar motion effect, delta-factor 1.16.

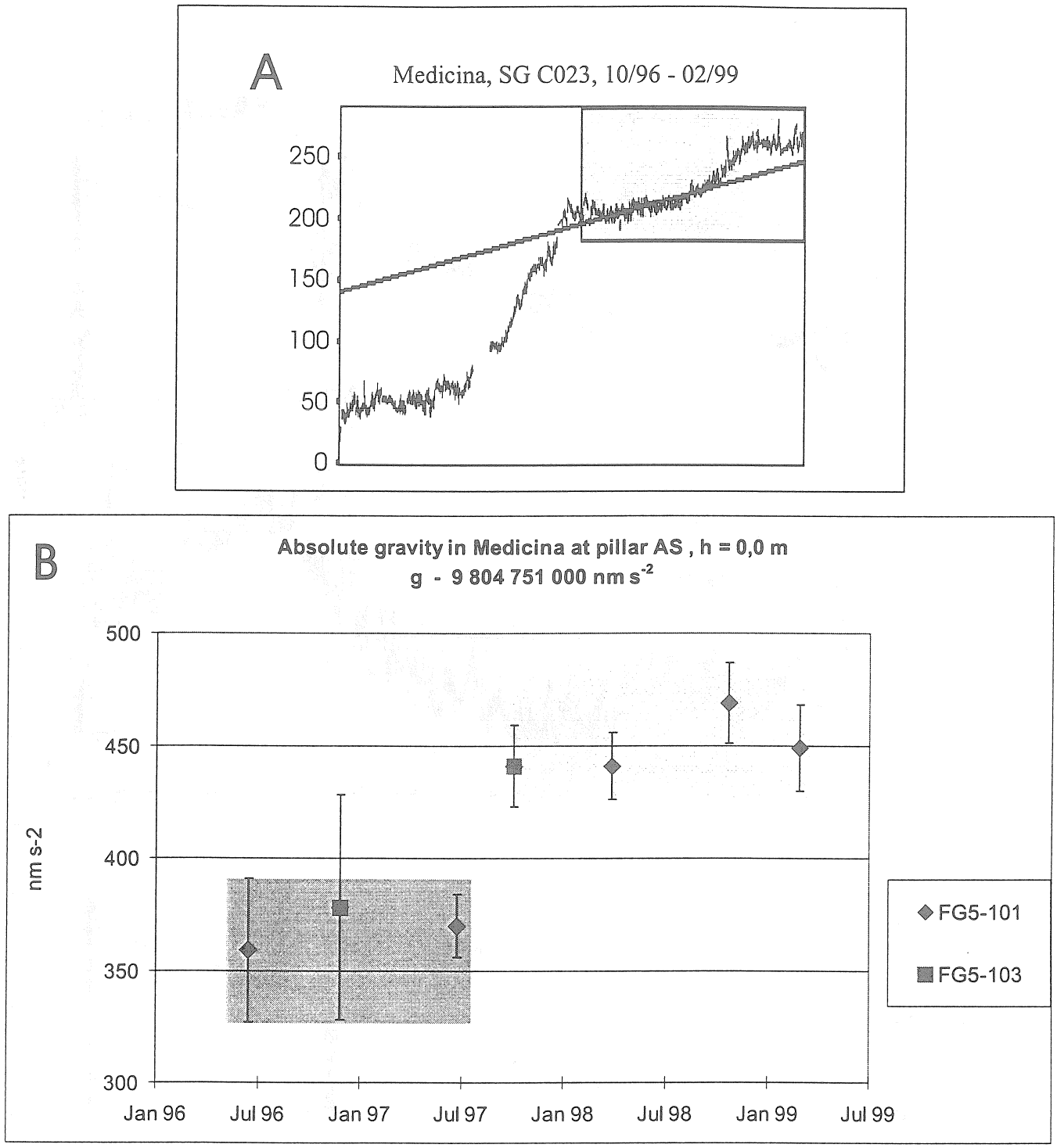

Fig. 10: Medicina site, gravity variations, observations using absolute and superconducting gravimeters reduced for tides, air pressure and polar motion effects (from top to bottom)
(A) - rough line: values according SG C023,

straight line: instrumental drift (45 nms^{-2}/year), determined by absolute measurements in the time interval marked by the shaded box, zoomed in Fig. 11.

(B) - values obtained with FG5-gravimeters. Two levels can be detected, marked by differently shaded areas, significantly separated by threefold amount of error bars.

Note the same time scale in both drawings.

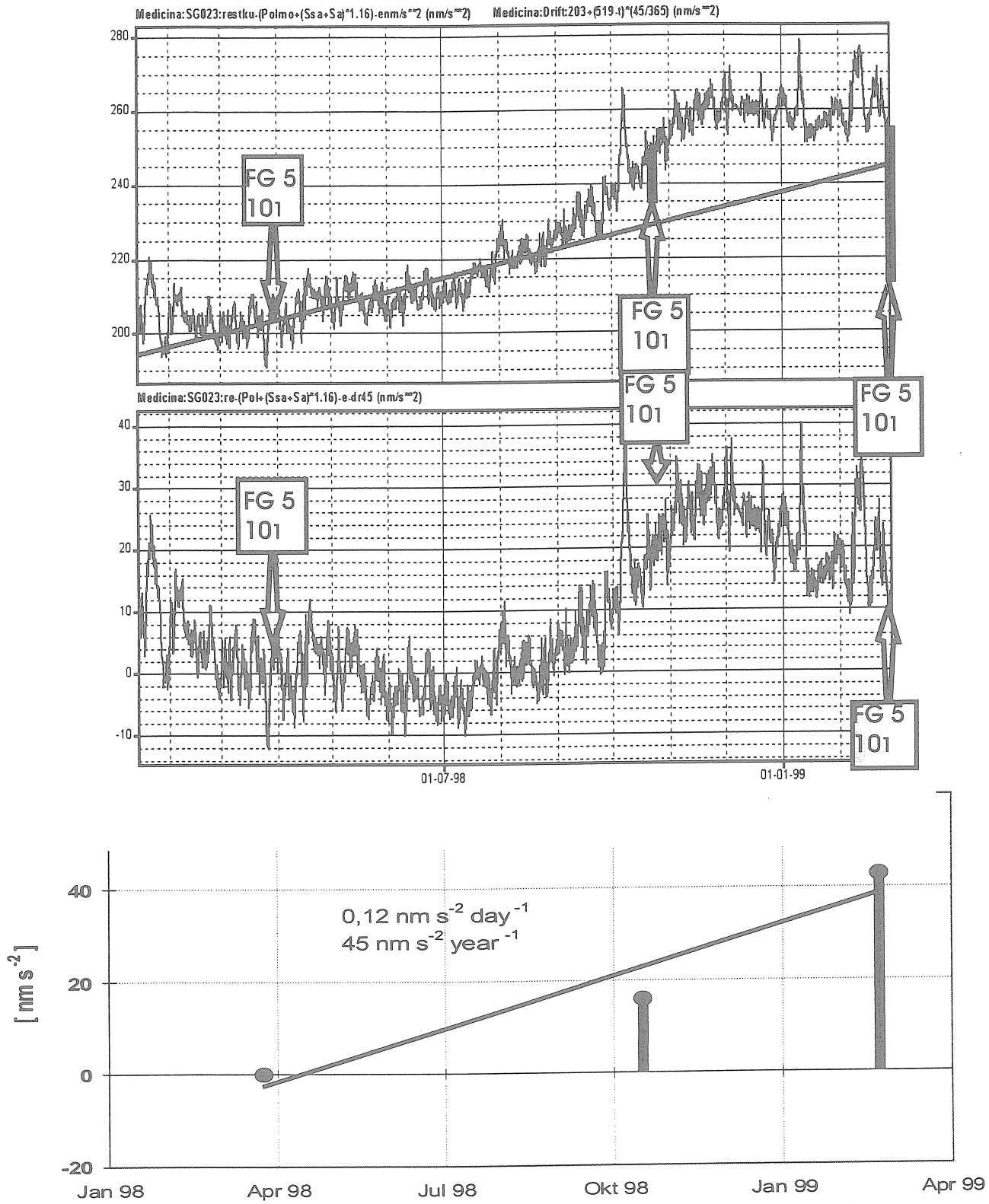

Fig. 11: Medicina site, determination (upper and lower box) and elimination (central box) of the instrumental drift of the superconducting gravimeter SG C023 on the base of absolute measurements and an uninterrupted time series of the SG C023 **without offsets**. The differences between the absolute readings (referred to March, 30 1998) and those of the SG C023, marked by black bars, reflect the instrumental behaviour expressed by a linear function in the order of 45 nms^{-2}/year. This term has been subtracted in the central box and for the whole gravity data set of SG C023.
Note the same time scale in all boxes.

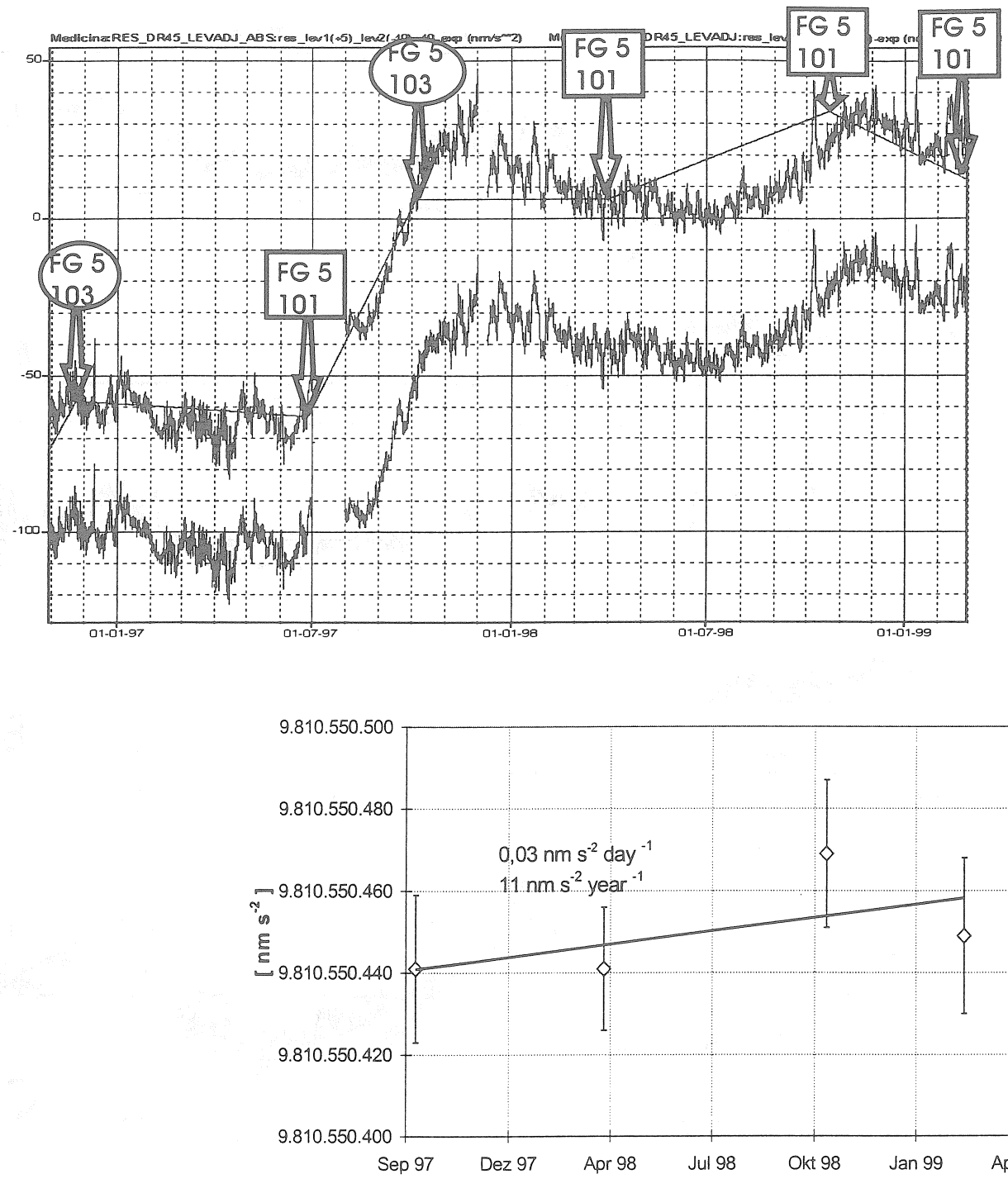

Fig. 12: Medicina site, fixing the levels of the single observation "blocks" of the SG C023 gravimetric time series (upper box) and determination of the "geophysical" linear trend (lower box) on the basis of absolute measurements .
In the upper box there are two functions with higher noise level. They differ (except for an offset) in the position of the second block (after fixing the relation of the first and third block to each other by using absolute measurements of the FG5-101 and FG5-103) : for the lower graph the hypothesis of the continuation of the previous level in the next block has been used, whereas for the upper one the absolute measurement of the FG5-103 in the first days of October 1997 has been used for the determination of the offset. The advantage of the latter consists in the pronounciation of the maximum in November 1997, which is consistent with the maximum in Nov. 98, see fig. 13a.
The temporal behaviour of the absolute values after the sharp gravity increase (lower box) can be expressed by a linear function in the order of 10 nms^{-2}/year. This term ("geophysical " linear trend) has been subtracted for the whole gravity data set of SG C023 (see fig. 13a, central box, rough function).
Note the same absolute time scale in all boxes.

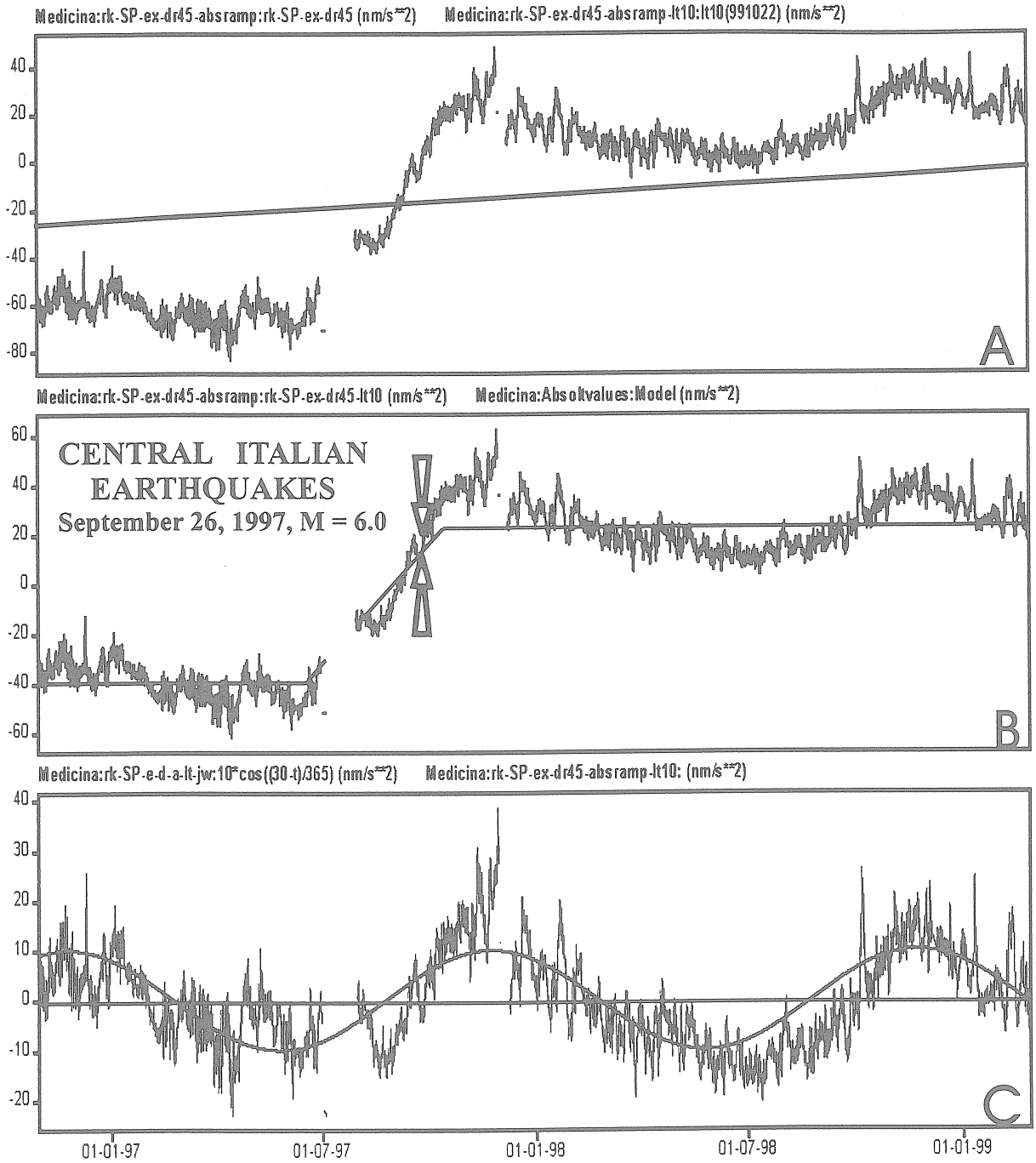

Fig 13a: Medicina site, gravity variations after offset determination based upon absolute measurements, stepwise elimination of probable geophysical models, Part I ((from up to down):

(A) - rough function: gravity variations after removal of the linear instrumental drift
- straight line: linear gravity increase of 10 nms^{-2}/year (**geophysical** linear trend) in accordance with subsidence rate of few mm in the Po river plain ,

(B) - rough function: gravity variations after subtraction of the linear geophysical trend
- straight line: the so-called "**ramp function**" models the linear gravity increase of approx. 63 nms^{-2} in the time interval June 15 till October 15, 1997, note the temporal position of the two large Central Italian earthquakes

C) -rough function : gravity variations after subtracting the geophysical linear trend and ramp function. Now the variations are in the same level and same signature.
- wavy thin line: **annual periodicity**, Ampl. approx. 10 nms^{-2}, maximum end of Nov./ beginning of December each year.

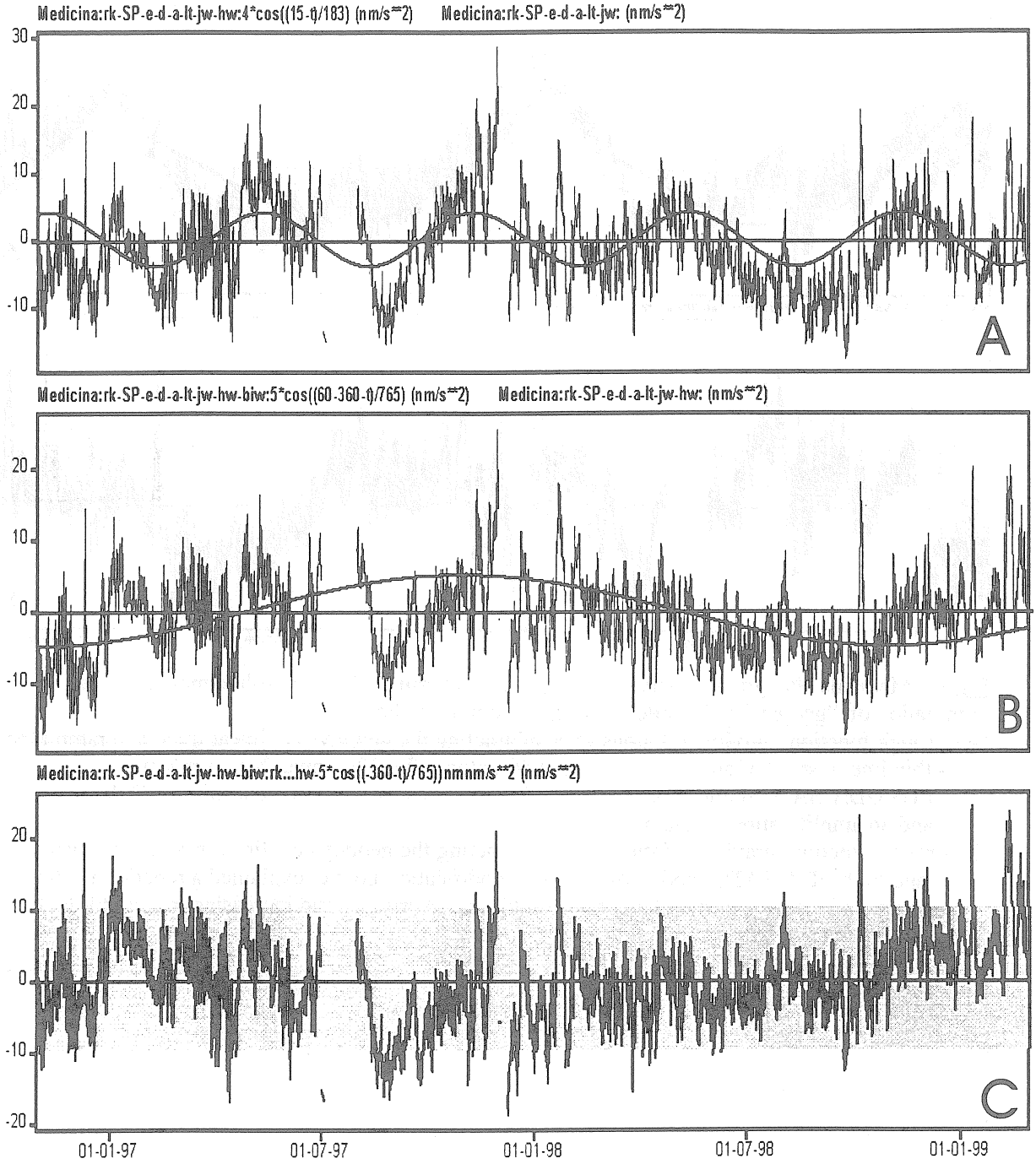

Fig 13b: Medicina site, gravity variations after offset determination by absolute measurements, stepwise elimination of "geophysical" models, Part II (for Part I see fig. 13a) (from up to down):

(A) - rough function: gravity variations after subtraction of the geophysical linear trend, ramp function and annual term,
- thin line: semi-annual periodicity, ampl. approx. 4 nms^{-2}, maximum. end of Nov./ beginning of December each year like the annual one.

(B) - rough function: gravity variations after subtraction of the geophysical linear trend, ramp function, annual and semi-annual periodicities,
- thin line: supposed bi-annual wave, ampl. approx. 5 nms^{-2}, maximum. end of Nov./ beginning of Dec of the odd years.

(C) - rough function: residual gravity variations after subtraction all the "geophysical" terms.
- shaded area: range of $|10|$ nms^{-2}. Final result: Using simple models the gravity variation can be reduced to noisy residuals in the order of $|10|$ nms^{-2} for the time span of 2.5 years.

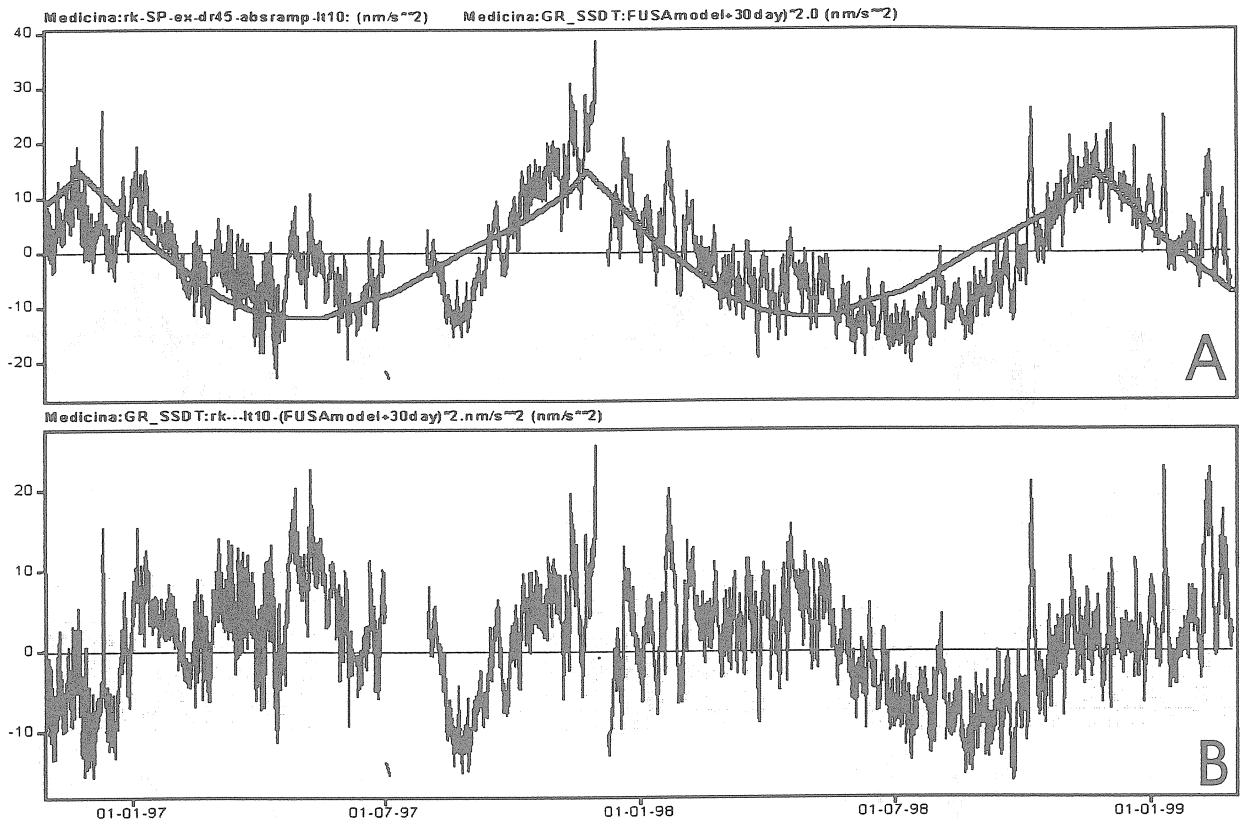

Fig 14: Medicina site, gravity variations after offset determination by absolute measurements, stepwise elimination of "geophysical" models, Part III (from top to bottom):

(A) - rough function: gravity variations after subtracting the geophysical linear trend and ramp function,
- thin line: instead of an annual periodicity (compare fig. 13a, lower box) a modified FUKUDA-SATO-model has been used. The modification consists in a shift of 30 days and an amplification by factor 2.

(B) - rough function: gravity variations after subtracting the geophysical linear trend, ramp function and FUKUDA-SATO-model. Besides the modification not yet explained a repetition pattern seems to be seen: constant level for Dec. till incl. April, de- and increasing in May till Nov.

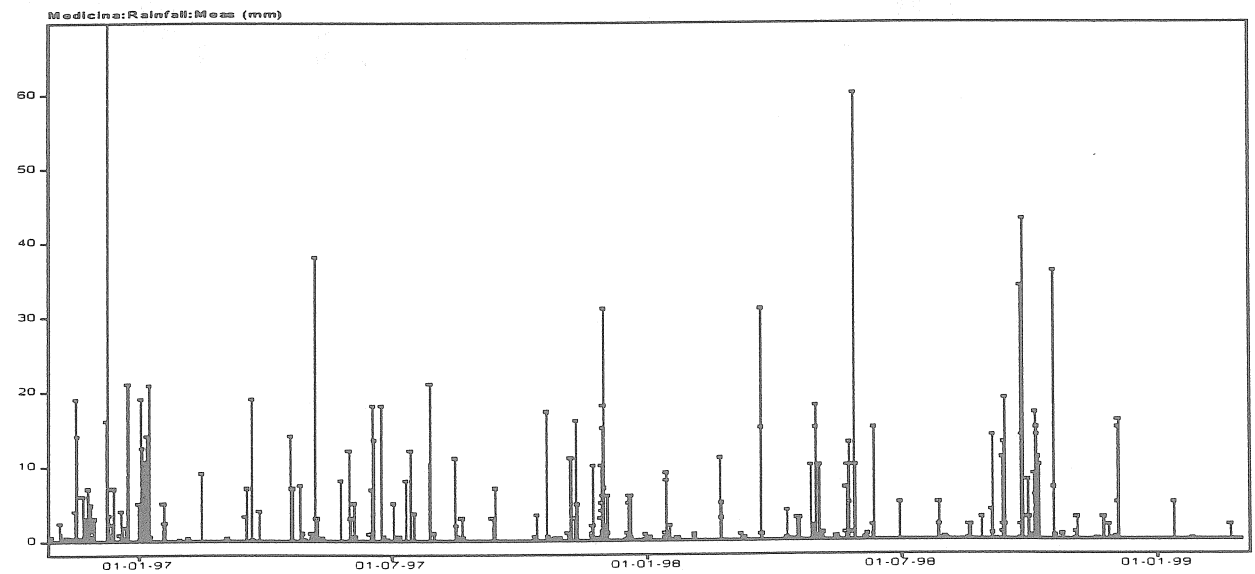

Fig. 15: Precipitation at Castel San Pietro Terme site (nearby Medicina site), unit [mm]: Few short-term anomalies in fig. 14 or 13b, lowest box, can be correlated with the precipitation. For instance the "needle" due to 152 mm precipitation at Dec. 10, 1996 can be detected in both time series.

The Dual Sphere Superconducting Gravimeter CD029 at Frankfurt a.M. and Wettzell. First Results and Calibration

M. Harnisch, G. Harnisch, I. Nowak, B. Richter, P. Wolf
Bundesamt für Kartographie und Geodäsie (BKG), Frankfurt a.M., Germany

Introduction

During the Thirteenth International Symposium on Earth Tides, Brussels 1997, B. RICHTER and R. WARBURTON announced the dual sphere gravimeter as a new type of superconducting gravimeters [2]. The BKG is owner of a first instrument of this type. In 1998 the CD029 was installed under very unfavourable conditions for a first test run at Frankfurt a.M. Since November 1998 the CD029 replaces the SG103 at the German Fundamental Station Wettzell, and as a contribution to the GGP again the data of the CD029 are transferred regularly to the ICET at Brussels. Based on data not only from the Wettzell station but also from the test measurements at Frankfurt a.M. some first results and experiences with this new type of gravimeters are reported.

1. History of operation of the dual sphere gravimeter CD029

Between July 28 and October 19, 1998 the CD029 was tested at Frankfurt a.M. For that purpose it was installed in a cellar room on the site of the BKG. The environmental conditions at this location did not meet the common standard for high precision measurements with this kind of instruments (no pillar, no air-conditioning, high noise level due to a railway line and heavy road traffic in short distances). Therefore the residual gravity derived from the observations at Frankfurt a.M., shows some perturbations, e.g. a lot of spikes. However, there are also some interesting features, which should be mentioned because they are different from the results obtained later under the much more favourable conditions at Wettzell.

After the test at Frankfurt a.M. the CD029 was transported to Wettzell. During the transportation the low temperature within the gravimeter was maintained. The CD029 replaces the SG103, registering at Wettzell up to September 24, 1998. Before the CD029 could be installed, the pillar had to be enlarged. Therefore a gap of 41 days occurred between the two time series. Since the November 4, 1998 the CD029 is again in continuous operation at Wettzell. The data are transferred daily to the Potsdam group of the BKG and from there in a monthly cycle to Brussels (ICET). This data series temporarily ended on May 5, 1999 with a serious break-down of the gravimeter. Therefore all the data up to this date are included in this report.

2. Some technical details of the CD029

A short description of the basic principles of the dual sphere superconducting gravimeter is given in [2]. It was developed with the aim of enhanced reliability of the recorded data and especially of a better drift monitoring. The dual sphere system is equivalent to two single systems combined in one instrument. The result is that the technical and financial expenditures are reduced considerably.

The cross section of the inner part of the instrument is given in fig. 1. The two gravimetric sensors are mounted one above the other at a vertical distance of 20 cm. The diameter of the spheres is one inch. The working temperature of the coldhead is about 3.2 K. Each gravity

system has its own set of electronics. Therefore each system can be operated like a separate single sphere instrument.

3. Data Structure

The data are recorded by a data acquisition system of the BKG as it was used - more or less modified and updated - since many years. The data are written into single "hourly files" which in turn are stored into hierarchic file systems. By this way the data of each hour may be accessed directly via a path name. Each of the hourly files starts with a header line. In the following main part a column structure is used with time information in the first three columns, the gravity signal of the lower system in the fourth, a channel identification number in the fifth and the information of the corresponding channel in the sixth column (fig. 2). The gravity signal of the upper system is stored into channel number 0. The channels are switched in turn. The described data structure leads to the following effective sampling rates, valid for the CD029 at Wettzell: lower system (main channel) 5 s, upper system (channel 0) 10 s, air pressure (channel 5) 1 min. During the test at Frankfurt a.M. the correspondent sampling rates were 10 s and 40 s for the two gravity channels and 1 min for the air pressure.

4. The difference signal

A characteristic and very helpful feature of the dual sphere gravimeter is the comparison of the gravity values measured by both systems. For that purpose the output voltages have to be multiplied with the corresponding scale factors. However, after the first attempts to do this it became clear, that also a small phase difference between the two gravity systems has to be taken into account. The difference signal is sensitive to all influences which are different for both systems or which are confined to one of them (e.g. steps, see fig. 9). In fig. 3 an example is given, which shows the reaction of the gravimeter on disturbances of the coldhead temperature. This slight effect probably could not be detected without the help of the difference signal.

The advantages of the difference signal become available only if both gravity systems are calibrated very carefully, at least to an accuracy of ±0.1 nm s^{-2}/V. On the basis of a nearly straight-lined section of the residual gravity fig. 4 gives an example of the influence of different scale factors on the shape of the difference signal. In the upper graph the scale factors -773.66 nm s^{-2}/V for the lower and -816.72 nm s^{-2}/V for the upper system were used, resulting from the acceleration calibration in October 1998 (see paragraph 10). In agreement with this calibration the phase shift between both systems was assumed to be $\Delta t = 0.0$ s. In the middle graph the scale factor for the upper system was changed to -815.84 nm s^{-2}/V. This value results from a trial and error procedure with the condition, that the undulations of the difference signal are minimised, i.e. that the mean square error of a fit to a third degree polynomial reaches a minimum value. The undulations are clearly diminished but not fully eliminated. The remaining undulations of the difference signal may not be further reduced by this procedure. If however, additionally a phase difference between both systems is included, the undulations of the difference signal nearly fully vanish as it may be seen from the lower graph. The optimum values of the calibration factor for the upper system and of the phase difference result to -815.82 nm s^{-2}/V and -4.7 s .

The existence of a small phase difference between both gravity systems is also confirmed by the disturbances arising from small earthquakes which may be seen also in the difference of the two gravity signals. If a phase difference is included, the disturbances are clearly reduced. Due to the comparatively fast earthquake oscillations on the one hand and the adjustment procedure used for the estimate of the time shifted gravity values on the other hand (time shift

less than the sampling rates of 5 and 10 s) one cannot reach a total elimination of the disturbances in practice.

5. Noise and Drift Rate

In comparison with other gravimeters the noise of the dual sphere gravimeter CD029 is very low. This may be seen already from the line widths of the residual gravity curves (figs. 5 and 11). In a more objective way at first the standard deviation may be estimated over short periods (e.g. 1 hour) where the influence of the drift may be neglected or eliminated by a linear model. In a second step these values are averaged over larger periods (e.g. 2 days). Even during the temporary installation at Frankfurt a.M. (13.-14.9.98) the noise was only m_0 = 0.44 nm s^{-2} (lower system) and 0.59 (upper system), later at Wettzell (11.-12.3.99) it diminished to 0.21 (lower system) and 0.19 (upper system). The corresponding values of the SG103 at Bad Homburg (25.3.99) and of the C023 at Medicina (17.-18.1.99) are 0.97 and 0.38 respectively (the m_0-values are given in fig. 5).

At Frankfurt a.M. the drift rates of both systems of the CD029 are very small (fig. 6). Only weak exponential constituents are present with decay times of 41.7 and 21.1 days for the lower and the upper system respectively. After subtracting these exponential constituents linear drift rates of (349.7 ± 1.7) nm s^{-2}/year and (413.9 ± 1.5) nm s^{-2}/year remain.

A quite different drift behaviour came out after the CD029 was installed at Wettzell. Both systems started with very large drift rates of about 23607.1 nm s^{-2}/year (lower system) and 8680.5 nm s^{-2}/year (upper system). After about 2 weeks the upper system reached steady values near zero while the very strong drift of the lower system continued. This may be explained by an exponential constituent with an extreme initial disturbance. The decay time was estimated to 25.2 days, i.e. a value in the same order of magnitude as during the testing period at Frankfurt a.M. In this way even after more than 3 months the decay of the exponential constituent of the lower system was going on (fig. 7). After correcting the exponential constituent of the lower system linear drift rates of (-1739.2 ± 2.6) nm s^{-2}/year and (+93.8 ± 4.4) nm s^{-2}/year were found (fig. 8).

As already mentioned in the beginning of May 1999 a total break-down of the CD029 happened. After a suspension of about six weeks it started with encouraging low drift rates of -308.8 nm s^{-2}/year of the lower and -497.5 nm s^{-2}/year of the upper system. No exponential constituents are visible in the first days of the new section of registrations. This drift behaviour corresponds to the first test period at Frankfurt a.M.

6. Steps

During the test measurements with the CD029 at Frankfurt a.M. altogether five steps could be detected in the difference signal. Three examples are given in fig. 9. Clearly it can be seen, that in this way steps down to a few nm s^{-2} may be detected with high significance as it was one of the aims of the dual sphere gravimeter. Another problem is whether the steps have to be corrected or not. At least for some of the steps a correction would introduce errors because the residual gravity after the steps slowly returns to the initial position without a second step backward. During the processing of other time series also the opposite behaviour was observed, which must not be corrected too: periods of slowly changing residual gravity ending suddenly by a step. During the measurements at Wettzell no steps down to the level of some nm s^{-2} occurred.

The results concerning steps may be summarised as follows. The measurements at Frankfurt a.M. show that steps down to some nm s^{-2} are clearly detected using the difference signal. On the other hand during the measurements at Wettzell no steps exceeding this level were ob-

served (apart from offsets due to failures of the diverse peripheral instruments or extensive maintenance activities). It means that, at least with modern gravimeters, the residual gravity is not seriously influenced by steps. Especially the assumed "hole" in the frequency distribution of steps [5], caused by an supposed multitude of small steps below the detection threshold obviously does not exist.

7. Influence of a break-down of the cooling water pump of the compressor

On January 27, 1999 a break-down of the cooling water pump happened. Also this very untypical event shows some interesting details in the reaction of the gravimeter (fig. 10). All the recorded environmental parameters (temperature of the cooling water, room temperature, tilts, etc.) reflect the disturbance more ore less suddenly. The nearly identical shape of the tilt signals seems to indicate a direct reaction of the electronics (e.g. temperature influences) as the primary reason of the tilt anomalies. Both gravity systems however, react quite differently. While the lower system remains nearly unaffected, the residual gravity of the upper system changes very clearly and nearly immediately. After the damaged pump was replaced by a new one, the residual gravity of the second system changed very rapidly in the opposite direction and after about 17 hours it reached nearly the same position as before the disturbance. Also the anomalies in the records of all the environmental parameters subsided very rapidly. But in fact the gravity signals of both systems did not reach exactly the same position as before. There seems to be a slight offset of the order of +27.2 nm s^{-2} in the lower and +22.0 nm s^{-2} in the upper system, while the difference signal with -5.3 nm s^{-2} remains nearly unaffected. Also a small change of the mean linear drift seems to occur.

8. Tidal Analysis (ETERNA)

The data recorded at Wettzell were analysed both with and without filtering. Due to the short data series of 161 days only subdivisions into 13 and 16 wave groups could be used. The results are given in tabs. 1 and 2. Roughly speaking the results are equivalent to those of the SG103 at the same station, based on a two-year series [7]. The tidal parameters of 5 selected waves are graphically presented in fig. 13.

If we compare first the δ-factors, significant differences between the gravimeters CD029 and SG103 become evident. These differences are due to uncertainties of the scale factors used for the analysis. On the other hand the very good agreement between the results of both systems of the CD029 is due to the consistent scale factors which were derived from an internal comparison of both gravity systems by means of the difference signal (see paragraphs 4 and 10). This agreement does not mean, that the results derived from the CD029 data are the "true" ones.

On the contrary the phases κ of both systems differ significantly. The differences range in the order of 5 to 10 seconds. In principle this result is confirmed by the investigations of the difference signal (see paragraph 4), however the values are about twice as large.

From the new analysis of the CD029 data no clear differences between the error bars of both systems may be derived as it seemed to be indicated by earlier analyses.

Tab. 1: Tidal Analysis (ETERNA), filtered Data, 13 Wave Groups
CD029, Wettzell, 4.11.1998 – 20.4.1999, 161.13 days, 2 Blocks
Numerical filter is PERTZEV59 with 51 coefficients.

Wave Group	Lower System		Upper System	
	δ	κ (°)	δ	κ (°)
Q1	1.14669 ± 0.00084	-0.1749 ± 0.0421	1.14752 ± 0.00030	-0.1886 ± 0.0151
O1	1.14846 ± 0.00016	0.0833 ± 0.0081	1.14868 ± 0.00006	0.1100 ± 0.0029
M1	1.15403 ± 0.00188	-0.0677 ± 0.0934	1.15214 ± 0.00067	0.0488 ± 0.0335
K1	1.13572 ± 0.00010	0.2135 ± 0.0050	1.13584 ± 0.00004	0.2457 ± 0.0018
J1	1.15579 ± 0.00194	0.1456 ± 0.0960	1.15754 ± 0.00069	0.2598 ± 0.0343
OO1	1.15898 ± 0.00488	0.4145 ± 0.2409	1.15660 ± 0.00174	0.3186 ± 0.0864
2N2	1.16283 ± 0.00138	2.0412 ± 0.0678	1.16269 ± 0.00117	2.0788 ± 0.0578
N2	1.17722 ± 0.00027	1.7669 ± 0.0132	1.17681 ± 0.00023	1.8246 ± 0.0112
M2	1.18494 ± 0.00005	1.3759 ± 0.0026	1.18510 ± 0.00005	1.4443 ± 0.0022
L2	1.21159 ± 0.00269	0.0761 ± 0.1274	1.21063 ± 0.00229	0.2419 ± 0.1086
S2	1.18298 ± 0.00012	0.2194 ± 0.0057	1.18319 ± 0.00010	0.2954 ± 0.0049
M3	1.06724 ± 0.00256	0.3506 ± 0.1374	1.06709 ± 0.00328	0.2661 ± 0.1759
M4	0.23471 ± 0.11933	11.7159 ± 29.1263	0.03885 ± 0.26956	9.3025 ± 397.4644
r_{air}	(-3.31585 ± 0.01361) nm s^{-2}/hPa		(-3.25956 ± 0.01438) nm s^{-2}/hPa	
m_0	± 0.631 nm s^{-2}		± 0.654 nm s^{-2}	

Tab. 2: Tidal Analysis (ETERNA), no Filter, 16 Wave Groups
CD029, Wettzell, 4.11.1998 – 20.4.1999, 161.13 days, 2 blocks

Wave Group	Lower System		Upper System	
	δ	κ (°)	δ	κ (°)
MM	1.15884 ± 0.22626	-1.3463 ± 11.6929	1.07497 ± 0.25613	0.7111 ± 14.2541
MF	1.07139 ± 0.08764	-1.6034 ± 4.6723	1.08370 ± 0.09908	0.0545 ± 5.2300
MTM	0.94088 ± 0.30203	2.8787 ± 18.3746	1.16263 ± 0.34143	7.5567 ± 16.8393
Q1	1.14788 ± 0.00291	0.0033 ± 0.1451	1.14879 ± 0.00273	-0.1267 ± 0.1363
O1	1.14883 ± 0.00058	0.0905 ± 0.0288	1.14897 ± 0.00054	0.1008 ± 0.0271
M1	1.15461 ± 0.00676	-0.2010 ± 0.3351	1.15683 ± 0.00635	0.0490 ± 0.3145
K1	1.13563 ± 0.00035	0.2093 ± 0.0178	1.13587 ± 0.00033	0.2313 ± 0.0167
J1	1.14950 ± 0.00687	0.0337 ± 0.3423	1.15335 ± 0.00646	0.1432 ± 0.3208
OO1	1.14393 ± 0.01680	0.7786 ± 0.8421	1.15309 ± 0.01579	0.3094 ± 0.7854
2N2	1.15663 ± 0.00459	1.7841 ± 0.2274	1.16339 ± 0.00461	1.8774 ± 0.2269
N2	1.17627 ± 0.00093	1.7327 ± 0.0453	1.17647 ± 0.00093	1.8082 ± 0.0454
M2	1.18477 ± 0.00018	1.3701 ± 0.0089	1.18498 ± 0.00019	1.4394 ± 0.0090
L2	1.22833 ± 0.00937	-0.1010 ± 0.4369	1.22193 ± 0.00940	-0.0671 ± 0.4409
S2	1.18345 ± 0.00039	0.2751 ± 0.0190	1.18394 ± 0.00039	0.3332 ± 0.0191
M3	1.05852 ± 0.00614	-0.1185 ± 0.3326	1.06548 ± 0.00734	0.2908 ± 0.3944
M4	0.96755 ± 0.38129	-53.9184 ± 22.5903	0.75912 ± 0.48411	-28.0420 ± 36.5568
r_{air}	(-2.80650 ± 0.02857) nm s^{-2}/hPa		(-2.80462 ± 0.03360) nm s^{-2}/hPa	
m_0	± 13.852 nm s^{-2}		± 16.295 nm s^{-2}	

9. Environmental Influences

Due to the increasing precision of the modern superconducting gravimeters, the environmental conditions get more and more influence on the gravity registrations.

It is common use to correct the influence of air pressure variations by means of a linear regression model. Therefore the local air pressure is used and the regression coefficient is estimated together with the tidal parameters during the tidal analysis. The first data from the CD029 showed significant differences between the air pressure regression coefficients of both gravity systems. From this the conclusion would have to be drawn, that also an instrumental constituent of the air pressure influence exists. However, recent data do not confirm this fear. Only the filtered data hint at a small difference near the significance level (tab. 1). The regression coefficients derived from the unfiltered data agree very well (tab. 2).

Although all gravimeter data are corrected for the influence of air pressure variations residual disturbances can remain. As an example fig. 11 shows nearly isochronous anomalies of the residual gravity at Wettzell and Medicina, which obviously are produced by insufficient air pressure corrections.

To an increasing extend also hydrological influences (precipitation, soil moisture, ground water) are to be taken into consideration. The seasonal variations of these influences may disturb all investigations of long-term effects (e.g. of the gravity effect of polar motions). – Fig. 12 shows precipitation and measured variations of the groundwater level along with the modelled gravity effect of the precipitation and the measured gravity variations. It should be noticed that also on mountain tops as it is the case at Wettzell considerable variations of the hydrological regime may occur.

10. Scale factors of the CD029

At the beginning only scale factors could be used, which were derived from comparisons with the theoretical tidal model. Because also tidal parameters, valid for the location of the measurements at Frankfurt a.M. were not available, the well known parameter set from the nearby station Bad Homburg (distance about 16 km) was used. As a first approximation the measured total tidal variation was compared with the correspondent theoretical tidal signal. Later, when time series became available, long enough for reliable tidal analysis, also single spectral components of the tidal signal could be compared. It should be noted, that all these estimations of scale factors using the comparison with theoretical tides are finally based on tidal registrations with the LCR-gravimeter ET-15, carried out at Bad Homburg between December 1983 and July 1984 in parallel with the TT40 [1].

Meanwhile the CD029 could be calibrated also directly by comparisons with absolute gravity measurements as well as by artificial accelerations, derived from small sinusoidal vertical displacements of the gravimeter ("platform calibration").

The principle of the calibration by comparison with absolute gravity measurements may be seen from fig. 14. In tab. 3 the results of 3 calibration campaigns are summarised. But only the first comparison (December 15 to 16, 1998) fulfils the requirements on such experiments. The second experiment (January 6 to 7, 1999) is affected by the low accuracy of the JILAG-5 gravimeter while during the third experiment (January 26 to 29, 1999) the break-down of the cooling water pump happened (see paragraph 7) which considerably influenced the data of the CD029 and in this way prevented a successful calibration. From this point of view it is only by luck that the mean values of both comparisons with the FG5-101 agree very well with the result of the platform calibration.

Tab. 3: Calibration of the CD029 by Comparison with Absolute Gravity Measurements

Date	Scale Factor nm s^{-2}/V	Δgmax nm s^{-2}	Absolute Gravimeter	N	Outliers	Remarks
15.-16.12.1998	-771.495 ± 3.293 -813.477 ± 3.472	1663.5	FG5-101	3550	50	
6. – 7.1.1999	-788.238 ± 6.361 -830.986 ± 6.701	1300.0	JILAG-5	2500	0	FGI, Mäkinen
26. – 29.1.1999	-774.448 ± 2.077 -818.888 ± 2.203	2066.85 2056.44	FG5-101	7333	29	CD029 disturbed (break-down of the cooling water pump)

The acceleration experiment (tab. 4) was carried out on October 22 and 23, 1998 at Frankfurt a.M. In addition to the scale factors of both systems also the phase shift of the tide filter could be estimated (the same value for both systems). It should be noticed that at Frankfurt a.M. the environmental conditions are not the best ones to carry out such high precision measurements. Under more favourable conditions a higher accuracy is to be expected as it is known from earlier acceleration experiments [3].

Tab. 4: Calibration of the CD029 by Inertial Accelerations ("Platform Calibration")

Date	Lower System nm s^{-2}/V	Upper System nm s^{-2}/V	Remarks
22.10.1998	-773.41 ± 0.36	-816.79 ± 0.33	Variable room temperature
23.10.1998	-773.91 ± 0.16	-816.65 ± 0.03	stable environmental conditions
Mean	-773.66 ± 0.2	-816.72 ± 0.2	
Phase Shift	(43.9 ± 0.1) s	(43.9 ± 0.1) s	up to now 38.0 s were used

The relationship of the scale factors to each other may be checked by means of the difference signal. The output voltages of both gravity systems have to be multiplied with the respective scale factors and the difference between the resulting gravity values ("difference signal") should have a constant value or randomly scatter around a mean value. This however is valid only if the scale factors are the "right" ones. If they are erroneous, the expected flat shape of the difference signal is disturbed by residuals of the tidal gravity variations as may be seen from the uppermost graph of fig. 4. In connection with the discussion of fig. 4 it was already mentioned that besides the scale factors also a small phase difference between both gravity systems has to be taken into account.

The sensitivity of the difference signal to errors of the calibration factors may be used to derive a consistent set of calibration parameters. Therefore the scale factor of the lower system resulting from the platform calibration was used as reference value and a trial and error procedure was started assuming a zero phase difference between both systems. Then the scale factor of the upper system and the phase difference were varied until the best fit to a third degree polynomial was reached (described by the mean square error m_0), i.e. until the undulations of the difference signal were minimised. The final results are given in tab. 5. The quantities between brackets are directly derived from the platform calibration. These values are consistent between each other but not necessarily without any errors. The problem of the "absolutely correct" calibration parameters may not be resolved as yet because from the point of view of the difference signal, even the very accurate method of the platform calibration, is not precise enough for this decision.

Tab. 5: Consistent set of calibration parameters of the CD029

	Lower System	Upper System
Scale factor	(-773.66 ± 0.2) nm s^{-2}/V	-815.82 nm s^{-2}/V
Phase	(43.9 ± 0.1) s	39.2 s

11. Final Remarks

First experiences with the new dual sphere gravimeter CD029 confirm the high quality and the high accuracy of this new type of superconducting gravimeters. In general the noise of the tidal signal and the drift rate are very low. The very strong exponential behaviour during the first operation period at Wettzell has to be considered as an exception. During the same time no steps occurred. The difference signal which compares the gravity values of both systems is a very helpful tool for the monitoring of the instrumental drift and the detection of disturbances of different kind. It also may be used to derive a consistent set of calibration factors and the phase lag between the two systems.

However, also this new type of gravimeters is not proof against failures. May be that some of the problems during the past were teething troubles of the first manufactured instrument. But for the use of all their advantages also these new gravimeters require the right handling and a very careful maintenance.

Acknowledgment

The authors thank Jaakko Mäkinen (Finnish Geodetic Institute, Helsinki) who granted permission to use the results of his absolute measurements at Wettzell as well as for the helpful discussions concerning the inclusion of these data into the calibration experiment.

References:

[1] Richter, B.
Das supraleitende Gravimeter
Dt. Geodät. Kommiss., R. C, H. 329, Inst. Angew. Geodäsie, Frankfurt a.M. 1987, 126 p.

[2] Richter, B., Warburton, R. J.
A New Generation of Superconducting Gravimeters
Proc. 13th Int. Symp. Earth Tides, Brussels 1997. Obs. Royal Belgique, Sér. Géophys., Brussels 1998, pp. 545 - 555.

[3] Richter, B., Wilmes, H., Nowak, I., Wolf, P.
Calibration of a Cryogenic Gravimeter (SCG TT60) by Artificial Accelerations and Comparisons with Absolute Measurements
Poster Presentation at the General Assembly IUGG, Boulder 1995, unpublished.

[4] Harnisch, M., Harnisch, G.
Processing of the data from two superconducting gravimeters, recorded in 1990 - 1991 at Richmond (Miami, Florida). Some problems and results
Working Group Bonn, 1994, Marées Terrestres Bull. Inf., 122, Bruxelles 1995, pp. 9141 - 9147.

[5] Harnisch, M., Harnisch, G.
Longtime behaviour of superconducting gravimeters derived from observed time series
Working Group Bonn, 1996, Marées Terrestres Bull. Inf., 127, Bruxelles 1997, pp. 9796 - 9805.

[6] Harnisch, M., Harnisch, G., Richter, B., Schwahn, W.
Estimation of polar motion effects from time series recorded by superconducting gravimeters.
Proc. 13th Int. Symp. Earth Tides, Brussels, 1997. Obs. Royal Belgique, Sér. Géophys., Brussels 1998. pp. 511 - 518.

[7] Harnisch, M., Harnisch, G., Jurczyk, H., Wilmes, H.
889 Days of Registrations with the Superconducting Gravimeter SG103 at Wettzell (Germany)
Proc. Second GGP Workshop Munsbach Castle (Luxembourg), 24-26 March 1999, in preparation.

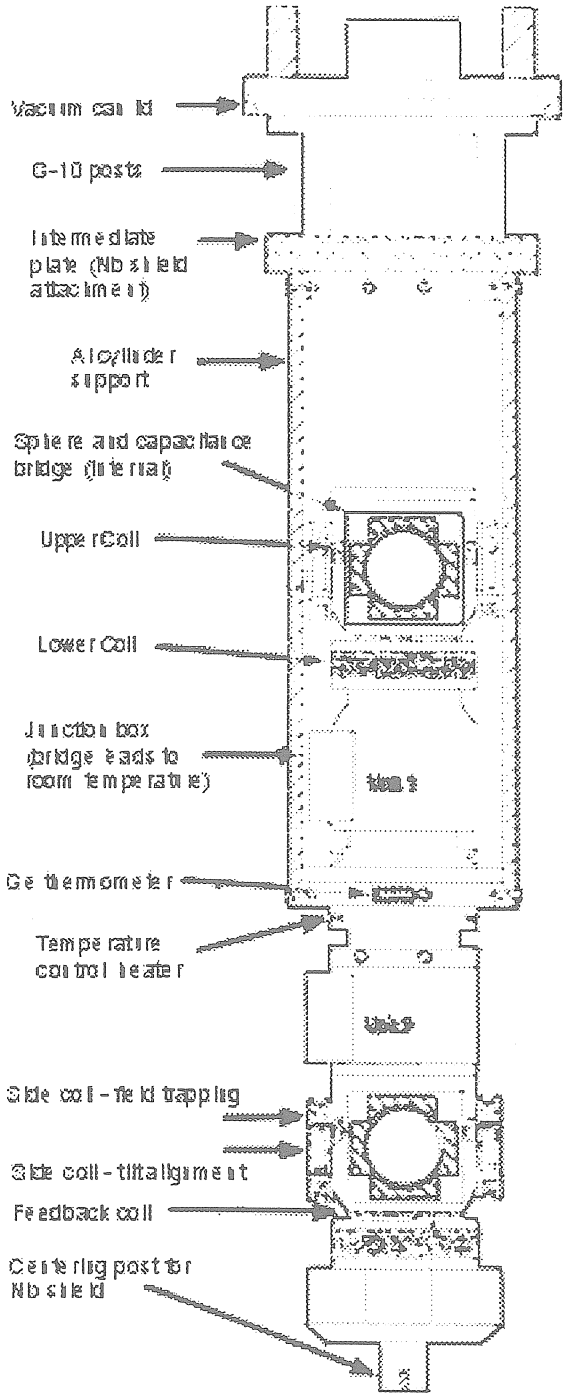

Fig. 1: Schematic cross section of the dual sphere gravimeter CD029 (after [2])

```
605608200 1999   3 11    9 1
    0 30  0    5.193840 0  1.43747e+000
    5 30  5    5.193890 3  5.03629e+000
   10 30 10    5.193900 0  1.43750e+000
   15 30 15    5.193890 4  5.07563e+000
   20 30 20    5.193830 0  1.43733e+000
   25 30 25    5.193720 5 -1.26588e+000
   30 30 30    5.193590 0  1.43698e+000
   35 30 35    5.193470 6  1.65930e+000
   40 30 40    5.193370 0  1.43657e+000
   45 30 45    5.193320 7  2.27315e-001
   50 30 50    5.193300 0  1.43633e+000
   55 30 55    5.193350 1 -2.50000e-004
   60 31  0    5.193420 0  1.43648e+000
   65 31  5    5.193550 3  5.03707e+000
   70 31 10    5.193730 0  1.43690e+000
   75 31 15    5.193970 4  5.07607e+000
   80 31 20    5.194170 0  1.43743e+000
   86 31 26    5.194360 5 -1.26592e+000
   90 31 30    5.194470 0  1.43765e+000
   95 31 35    5.194570 8  2.23311e-001
  100 31 40    5.194580 0  1.43772e+000
  105 31 45    5.194510 9  1.84856e-001
  110 31 50    5.194380 0  1.43773e+000
  115 31 55    5.194210 2 -2.60000e-004
  120 32  0    5.194030 0  1.43778e+000
  125 32  5    5.193890 3  5.03793e+000
  130 32 10    5.193820 0  1.43780e+000
  135 32 15    5.193810 4  5.07702e+000
 ...
```

Fig. 2: Data structure of the "Hourly Files"

Example: 11.3.1999, 8:30 ... 9:30 UT
Header line: date, time (hour)
Column 2: minutes
Column 3: seconds
Column 4: main channel (lower system)
Column 5: channel number (0 ... 9)
Column 6: channel information (Volt)
Upper system: channel number 0
Air pressure: channel number 5

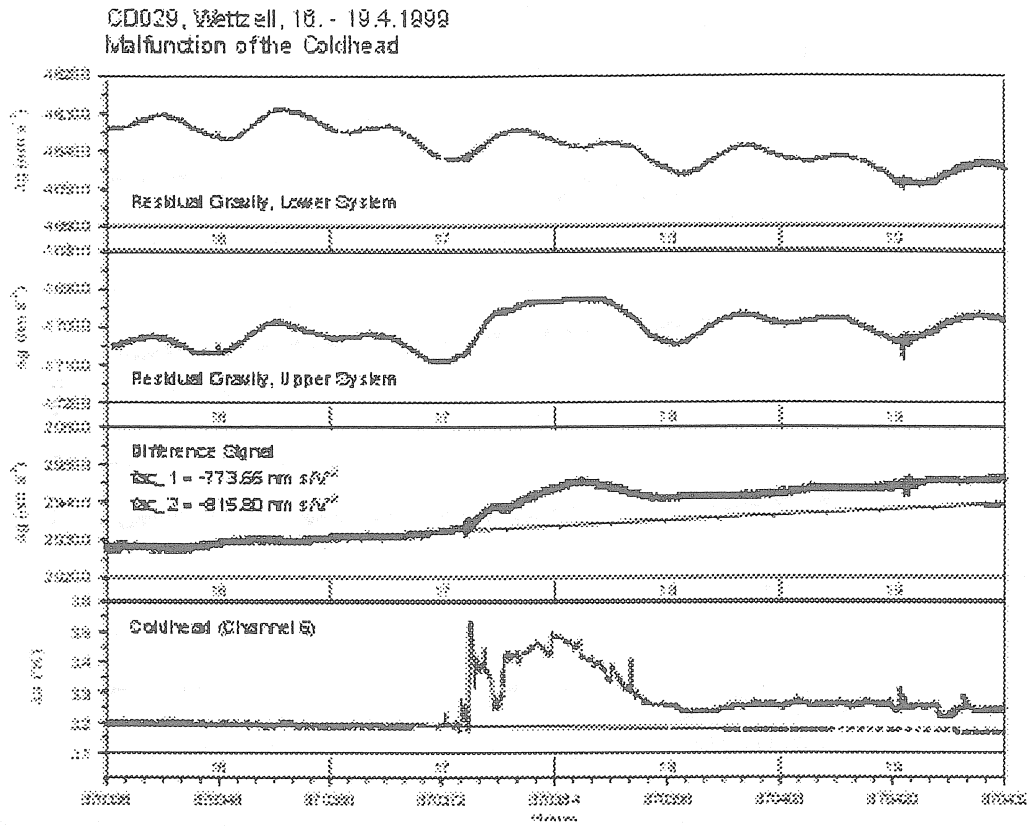

Fig. 3: Malfunction of the coldhead. The disturbances of the residual gravity are masked by residual tidal influences due to an unsuited (elder) set of tidal parameters. They are clearly detected by the difference signal. Also a systematic shift of the difference signal is to be seen.

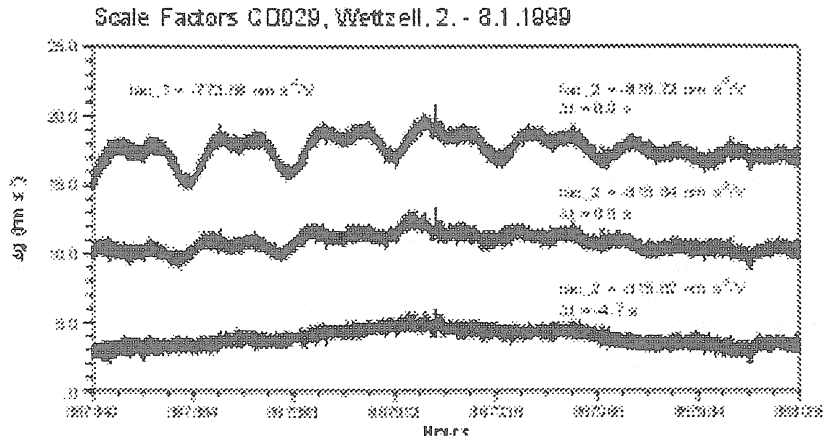

Fig. 4: Influence of the scale factors on the difference signal. Top graph: All calibration parameters taken from the platform calibration (October 1998). Middle graph: Calibration factor of the upper system adjusted. Bottom graph: Calibration factor of the upper system and phase difference adjusted.

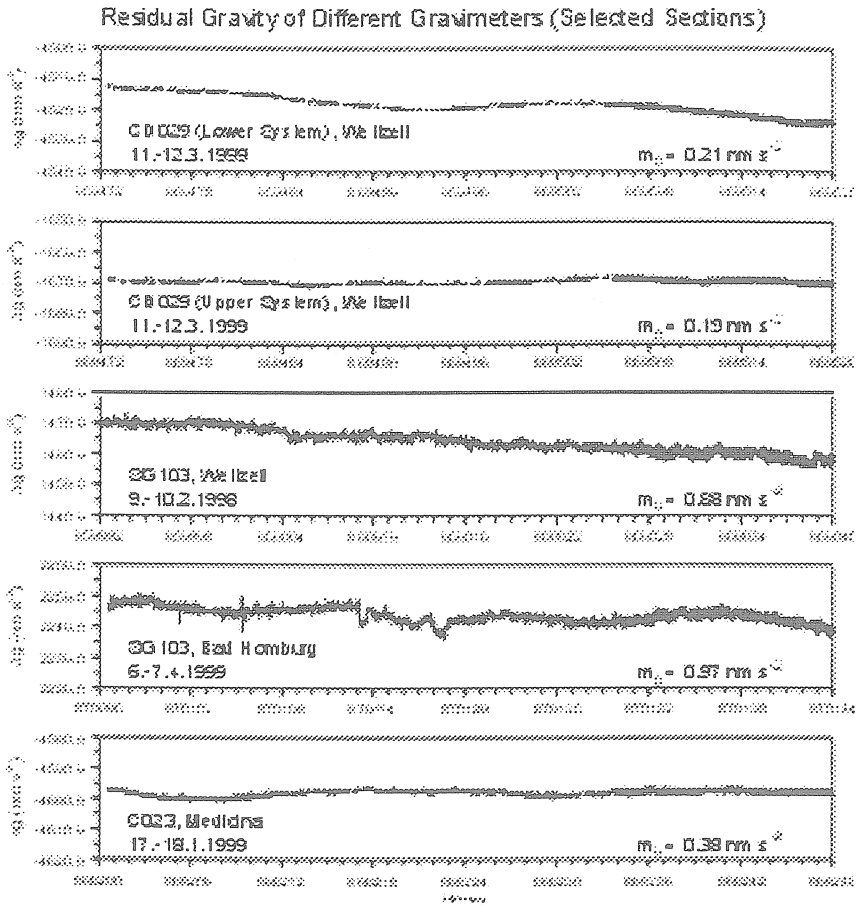

Fig. 5: Selected parts of the residual gravity curves. Line width gives an impression of the instrumental noise

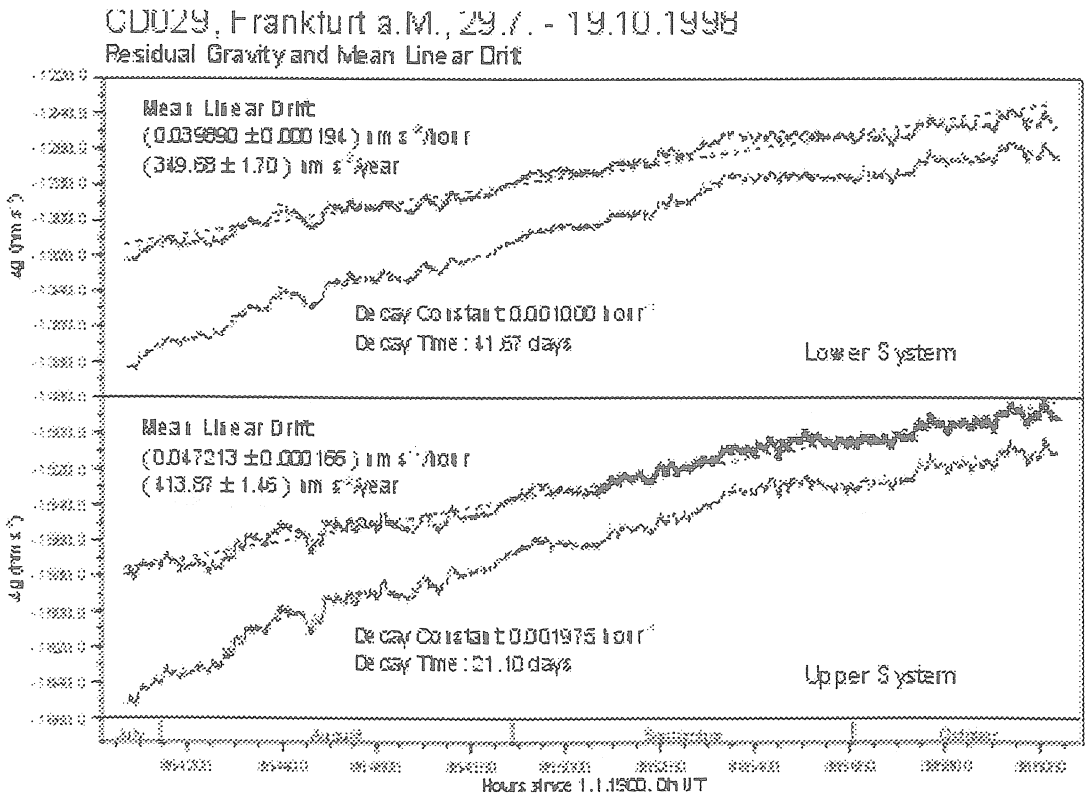

Fig. 6: Drift rates during the test measurements at Frankfurt a.M. Lower curves: exponential constituent included. Upper curves: exponential constituent eliminated.

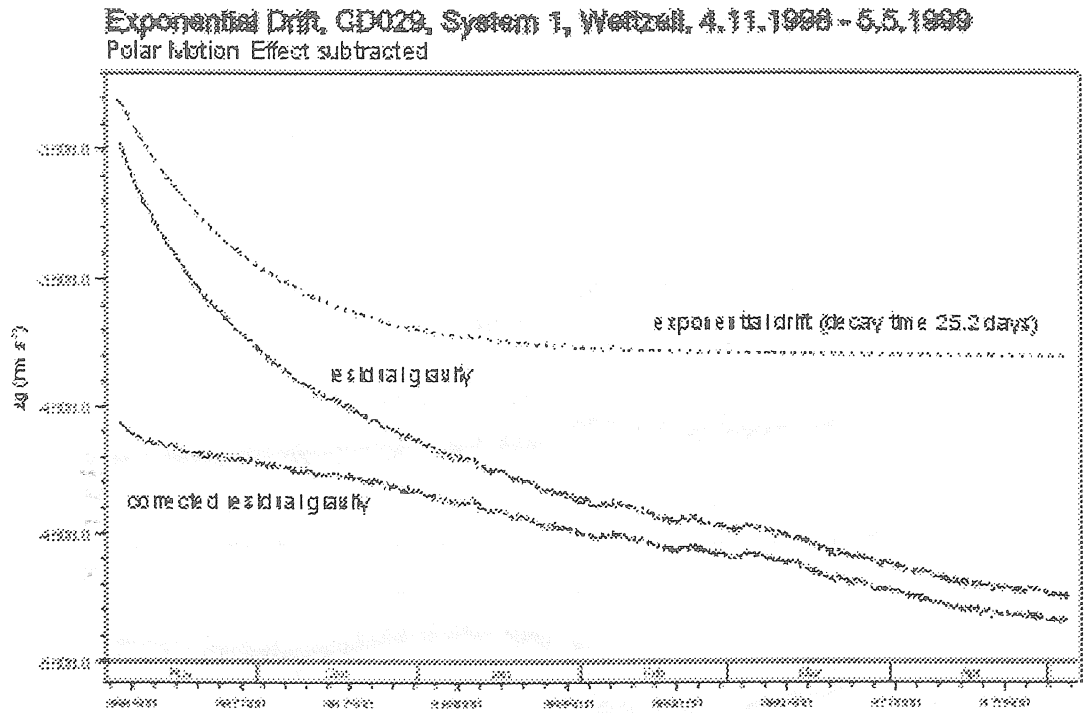

Fig. 7: Drift behaviour of the CD029, lower system. The drift of the lower system was dominated by an exponential constituent with a very large initial disturbance, decay time 25.2 days.

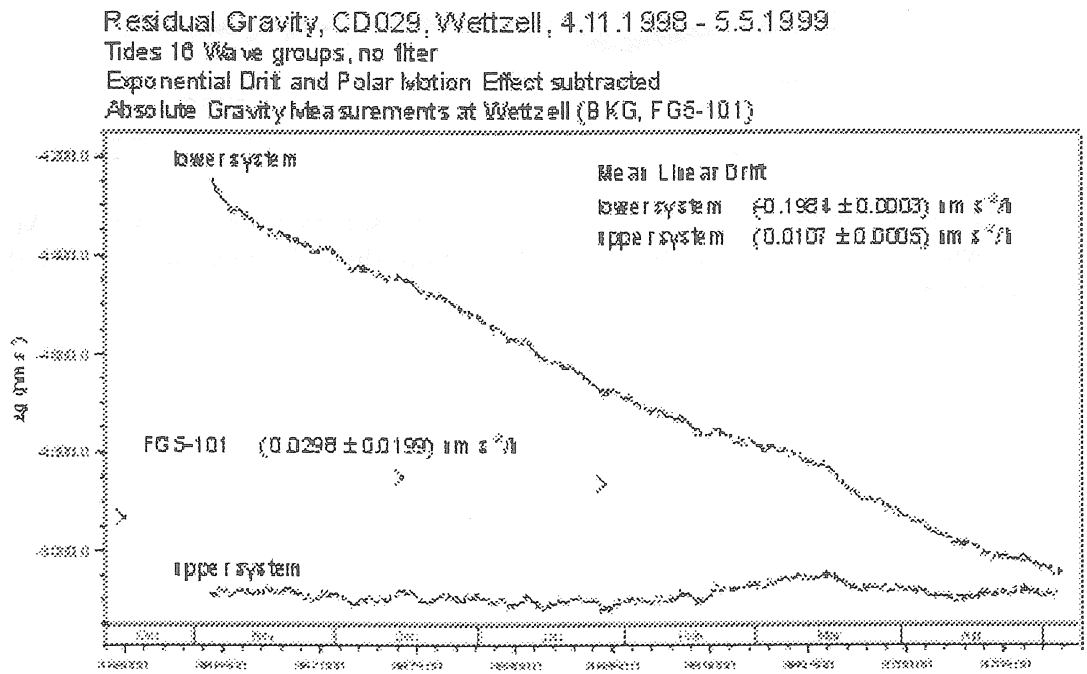

Fig. 8: Drift behaviour of the CD029. Exponential constituent (only lower system) and influence of polar motions subtracted. Comparison with three absolute gravity measurements (FG5-101).

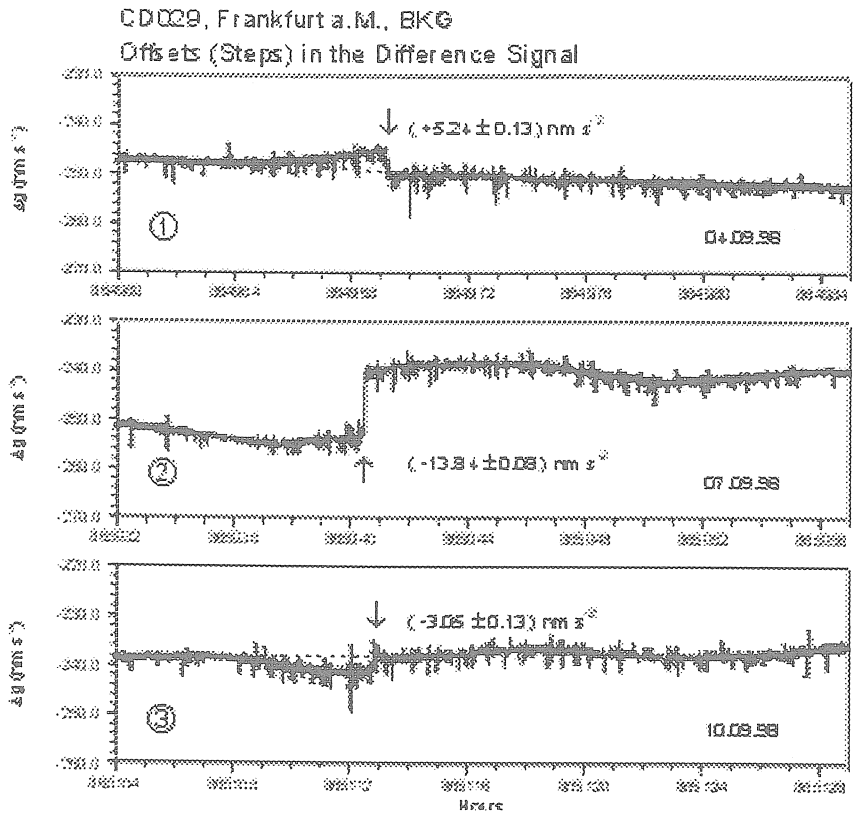

Fig. 9: CD029, Examples of steps during the test measurements at Frankfurt a.M. Steps down to some nm s^{-2} may be clearly detected in the difference signal. Only the step in the middle diagram has to be corrected.

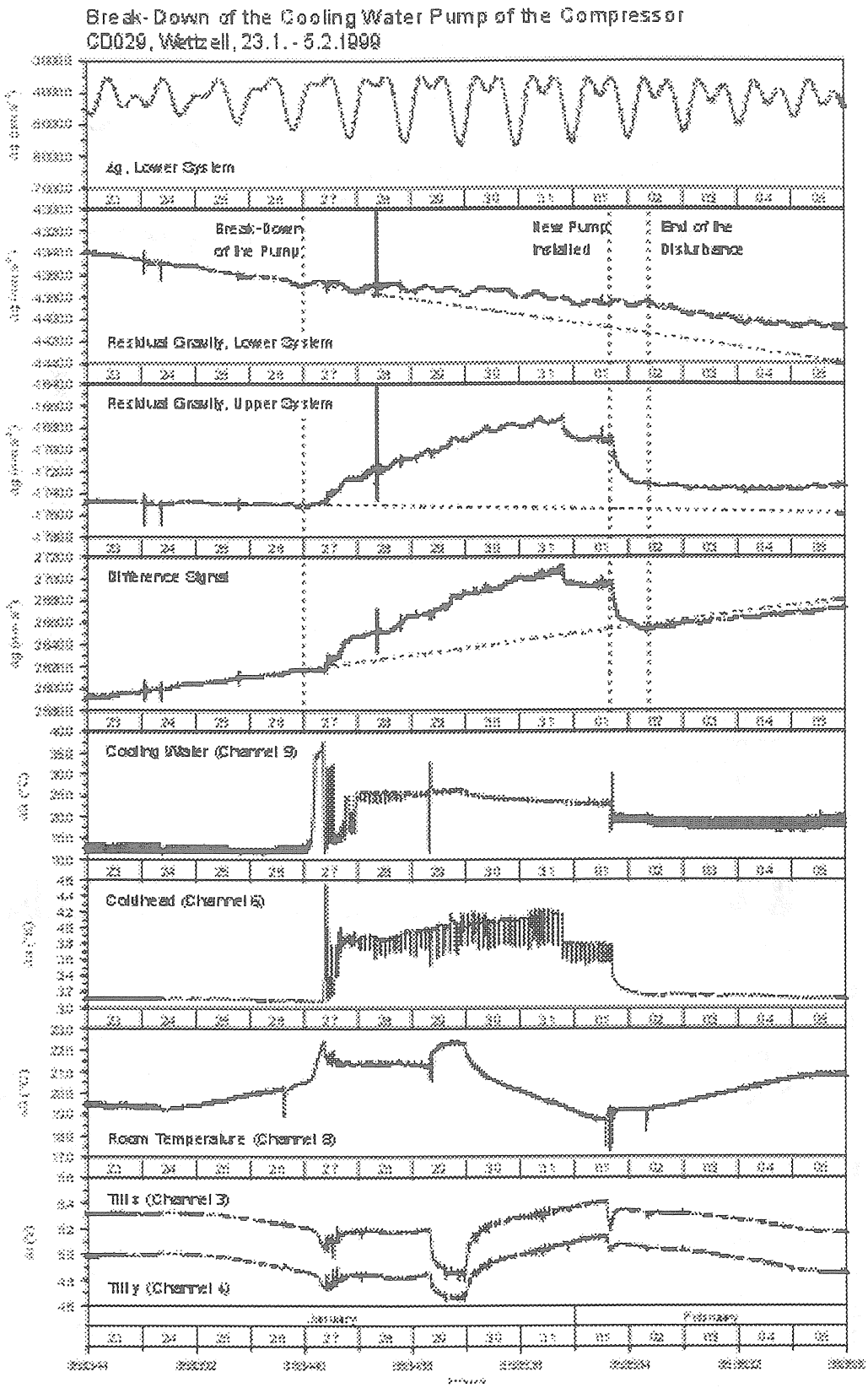

Fig. 10: Break-down of the cooling water pump of the compressor. Influence on both systems of the CD029, on the difference signal and on different instrumental and environmental parameters.

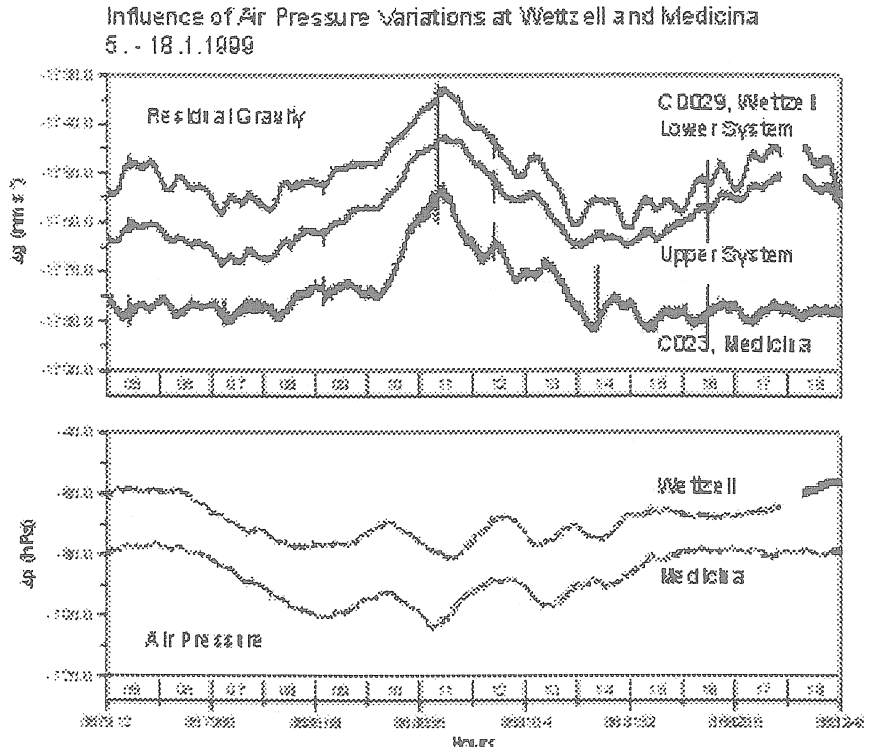

Fig. 11: Residual air pressure influences at Wettzell and Medicina (5. - 18.1.1999)

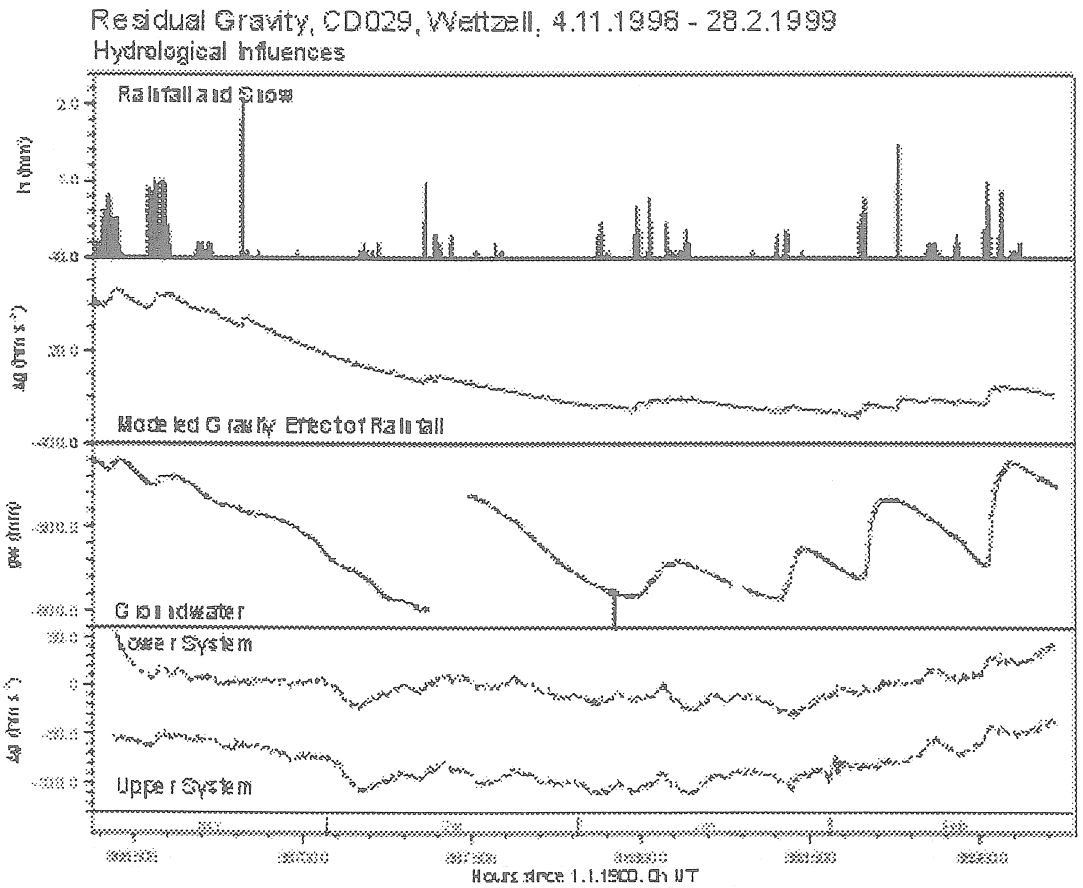

Fig. 12: Hydrological Influences at Wettzell. Measured rainfall, snow and groundwater variations. Modelled gravity effect of rainfall. Measured gravity variations, exponential constituents and linear drift eliminated.

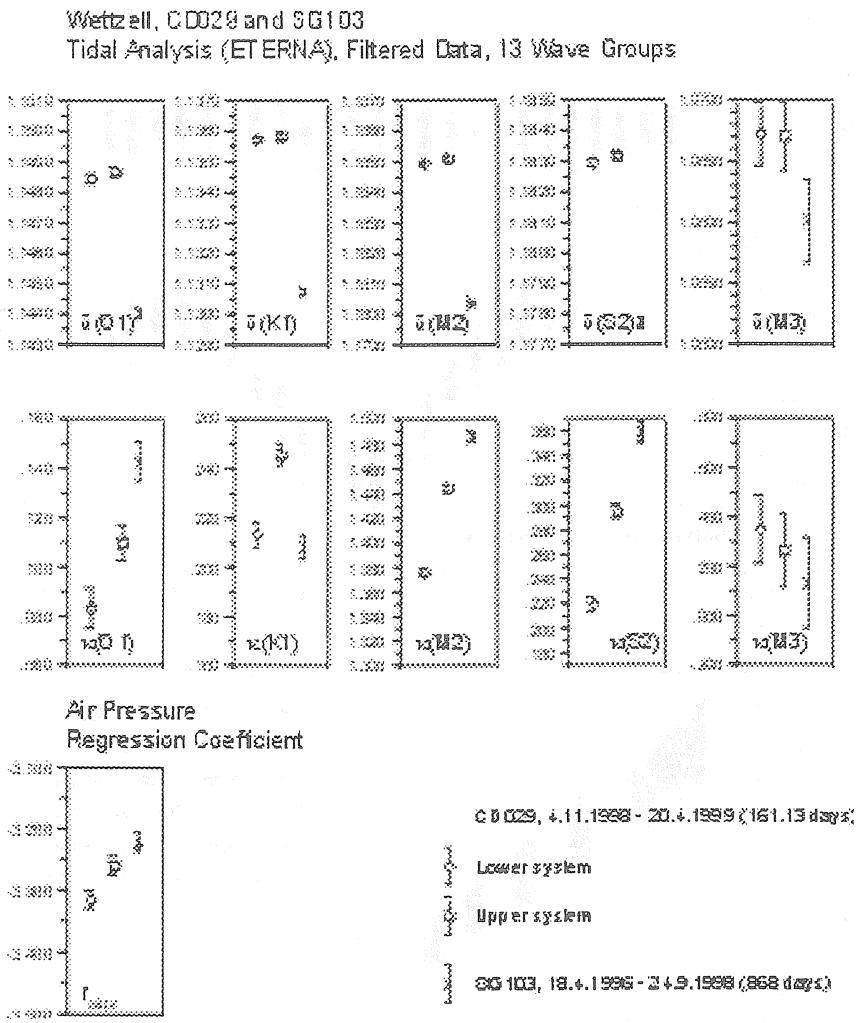

Fig. 13: Tidal parameters O1, K1, M2, S2 and air pressure regression coefficients derived from both systems of the CD029 (Wettzell, 4.11.1998 – 20.4.1999) in comparison with the correspondent data of the SG103 (Wettzell, 18.4.1996 – 24.9.1998)

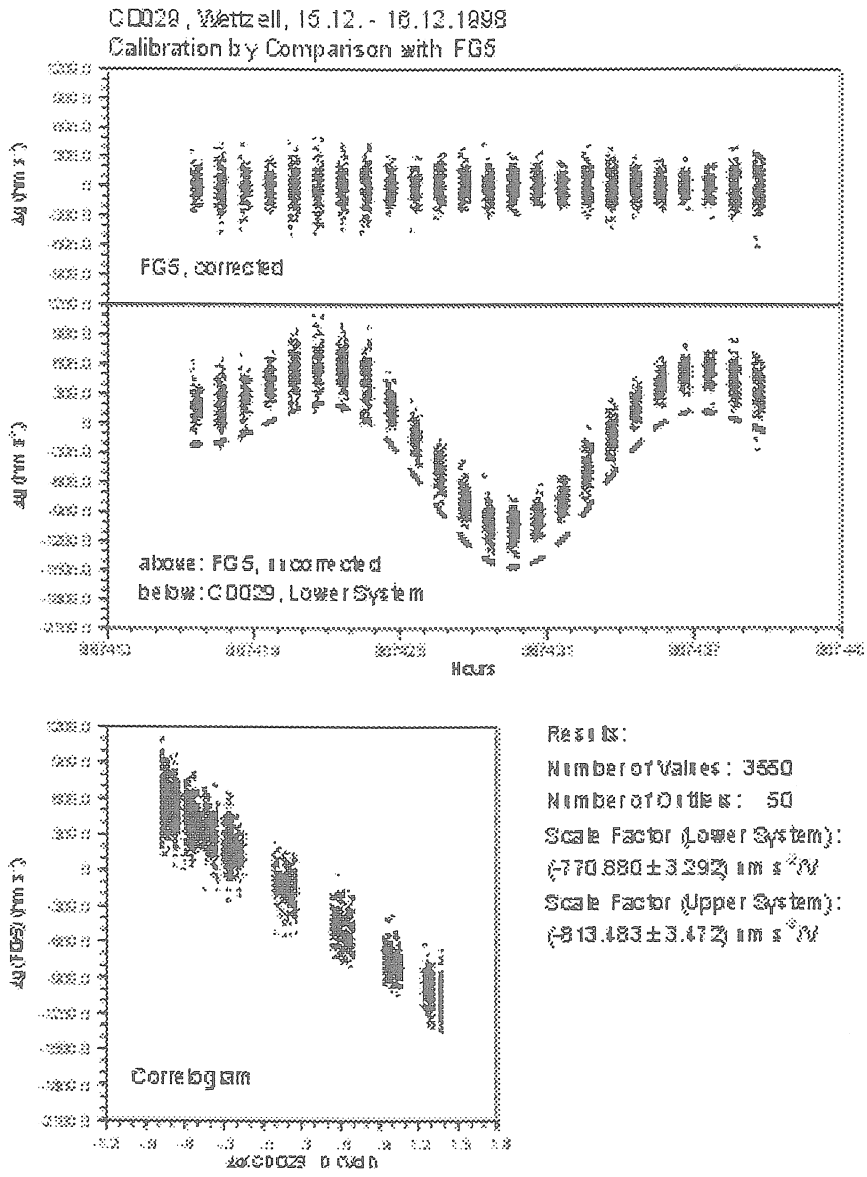

Fig. 14: Calibration of the CD029 by comparison with the absolute gravimeter FG5-101, Wettzell, 15. – 16.12.1998

889 Days of Registrations with the Superconducting Gravimeter SG103 at Wettzell (Germany)

M. Harnisch, G. Harnisch, H. Jurczyk, H. Wilmes
Bundesamt für Kartographie und Geodäsie (BKG), Frankfurt a.M.

Introduction

The SG103 was one of the gravimeters, announced to participate in the GGP. Since 1996 data were transferred weekly to the ICET. But already in November 1998, the registrations of the SG103 were cancelled and after a break of about six weeks the instrument was replaced by the dual sphere gravimeter CD029 [6]. With regard to this decision in the following a short information is given on the results and problems of the SG103.

1. History of operation of the SG103

Between August 8, 1993 and August 25, 1995 the SG103 was in operation at Bad Homburg. Noise and drift rate of this instrument were very promising in the first time of operation. Unfortunately between October 13 and November 10, 1994 the registration was broken by a gap of about 29 days into two main sections with significant different drift rates. This fact decisively complicates a new determination of the gravity effect of polar motions. At the same station between 1981 and 1984 the TT40 produced the first data series which very well reflected the gravity effect of polar motions [2]. Some results and problems of these older series were discussed during the workshop 1996 at Bonn [3] and on the Earth Tides Symposium 1997 at Brussels [1].

In April 1996 the SG103 was installed at Wettzell. It replaced the elder TT60, registering there since 1989. As a contribution to the GGP the data of the SG103 were transferred weekly to Brussels (ICET). The noise of these data was relatively high and the drift rate very large and not quite stable. As on the other hand higher accuracy gravimeters became available, the registrations of the SG103 at Wettzell were cancelled in September 1998. The SG103 was replaced by the new dual sphere gravimeter CD029, recording there since November 4, 1998. Since that time the CD029 data are transferred again to the ICET [6].

The SG103 was moved back to Bad Homburg where it was in operation since December 1998. But the quality of the data decreased more and more, so that in the beginning of April 1999 the registrations of the SG103 were stopped definitively.

2. Remarks on some technical details of the SG103

The SG103 is a single sphere instrument. It is the only instrument using a sphere of 0.5 inch in diameter. Its coldhead works at a temperature of about 20 Kelvin.

The analogue data are digitised by two AD-converters with different resolutions. The data are stored in an interleaved structure, which is used successfully since many years at the BKG. The basic sampling rate is 10 s, used for the gravity signal from the tide filter output. With the same sampling rate additional information of up to 10 channels is stored in parallel. The channels are switched in alternating order. In this way the air pressure is stored with an effective sampling rate of 1 min.

3. Instrumental drift

The instrumental drift may be derived from the residual gravity. Fig. 1 gives an impression of the drift behaviour of the SG103 during the different operation periods at Bad Homburg and Wettzell. Obviously after severe disturbances considerable changes of the instrumental drift may occur. Altogether five main periods have to be separated. The strongest changes occurred after the SG103 was moved from Bad Homburg to Wettzell (without changing the temperature inside the gravimeter). During the first time at Bad Homburg the gravimeter had a moderate positive drift. After the transportation to Wettzell the drift changed its sign and the residual gravity decreased rapidly with about -0.2 nm s^{-2}/hour. All attempts to reduce the drift rate remained without long-term success. Later in November 1996 with the beginning of the winter time the drift rate changed to -0.3 nm s^{-2}/hour without any evident cause. Since this time up to the end of the registrations at Wettzell in September 1998 the drift rate conserved this larger value. Back at Bad Homburg, again a moderate drift occurred, however with negative sign.

During none of the operation periods any significant exponential constituent could be observed in the instrumental drift as it has been often found in the behaviour of other instruments, e.g. the TT40 and the lower system of the CD029 [1][6].

4. Quality of the data and disturbances

The Wettzell data set under consideration is nearly complete. No gap longer than about one week did occur.

Gaps, arising from losses of single hourly files (e.g. during the data transmission from the gravimeter site at Wettzell to Potsdam) can be closed without any problem. If the gaps are too large (more than 48 hours) or are caused by serious perturbations, the data series has to be broken into blocks. In the case of the SG103 at Wettzell a subdivision into six of such blocks must be introduced. One of the larger gaps was caused by the attempt to reduce the drift rate (September 10 to 12, 1996), another by problems with the barometer and its replacement by a new one (February 1997).

During the whole two-year data series altogether 14 steps had to be corrected. The corresponding offsets ranged from 9 to 2500 nm s^{-2}. The frequency of the steps diminished to the end of the observations at Wettzell.

5. Tidal analyses and their results

The original gravity data were recorded with a sampling rate of 10 s. These data are decimated to 1 minute intervals by a fitting procedure, based on the adjustment of non overlapping sections of the data by polynomials of second degree. The 38 seconds phase shift of the tide filter is also taken into consideration during this step of the data processing. For the further data handling the PRETERNA software is used together with some graphically supported tools, specially developed for the interactive processing on HP workstations. In this way it is possible to monitor offsets and to avoid falsifications of the drift caused by inappropriate step corrections. Also big disturbances like earthquakes may be corrected by interpolation. In the last step of the preprocessing the data are despiked by the PRETERNA software. The resulting hourly values were first analysed by the ETERNA program separately for each of the six blocks.

In tab. 1 the results of a tidal analysis of all the six single blocks are shown, based on filtered data and a subdivision into 13 wave groups (without zonal tides). In a second analysis no fil-

tering was applied, the drift was modelled by Tschebyscheff-polynomials up to the second degree and 16 wave groups were used including zonal tides up to a period of 1 month. The results of this analysis are shown in tab. 2. The drift (last column) was estimated using a linear model in a separate step independently from the tidal analyses. The values are comparable to those given in figure 1 for subsets 3 and 4.

Tab. 1: Tidal Analysis (ETERNA), Filtered Data, 13 Wave Groups, 6 single blocks
first line: δ, second line: κ

block	Days	m_0	O1	K1	M2	S2	M3	M4	r_{air}
I	52.6	1.747	1.14213 0.1417	1.13067 0.0267	1.18066 1.5544	1.17264 0.5141	1.08105 -0.6652	1.28446 -168.193	-3.48394
II	89.0	2.521	1.14359 0.1422	1.12913 0.1351	1.18091 1.4976	1.17633 0.5021	1.04205 -1.5973	0.45196 135.789	-3.32578
III	112.1	2.520	1.14273 0.1457	1.12980 0.2677	1.18013 1.4849	1.17673 0.4511	1.03178 -0.7178	1.45802 41.0750	-3.16349
IV	39.0	1.094	1.14525 0.0894	1.13175 0.2833	1.18039 1.5137	1.17798 0.3068	1.08081 -0.0315	0.64640 -53.5830	-3.27165
V	251.5	1.402	1.14424 0.1523	1.13142 0.1944	1.18016 1.4813	1.17756 0.3173	1.06034 1.0970	0.62276 60.6532	-3.36094
VI	324.2	1.071	1.14460 0.1420	1.13099 0.2335	1.18039 1.4770	1.17881 0.3005	1.06902 0.2629	0.35879 113.141	-3.19070
total	868.4	1.743	1.14403 0.1428	1.13074 0.2084	1.18035 1.4859	1.17771 0.3590	1.06012 0.1347	0.39417 76.7810	-3.22187

m_0: standard deviation nms^{-2}, r_{air}: air pressure regression coefficient nms^{-2}/hPa

Tab. 2: Tidal Analysis (ETERNA), no Filter, 16 Wave Groups, 6 Single Blocks
first line: δ, second line: κ

block	days	m_0	Mf	O1	K1	M2	S2	r_{air}	drift
I	52.6	6.535	1.07724 -6.7676	1.14123 0.1524	1.13072 0.0905	1.18115 1.5596	1.17685 0.6811	-1.58056	-0.27900
II	89.0	8.652	1.29006 -1.7095	1.14338 0.1423	1.12920 0.1582	1.18093 1.4989	1.17789 0.5742	-2.41304	-0.20647
III	112.1	40.618	1.14690 4.2764	1.14268 0.1150	1.12995 0.2878	1.18047 1.4742	1.17792 0.5203	-2.51890	-0.21724
IV	39.0	3.009	1.31848 1.0152	1.14494 0.1057	1.13165 0.2791	1.18024 1.5121	1.17819 0.2963	-3.37892	-0.26244
V	251.5	21.515	1.17248 1.0899	1.14435 0.1534	1.13147 0.2304	1.18015 1.4766	1.17996 0.4517	-1.82711	-0.30399
VI	324.2	28.271	1.13461 3.3276	1.14446 0.1255	1.13099 0.2429	1.18059 1.4769	1.17971 0.3435	-2.52248	-0.28478
total	868.4	25.950	1.15328 1.9276	1.14388 0.1317	1.13077 0.2237	1.18050 1.4850	1.17913 0.4332	-2.31448	

m_0: standard deviation nms^{-2}, r_{air}: air pressure regression coefficient nms^{-2}/hPa, drift: linear drift rate nms^{-2}/h

For the determination of the residual gravity (fig. 2) only the results of the analyses of the unfiltered data (tab. 2) were used.

The air pressure regression coefficients vary strongly between the single blocks (from -1.6 to -3.4 nm s^{-2}/hPa). For most of the cases the absolute value is very low (table 2, lines 1 to 6). A low coefficient also results from a common analysis of all blocks (table 2, last line). If the diurnal tidal band is resolved in more detail and the half yearly as well as the yearly tides are included (altogether 23 wave groups) the analysis of the whole data set yields an air pressure coefficient of -2.6 nm s^{-2}/hPa (tab. 3).

The variations of the air pressure coefficient may be caused by failures of the barometer during the first, the fourth and the first two weeks of the fifth block. After a new barometer was installed, the coefficients became stable again, but their absolute values remained comparatively low.

The analyses of the total data set with different resolutions – 16 (table 2) and 23 (table 3) wave groups – seem to give hints on a relation between the number of wave groups and the amount of the air pressure regression coefficient. The higher the number of wave groups the more the estimated air pressure regression coefficient tends towards the "usual" value in the order of r_{air} = -3.0 nm s^{-2}/hPa. That means that a higher resolution of the analysis should improve the effectiveness of the air pressure correction. The reliability of the air pressure correction on the other hand influences the estimate of the drift rates. From table 2 it may be seen, that the two lowest values of r_{air} correspond to the highest drift rates.

The stability of the drift and the reliable determination of the drift rate are decisive conditions for the study of long-term gravity variations, especially the gravity effect of the polar motions. The estimation of the drift rate is complicated by the existence of the six single blocks, each of them with its own drift behaviour. Comparing the drift rates within the single blocks it becomes evident, that all values are large and quite different, but the sign and the general tendency are the same over the whole data set. This gives a possibility to estimate reliable parameters for the long-term gravity variations, if it is possible to replace the individual drift rates by one common value.

If the linear drift, valid for the respective block, and the gravity effect of polar motions are subtracted from the gravity residuals and the values within each block are shifted by suitable chosen offsets to a mean common level, we obtain the residual fluctuations shown in fig. 2. Surprisingly this very troubled picture is in good agreement with the gravity variations detected by absolute gravity measurements carried out at the same site during the registration period of the SG103 (marked by small circles). On the one hand the apparent drift values, calculated for the six blocks, are realistic within their estimated precision and in the mean they are confirmed by the absolute values. On the other hand the correspondence with the residual gravity curve of the SG103 shows, that the variations of the absolute gravity values are not only uncertainties of the measuring process. Obviously there are also small real non-periodic gravity variations of unknown origin as yet. A possible explanation could be found in hydrological influences.

Hydrological influences could not be included into the considerations because rainfall data became available only in the last months of the recording period. But from fig. 3 it may be seen, that generally hydrological influences are of great importance for the study of long-term gravity variations also in regions of moderate precipitation as Middle Europe. The hydrological influences onto the measured gravity variations were discussed in more detail during the workshop at Jena 1998 [4].

For the analysis of the data set as a whole in the following considerations 23 wave groups were used (tab. 3). With the resulting set of tidal parameters the residual gravity may be derived again only for the separate sections (blocks) of the data series. But these may be interconnected by offsets which are determined like steps between adjacent blocks. The result is shown in fig. 1 (sections 3 and 4). The general impression is that of a homogeneous curve.

Tab. 3: Tidal Analysis (ETERNA), no Filter, 23 Wave Groups

Wave Group	Without Elimination of Polar Motion Effect		Polar Motion Effect Subtracted With Theoretical Value δ=1.16		Polar Motion Included as Additional Channel	
	δ	κ	δ	κ	δ	κ
Sa	3.29312 ±19.52256	47.6922 ±500.2698	4.25402 ±18.83571	-90.7192 ±385.4711	17.18206±107.25032	-104.3514±101.9814
Ssa	1.26384 ± 1.40125	-11.0672 ± 49.8145	1.22534 ± 1.36551	-15.4998 ± 51.5841	1.17502 ± 1.32429	-24.3587 ± 67.1287
Mm	1.21548 ± 0.09883	-1.0984 ± 4.6783	1,21978 ± 0.09743	-1.0267 ± 4.5958	1.22774 ± 0.09692	-0.8952 ± 4.5371
Mf	1.15079 ± 0.04348	1.3330 ± 2.1710	1.14683 ± 0.04286	1.3621 ± 2.1476	1.13950 ± 0.04264	1.1464 ± 2.1475
Mtm	1.21950 ± 0.14942	-3.5540 ± 6.9972	1.22643 ± 0.14730	-3.5560 ± 6.8590	1.23928 ± 0.14637	-3.5596 ± 6.7438
Q1	1.14053 ± 0.00199	-0.0193 ± 0.1000	1.14044 ± 0.00195	-0.0234 ± 0.0981	1.14026 ± 0.00192	-0.0310 ± 0.0965
O1	1.14398 ± 0.00039	0.1345 ± 0.0196	1.14399 ± 0.00038	0.1355 ± 0.0192	1.14401 ± 0.00038	0.1374 ± 0.0189
M1	1.15217 ± 0.00358	0.0958 ± 0.1779	1.15229 ± 0.00351	0.1047 ± 0.1745	1.15251 ± 0.00345	0.1212 ± 0.1715
P1	1.14422 ± 0.00069	0.1925 ± 0.0344	1.14423 ± 0.00067	0.1939 ± 0.0338	1.14426 ± 0.00066	0.1965 ± 0.0332
S1	1.30968 ± 0.04101	9.6753 ± 1.7948	1.30910 ± 0.04024	9.7151 ± 1.7618	1.30803 ± 0.03955	9.7890 ± 1.7330
K1	1.13116 ± 0.00026	0.2369 ± 0.0132	1.13114 ± 0.00026	0.2363 ± 0.0129	1.13110 ± 0.00025	0.2353 ± 0.0127
Θ1	1.22845 ± 0.02960	-0.6549 ± 1.3812	1.22903 ± 0.02904	-0.7042 ± 1.3546	1.23010 ± 0.02854	-0.7954 ± 1.3302
M1	1.16887 ± 0.01581	1.0280 ± 0.7751	1.16873 ± 0.01551	1.0318 ± 0.7606	1.16847 ± 0.01525	1.0390 ± 0.7477
J1	1.15220 ± 0.00492	0.1677 ± 0.2444	1.15250 ± 0.00482	0.1771 ± 0.2398	1.15305 ± 0.00474	0.1945 ± 0.2355
OO1	1.15168 ± 0.01176	0.3285 ± 0.5850	1.15143 ± 0.01154	0.3421 ± 0.5741	1.15096 ± 0.01134	0.3673 ± 0.5645
2N2	1.15699 ± 0.00533	2.2130 ± 0.2640	1.15682 ± 0.00524	2.2104 ± 0.2593	1.15651 ± 0.00515	2.2056 ± 0.2551
N2	1.17384 ± 0.00109	1.9900 ± 0.0533	1.17387 ± 0.00107	1.9900 ± 0.0523	1.17393 ± 0.00105	1.9899 ± 0.0515
M2	1.18044 ± 0.00021	1.4847 ± 0.0101	1.18043 ± 0.00020	1.4846 ± 0.0099	1.18043 ± 0.00020	1.4845 ± 0.0097
L2	1.17336 ± 0.00603	0.0718 ± 0.2947	1.17325 ± 0.00592	0.0687 ± 0.2894	1.17306 ± 0.00583	0.0629 ± 0.2847
S2	1.17869 ± 0.00047	0.4115 ± 0.0226	1.17871 ± 0.00046	0.4127 ± 0.0222	1.17874 ± 0.00045	0.4150 ± 0.0218
K2	1.18029 ± 0.00225	0.5187 ± 0.1091	1.18025 ± 0.00221	0.5234 ±.0.1071	1.18016 ± 0.00217	0.5319 ± 0.1054
M3	1.06036 ± 0.00885	0.0710 ± 0.4784	1.06053 ± 0.00868	0.0628 ± 0.4691	1.06083 ± 0.00852	0.0477 ± 0.4603
M4	0.56597 ± 0.52566	75.2919 ± 53.2171	0.54035 ± 0.51545	75.6100 ± 54.6569	0.49295 ± 0.50577	76.2867 ± 58.7877
r_{air}	-2.56749 ± 0.01997		-2.55283 ± 0.01964		-2.52567 ± 0.01943	
r_{pole}					2.85260 ± 0.08020	
m_0	19.541		19.214		18.972	

r_{air}: air pressure regression coefficient nms^{-2}/hPa, r_{pole}: effective amplitude factor of the gravity effect of polar motions, m_0: standard deviation nms^{-2}

The different drift rates within the single blocks seem to be of less importance. Clearly they are dominated by a common tendency.

As already mentioned in paragraph 3 in November 1996 the drift rate changed from –0.2 nm s^{-2}/hour to –0.3 nm s^{-2}/hour. Both drift rates differ significantly but they are quite stable. Therefore in the following considerations a splitting into two sections is necessary corresponding to the two main drift rates identified in figure 1.

6. Long-term effects (Polar motions)

A formal simple way to estimate the contribution of polar motions is a multi-channel tidal analysis in which the gravity effect of the polar motions (with the a priori value $\delta = 1.16$) is included as an additional channel. At first 23 wave groups were used. In this way we obtain $\delta = 2.85$ as an effective value of the total polar motion influence (tab. 3, right columns), which is very different from the values determined by the fitting procedure described below. If in the same way a multi-channel tidal analysis with 22 wave groups is carried out (without the S_a wave), the δ-factor changes to 0.49. Both very contrary values of the δ-factor are absolutely unsuited to describe the gravity effect of the polar motions. That means that the multi-channel analysis must not be applied, if the time series is not freed from disturbing influences near the same period as the investigated one.

For the study of long-term gravity variations all known disturbing influences have to be subtracted from the measured gravity data. In the present case of polar motions above all the Earth tide variations and the influence of the air pressure have to be eliminated. The tidal parameters with 23 wave groups resulting from the analysis of the total data set (tab. 3, middle column) are used for that purpose. The influence of air pressure variations is eliminated using the measured local air pressure together with the air pressure regression coefficient taken from the same analysis. Hydrological influences also should be eliminated, but this was not possible because neither soil moisture nor groundwater data were available as mentioned above.

The right choice of the wave groups is difficult and connected with some severe problems. In principle it would be necessary to enclose the yearly tidal wave into the tidal model. But none of the six blocks is extended over a time span longer than one year. Therefore at first three variants of the tidal analysis have been tried in which the S_a wave was included and the influence of the polar motions was handled in different ways (see table 3). The mean square errors of the S_a wave resulting from all three kinds of analyses are very large and the δ- and the κ-values itself are quite different and unreliable. Therefore also a set with 22 wave groups was tried, limited to periods up to the half yearly wave.

The elimination of the drift of the whole data set is based on the two main sections of the data set (see paragraph 5). Both are handled separately and afterwards the results are combined to a unique set of residual gravity.

The corrected gravity residuals (23 WG, drift free) show a long-term periodicity (fig. 4). To resolve completely Chandler and annual periods more than five years should be required. Because the data set available here is much shorter, the residuals were fitted to a model with two periodic functions superposing each other. The first of them is exactly the period of one year. For the second one, which represents the Chandler wave, 420.75 days were used. This period was derived by fitting the model of two periodic functions to the calculated gravity effect of the observed polar motions in the time range under consideration. The best fit was found by stepwise variation of the larger period. The result of the correspondent fit of the observed gravity variations using the same model and the two periods mentioned above is shown in fig.

4. The resulting δ-factors of both periods are small in comparison to the expected value of 1.16 (table 4, upper line).

Tab. 4: Results of the Gravity Effect of Polar Motion depending on Annual Tidal Wave

Tidal Analysis	Annual Wave		Chandler-Wave	
	δ	κ	δ	κ
23 Wave Groups	0.962	10.22°	0.704	-14.05°
22 Wave Groups	1.324	52.42°	0.990	-14.26°

If the parameter set with 22 wave groups is used, the procedure of the determination of the polar motion effect remains the same as described above. The drift rates of the two sections of the whole data set are nearly the same and the graph of the drift free residual gravity is similar to that shown in figure 4. But if the data set is fitted to the superposition of the two periodic functions with the same periods (365.25 days and 420.75 days) the resulting δ-factors are quite different (table 4, lower line). The modified handling of the yearly constituent results in a δ for the Chandler-wave which is closer to the expected value of 1.16 while the phase lag is not changed.

7. Scale factor of the SG103

All data of the SG103 were processed with a scale factor of -981.0 nm s^{-2}/V. This value was derived from comparisons between the observed gravity variations and the well known tidal parameters (especially O1) at Bad Homburg. In this way the scale factor of the SG103 finally is based on tidal registrations with the LCR ET-15, carried out between December 1983 and July 1984 [2].

Meanwhile also comparisons with absolute gravimeters became available, which could be used for the estimation of the scale factor of the SG103. Table 5 summarises the results of all inter-comparisons during the registration period of the SG103 at Wettzell and of some later experiments at Bad Homburg.

The calibration by comparison with absolute measurements has the great advantage, that the operation of the superconducting gravimeter has not to be interrupted. In addition the absolute values may be used to check and to correct the drift of the superconducting gravimeter. Problems arise from the very different accuracies of the superconducting and of the absolute gravimeters. This and the principle of the evaluation procedure may be seen from fig. 5. First of all the elimination of outliers from the absolute measurements is of greatest importance. For that purpose a distribution-free test on the basis of the median and quartils is used. After the outliers are eliminated, a normal distribution of the measured values is assumed and the scale factor may be derived by linear regression. But some small systematic effects seem to remain (fig. 6). Their elimination could contribute to a slight increase of the calibration accuracy. However, it seems that until further improvements of the techniques of absolute measurements the calibration of superconducting gravimeters by comparison with absolute measurements is limited to accuracies in the order of 1 nm s^{-2}/V i.e. ≅ 0.1%.

Tab. 5: Scale factor of SG103 Determined by Comparison with Absolute Gravity Measurements

Period	Scale factor	Δg_{max}	Gravimeter	N	Out-liers	Comments
Wettzell						
18.-20.6.96	-988.495 ± 3.155	1597.52	FG5-101	4941	9	
19.-22.11.96	-988.385 ± 4.010	1670.9	FG5-101	12517	83	
21.-23.11.96	-987.446 ± 2.000	1851.8	FG5-103	9380	20	T. Baker
28.-31.1.97	-984.573 ± 5.825	1088.12	FG5-101	10759	41	
23.-24.6.97	-956.816 ± 3.102	1776.66	FG5-101	4755	45	
30.9.-2.10.97	-986.447 ± 2.453	1244.93	FG5-103	9600	0	T. Baker
8.-10.10.97	-965.761 ± 6.609	1253.65	FG5-101	5508	192	
12.-15.5.98	-983.226 ± 5.746	1815.58	FG5-101	8600	100	
28.-29.7.98	-971.062 ± 8.243	1064.19	FG5-101	3128	22	
Weighted Mean of 9 Calibrations: (-982.145 ± 3.827) nm s^{-2}/V						
Bad Homburg						
19.-21.12.98	-983.578 ± 2.144	1961.1	FG5-101	4302	48	
14.-20.1.99	-988.791 ± 2.145	2409.19	FG5-101	18317	93	SG103 dis-
22.-25.1.99	-987.278 ± 3.944	1139.8	FG5-101	4286	6	turbed
3.-5.2.99	-995.050 ± 4.078	1311.96	FG5-101	4329	171	dto.
Weighted Mean of 10 Calibrations (without the last 3 at Bad Homburg): (-982.457 ± 3.197) nm s^{-2}/V						

Calibration experiments using the method of inertial accelerations ("platform calibration") should give a higher accuracy. Results from the gravimeters TT60, C023 and CD029 indicate, that an increase by more than one order of magnitude seems to be possible [5]. The SG103 however, was not calibrated by this method.

Final Remarks

The registration period of the SG103 covers a time span of more than two years. The expected influence of the polar motions on the recorded gravity variations could be detected clearly. However, some of the numerical results are uncertain. The estimated δ-factor of the Chandler wave is too small. The results depend on the details of the method used for the data processing. The main reason for the unsatisfying results are the short time interval of the data series and the inhomogeneity of the data, resulting from different interruptions, which on their part may be connected with changes of the drift rate. The large amount of the drift rate itself seems to be of secondary importance.

From several comparisons with absolute gravimeters a reliable scale factor could be derived. Comparisons with absolute measurements do not disturb the registrations and additionally they may be used to check and to correct the drift of the superconducting gravimeter. At the present time only the method of inertial accelerations would give a significant higher accuracy. But this calibration method should be applied only before and after long-time gravity registrations because it seriously affects the homogeneity of the data series.

Acknowledgments

The authors thank Trevor Baker (Bidston Observatory, U.K.) who made available the results of his absolute measurements with the FG5-103 at Wettzell. Reinhard Falk (BKG) kindly prepared and compiled the correspondent data of the BKG, measured between 1996 and 1999 with the FG5-101 at Wettzell and Bad Homburg.

References:

[1] Harnisch, M., Harnisch, G., Richter, B., Schwahn, W.
Estimation of polar motion effects from time series recorded by superconducting gravimeters.
Proc. 13th Int. Symp. Earth Tides, Brussels, July 1997. Obs. Royal Belgique, Brussels 1998. pp. 511 - 518.

[2] Richter, B.
Das supraleitende Gravimeter
Dt. Geodät. Kommiss., R. C (Dissertationen), H. 329, 126 S., Inst. Angew. Geodäsie, Frankfurt a.M. 1987

[3] Harnisch, M., Harnisch, G.
Longtime behaviour of superconducting gravimeters derived from observed time series
Working Group, Bonn 1996. BIM no. 127, p. 9796-9805

[4] Harnisch, M., Harnisch, G.
Hydrological Influences in the Registrations of Superconducting Gravimeters and Ways to their Elimination
Workshop, Jena 1998, BIM no. 131, p. 10161-10170

[5] Richter, B., Wilmes, H., Nowak, I., Wolf, P.
Calibration of a Cryogenic Gravimeter (SCG TT60) by Artificial Accelerations and Comparisons with Absolute Measurements
Poster Presentation at the General Assembly IUGG, Boulder 1995, unpublished

[6] Harnisch, M., Harnisch, G., Nowak, I., Richter, B., Wolf, P.
The Dual Sphere Superconducting Gravimeter CD029 at Frankfurt a.M. and Wettzell. First Results and Calibration
Proc. Second GGP Workshop Munsbach Castle (Luxembourg), 24-26 March 1999, in preparation

[7] Crossley, D .J., Xu, Su, van Dam, T.
Comprehensive Analysis of 2 years of SG Data from Table Mountain, Colorado
Proc. 13th Int. Symp. Earth Tides, Brussels, July 1997. Obs. Royal Belgique, Brussels 1998. pp. 659 – 668.

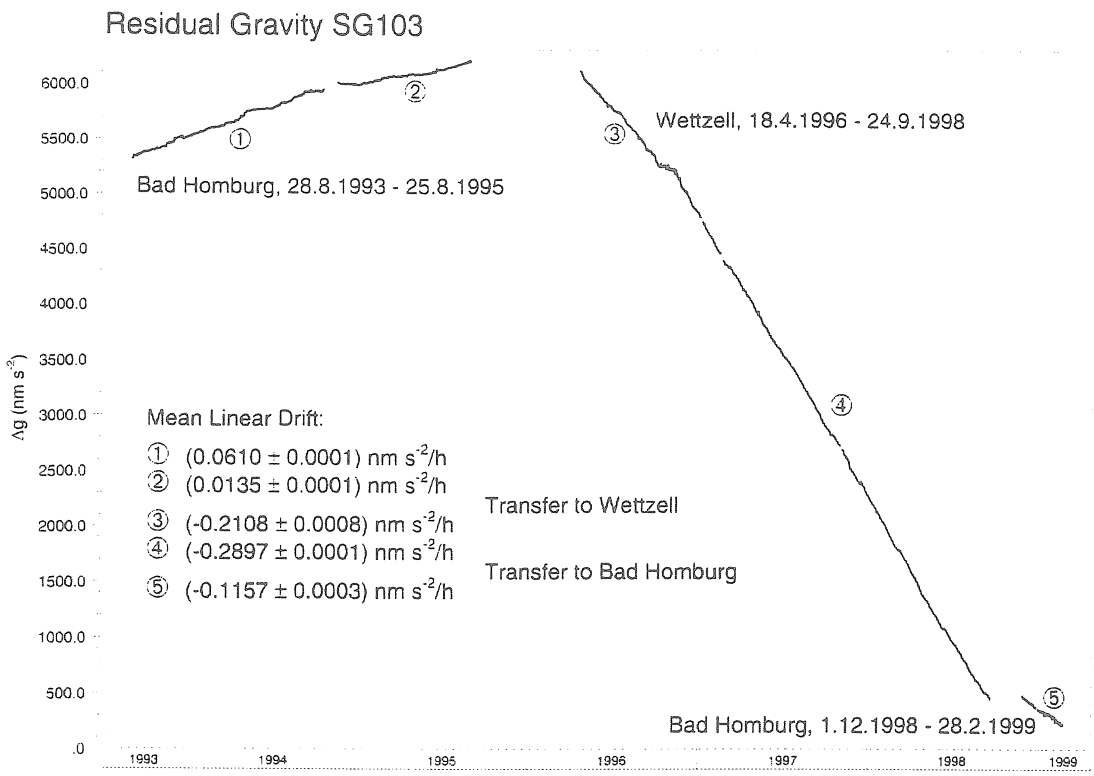

Fig. 1: Residual Gravity and Drift Behaviour of the SG103 between 1993 and 1998 at Bad Homburg and Wettzell

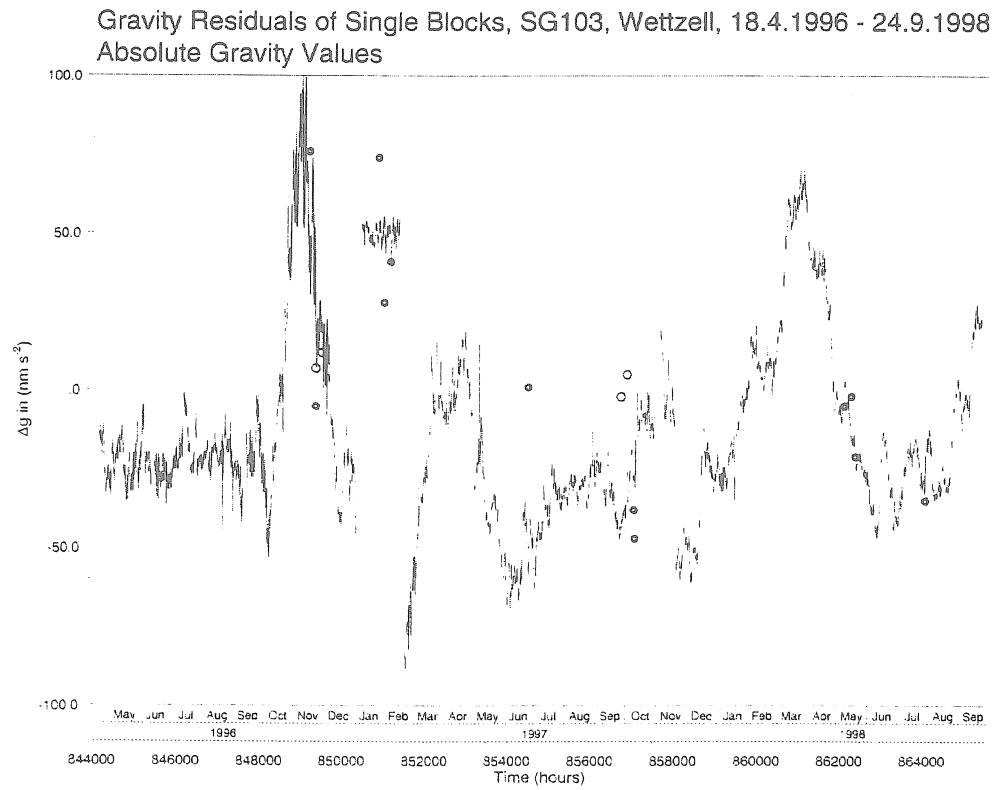

Fig. 2: Residual Gravity of the SG103 at Wettzell, April 18, 1996 – September 24, 1998. Comparison with Absolute Gravity Measurements. Dark circles: FG5-101, light circles: FG5-103 (T. Baker)

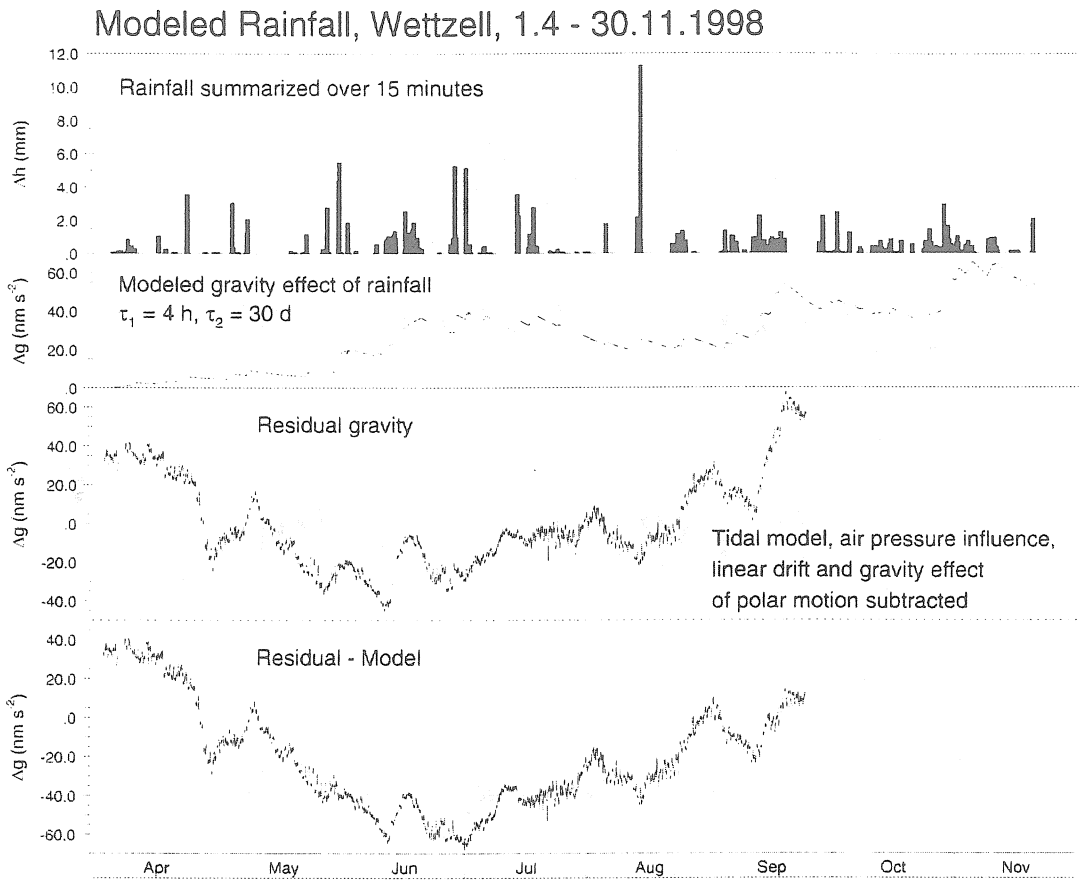

Fig. 3: Gravity Effect of Rainfall at Wettzell, April 1 – November 30, 1998, Modelled after Crossley and van Dam [7]. Simultaneous Residual Gravity of the SG103, Rainfall Effect Corrected

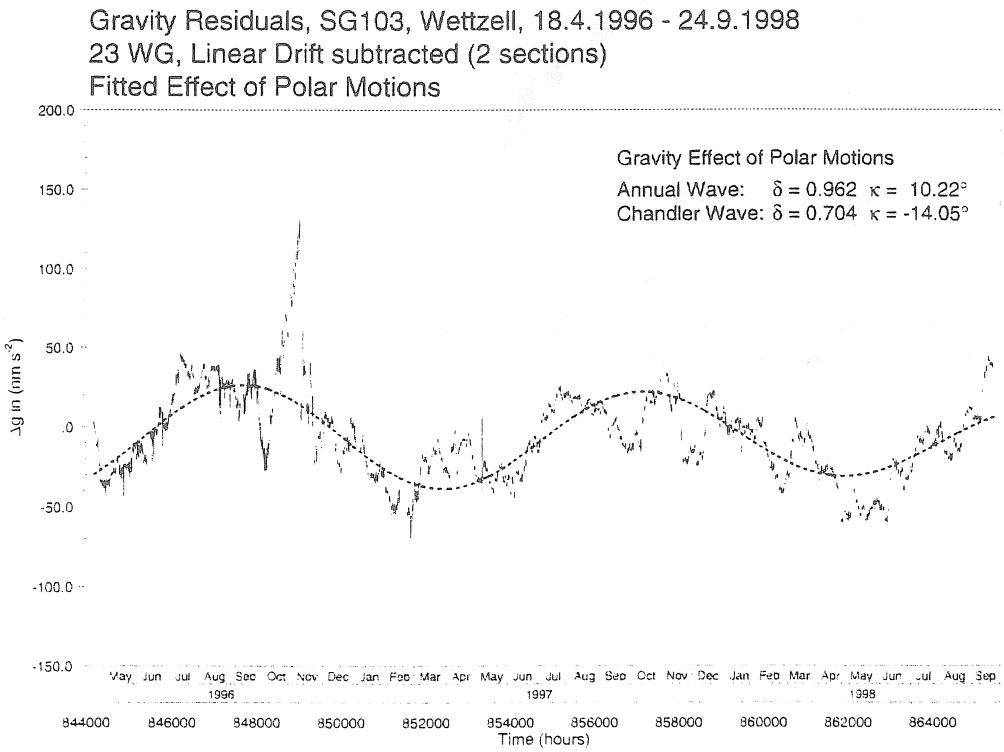

Fig. 4: Residual Gravity of the SG103 at Wettzell, 1996 – 1998. Gravity Effect of Polar Motions fitted to the Residual Gravity

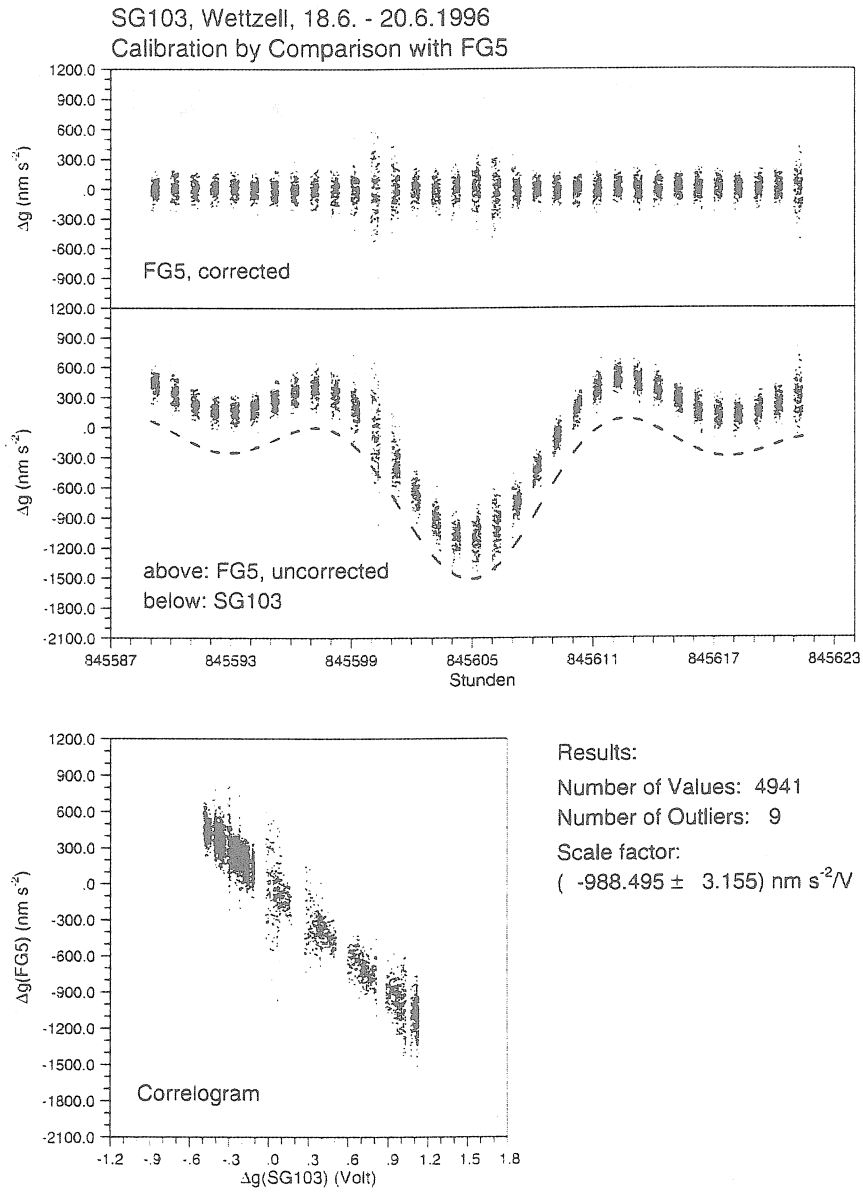

Fig. 5: Calibration of the SG103 by Comparison with Absolute Gravity Measurements at Wettzell, June 18 – 20, 1996

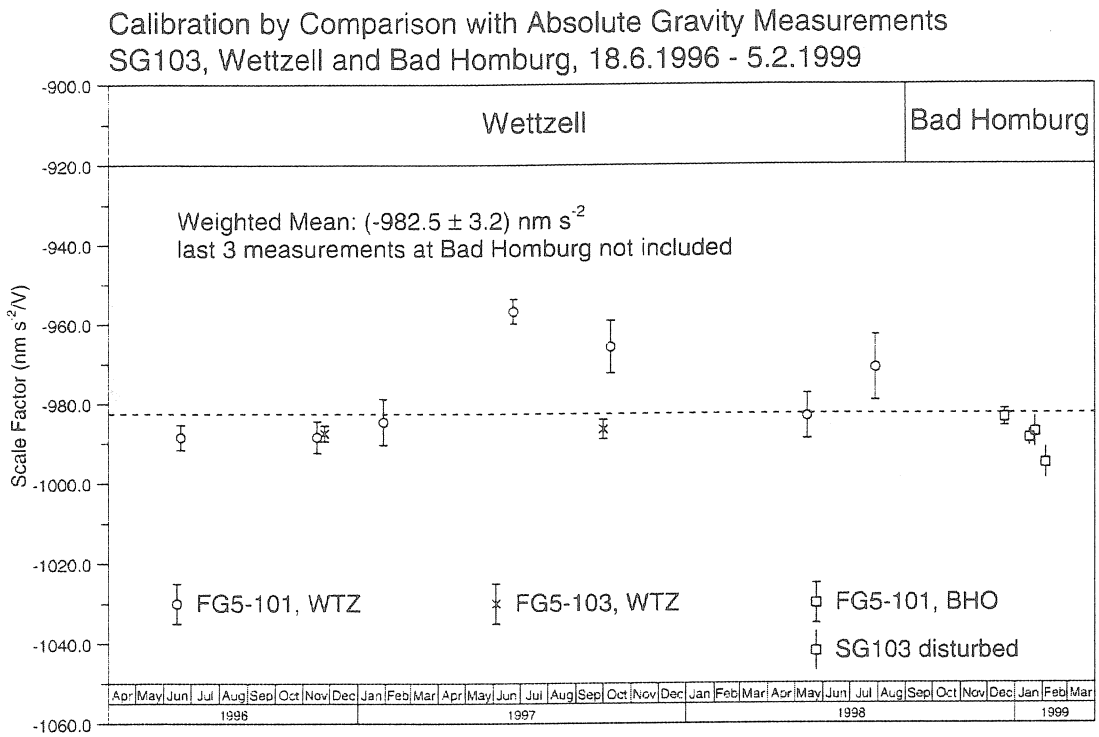

Fig. 6: Calibration of the SG103 by Comparison with Absolute Gravity Measurements at Wettzell and Bad Homburg. Results of all Campaigns with FG5-101 and FG5-103, 1996 – 1999

Final Results of the SG-Registration in Potsdam

by Hans-Jürgen Dittfeld

GeoForschungsZentrum Potsdam
Section 1.3: Gravity Field and Figure of the Earth
Telegrafenberg, D-14473 Potsdam, Germany
e-mail: ditti@gfz-potsdam.de

Summary
Operating from June 1992 till October 1998 the Superconducting Gravimeter (SG) GWR TT70 No. 018 yielded 2250.08 days of registration in Potsdam.
Using the **ETERNA 3.3** tidal analysis package (*Wenzel* 1996), a standard deviation of ±9.13 nm/s² was obtained for a model including, besides the diurnal(D), semi-diurnal(SD) and ter-diurnal(TD) waves, 10 long-period constituents and TCHEBYCHEFF polynomials for drift evaluation. The regression coefficient for the pole tide is 1.1268±0.518. The smallest errors on the amplitude factors of long-period wave-groups reach a few percent.
For the analysis of the filtered series including 47 wave groups, without long period tides, the standard deviation is ±0.84 nm/s² . The results corrected for the indirect effect of the oceans based on Schwiderski cotidal maps, agree with the WAHR-DEHANT-ZSCHAU Earth model (*Dehant*, 1987).
Computations including regressions with other environmental parameters than the air pressure have not given significantly different results.

1.The measurements

The gravimeter was installed next to the Potsdam absolute gravity site. Registrations were performed by the Data Acquisition and Monitoring System DDAS-1, delivered together with the gravimeter by GWR INSTRUMENTS , San Diego, California.
Data were digitised every five seconds with 22 bits A/D converters for the gravimeter and air pressure signals. For the environmental data such as the room temperature or the inclinations of the instrument the sampling was made every two minutes with 16 bits only.

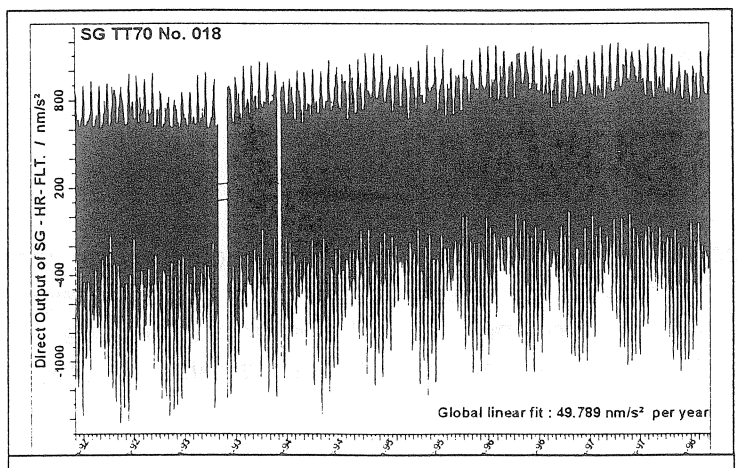

Fig. 1 Data-plot of the measurement

In Fig. 1 two longer interruptions are visible: the first one of about one month caused by a hard-disc crash, the second one of about 10 days due to a lightning stroke during a thunderstorm.
A number of shorter interruptions have been interpolated on the basis of former tidal results in Potsdam. So for instance about sixty so called "Read Time-Outs" interruptions of the high resolution Analogue-Digital Converter during the first 18 months of registration, altogether nearly 300 hours.
Altogether ten refillings, in each case with nearly 180 litres of liquid Helium, were made during more than six years of registration. The loss of liquid Helium was in the order of 0.2 to 0.3% per day. A higher loss took place only in case of stops or failures of the compressor for the cool head and of course at the end when the compressor was definitely switched off.

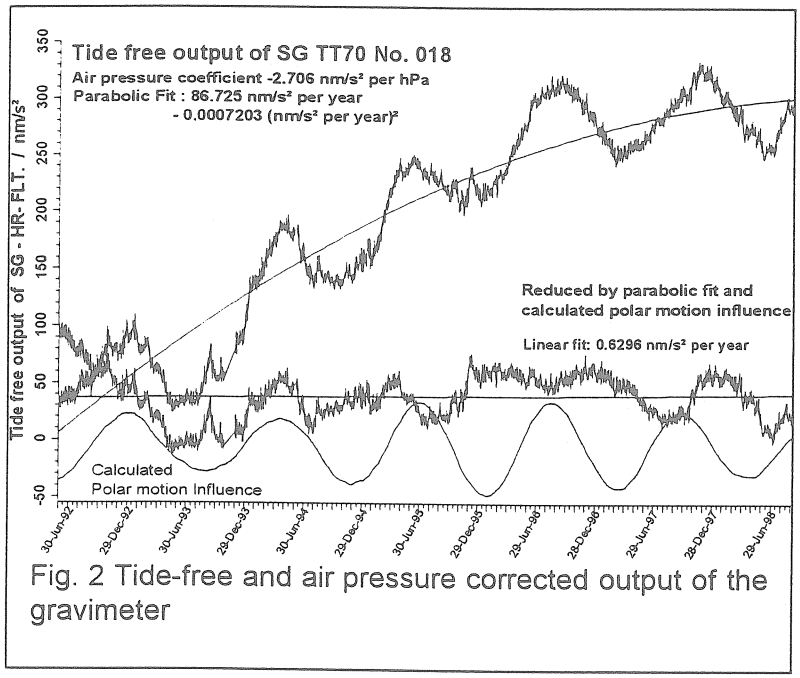

Fig. 2 Tide-free and air pressure corrected output of the gravimeter

The tide free and air pressure corrected output or **drift curve**(Fig. 2) has been extended with respect to the previous presentation in *Dittfeld* 1998a. While in the first years a linear fit was optimal for a global description of the trend, by now a polynomial of 2nd or 3rd degree seems to fit better. For the simple linear fit the drift is 47.2 nm/s² per year. It is very similar to the corresponding straight line fit on the direct data plot of Fig. 1 (49.8 nm/s² per year).
Subtracting the fitted function and the polar motion influence computed by means of the International Earth Rotation Service data (lowermost thin curve in Fig. 2) we get residuals that show during the first year a possible (but not sure) initial downwards drift and later on irregular oscillations of the order of 20 nm/s². Similar features are observed also with other SGs. Especially there are typical outbreaks lasting less than a dozen of days. This has to be modelled in the future for a better understanding of the behaviour of the instrument.

2. Tidal analysis

ETERNA 3.3 tidal analysis program was used in spite of the fact that the mean square errors for long period tidal waves are much larger than in the foregoing ETERNA versions (*Dittfeld* 1998a) - in the hope, that these errors are the most realistic. So the precision of the long-periodic parameters seems a little bit disappointing.

3. Polar motion effect

Because the polar motion influence is clearly seen in Fig. 2, one expects significant numerical results from the corresponding regression analysis. However the mean square error of the coefficient was very high in the beginning. For the first 1028 days the result is indeed near to the value expected by model calculations (1.162) but with an internal error of 1.041 (see table).

Pole tide Regression Coefficient during Prolongation of the Measurement

Length [d]	Pole tide Coeff.	Stdv. [±nm/s²]
395.3	0.707 ± 29.484	5.94
750.6	1.736 ± 1.941	6.69
1028.4	1.162 ± 1.041	7.82
1280.2	0.789 ± 0.534	7.82
1410.4	0.974 ± 0.825	7.97
1662.8	0.855 ± 0.581	9.39
1970.7	1.024 ± 0.582	9.03
2250.1	1.127 ± 0.518	9.13

When increasing the measurements length the correspondence to the model was going from bad to worse, but at the end it became better again.
Fig.3 shows the resulting coefficients with their errors versus the increasing time span.

We can see an asymptotic approach towards 1.16 and a very slow decrease of the still very high error bars.
Using a polynomial fit of degree 2 instead of 3 to remove the drift in each data block, the errors of all the single parameters were enlarged and the total standard deviation of the analysis was increased by a factor of about two (!).

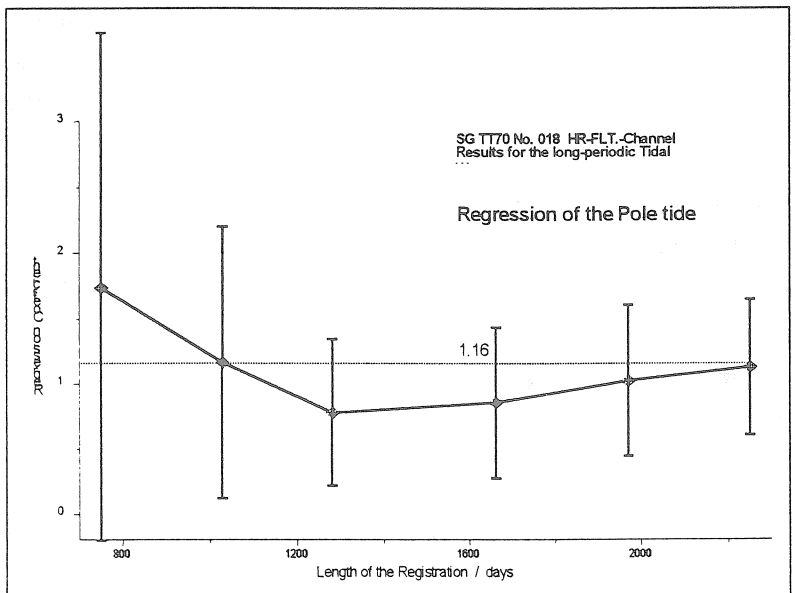

Fig. 3 Results for the pole tide during prolongation of the measurement

The use of other options of the ETERNA program as the length of day correction gave absolutely the same results. The application of a pole tide correction instead of the pole tide regression gave clearly higher standard deviations of the analyses.

The introduction of additional environmental parameters besides the air pressure did not provide better results too (see §6).

4. Tidal analysis results

The global analysis results are given for 47 wave groups (appendix 1) or 57 wave groups (appendix 2). The δ-factors of the analysis without long period constituents are shown as diamonds in Fig. 4 together with the model values (dotted line) and - additionally as crosses - after the correction of the indirect effect of the oceans for the eight main waves of the Schwiderski models.

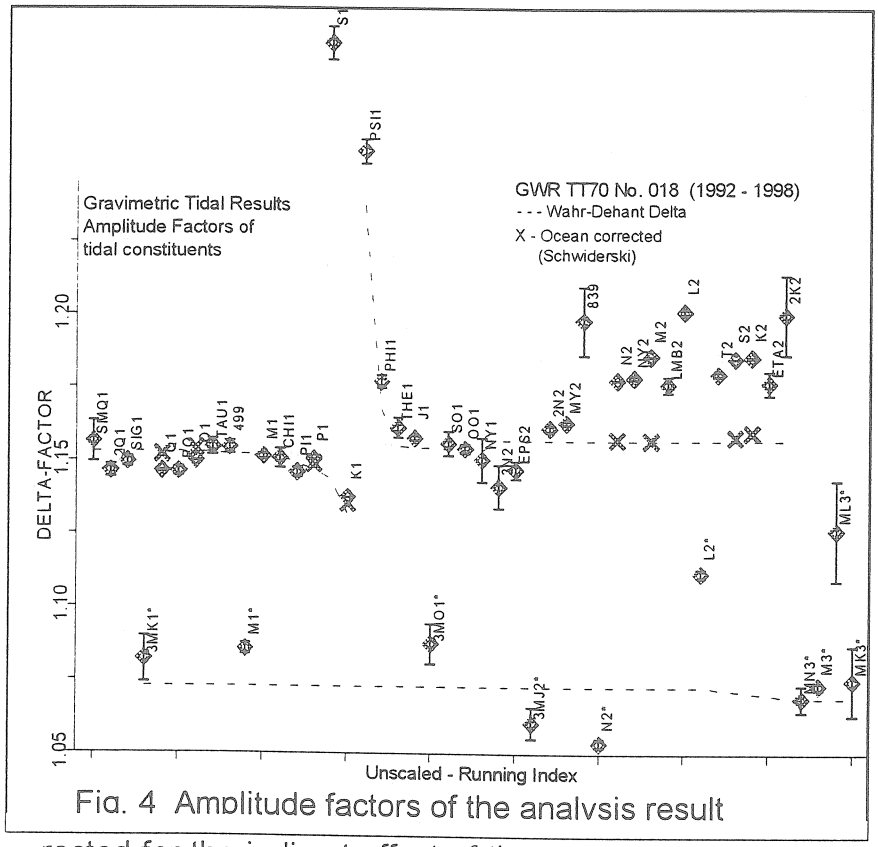

Fig. 4 Amplitude factors of the analysis result

Besides the TD waves , several D and SD constituents deriving from the third degree potential are separated. There is a risk of course to analyse waves which require normally more than eight registration years using only 2250 days. However, when comparing these results with those of the already published 25 year's registration with a spring gravimeter in the very neighbourhood (*Dittfeld* 1998b), no significant differences have been found.

Looking on those wave groups that can be corrected for the indirect effect of the oceans, we find in the table below the observed parameters of the 9 main waves.

Superconducting Gravimeter GWR TT 70 No. 018
Results corrected for the indirect effect of the oceans (SCHWIDERSKI)

Analysis program: ETERNA 33
2250 days in 1992 / 98

Wave	Observation		Indirect effect corrected			δmod	δc/δmod
	δ	κ°	[nm/s²]	δ_c	κ°		
MF	1.14036 ±0.01041	0.2545 ±0.5223	65.348	1.16130	0.1988	1.16442	0.99732
Q1	1.14631 ±0.00030	-0.1785 ±0.0148	66.365	1.15198	0.0061	1.15289	0.99921
O1	1.14980 ±0.00005	0.1317 ±0.0025	347.251	1.15408	0.0249	1.15269	1.00121
P1	1.15039 ±0.00009	0.0941 ±0.0047	160.887	1.14890	-0.0477	1.14716	1.00152
K1	1.13738 ±0.00003	0.1966 ±0.0017	480.369	1.13520	0.0775	1.13168	1.00311
N2	1.17781 ±0.00012	1.9311 ±0.0060	62.317	1.15755	0.0956	1.15708	1.00041
M2	1.18596 ±0.00002	1.3609 ±0.0010	325.397	1.15723	-0.0456	1.15708	1.00013
S2	1.18516 ±0.00005	0.1585 ±0.0023	151.538	1.15838	-0.2505	1.15708	1.00112
K2	1.18570 ±0.00021	0.4188 ±0.0100	41.297	1.15992	0.1414	1.15708	1.00245

After correction the phases are almost reduced to zero with a biggest deviation of 0.25° for S2.

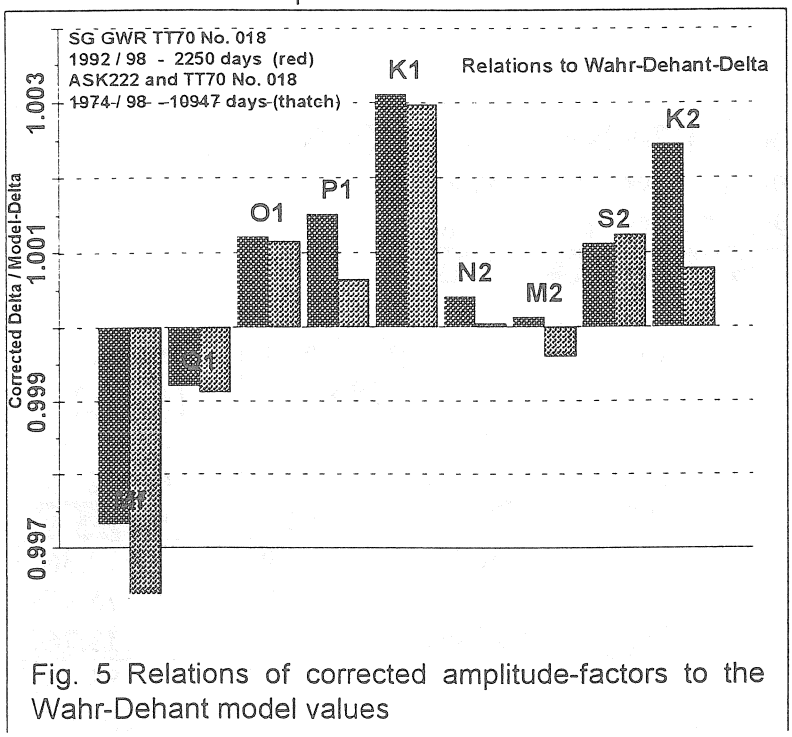

Fig. 5 Relations of corrected amplitude-factors to the Wahr-Dehant model values

We introduced also the Wahr-Dehant-Zschau δ_{mod} values. The deviations from unity of the ratio δ_c/δ_{mod} (last column) are generally smaller than 0.3%. For K1 only we get 0.31% (see also Fig. 5, left blocks). This can also confirm the calibration a posteriori.

It may be noticed that a common analysis of the SG data together with those of the long-term series of the ASKANIA GS15 No. 222 gravimeter (altogether with about 30 years of registration) comes even a little bit nearer to the model (Fig. 5, right blocks).

5. Long period tidal constituents

SG GWR TT70 No. 018
1992 07 - 1998 10 (2250.1 days) - ETERNA 33

Longperiodic Tidal Waves

Wave	Amplitude [nm/s²]	δ-factor	stdv. ±	Phase Lead [deg.]	stdv. [±deg.]
SA	18.450	4.4179	3.6889	-40.421	46.476
SSA	29.746	1.1312	0.2345	-2.220	11.767
STA	2.114	1.3772	2.6135	62.382	107.284
MSM	6.021	1.0547	0.1654	3.748	8.967
MM	33.971	1.1379	0.0280	0.616	1.401
MSF	5.989	1.2093	0.0943	-3.062	4.603
MF	64.389	1.1393	0.0103	0.324	0.515
MSTM	2.471	1.2026	0.1651	-1.222	7.864
MTM	12.511	1.1561	0.0362	-1.148	1.792
MSQM	1.840	1.0647	0.1293	0.361	6.954

One of the main reasons to use SGs is the hope to get more accurate tidal parameters for the long period tidal waves too. Among 10 long period waves, assuming a mean square error of a few percent as significance level, we found significant results only for three of them, namely MM, MF and MTM. These are marked in the table close by. But even for these wave groups the error of the phases is higher than their values so that also a zero phase difference may be assumed as true.

Looking for a trend in the results we analysed periods with increasing length i.e. 1993/96, 1992/97 and 1992/98 (see next table). One can detect some trends only in a few cases but almost no tendencies are evident.

SG GWR TT70 No. 018 in Potsdam

1993 03 - 1996 02 (1028.4 days)

1992 07 - 1997 02 (1662.8 days)

1992 07 - 1998 10 (2250.1 days)

Wave Group	Amplitude [nm/s^2]	δ-factor	stdv. ±	ph. Lead [deg.]	stdv. [±deg.]
SA	18.314	4.3854	7.3978	-19.693	487.331
	10.447	*2.5017*	*4.6872*	*-2.170*	*252.251*
	18.450	4.4179	8.6889	-40.421	463.776
SSA	26.941	1.0244	0.3079	-3.339	17.864
	30.035	*1.1421*	*0.3227*	*-3.510*	*18.974*
	29.746	1.1312	0.2345	-2.220	11.767
STA	3.972	2.5865	3.3504	101.383	188.703
	2.068	*1.3468*	*3.6149*	*-6.055*	*207.330*
	2.114	1.3772	2.6135	62.382	107.284
MSM	5.559	0.9736	0.2063	0.741	11.842
	5.858	*1.0260*	*0.2352*	*0.511*	*13.478*
	6.024	1.0547	0.1654	3.748	8.967
MM	33.892	1.1353	0.0351	1.068	1.978
	33.817	*1.1328*	*0.0397*	*0.688*	*2.260*
	33.972	1.1379	0.0280	0.616	1.401
MSF	6.165	1.2451	0.1198	-6.214	6.847
	6.184	*1.2490*	*0.1369*	*-5.155*	*7.827*
	5.989	1.2093	0.0973	3.062	4.603
MF	64.015	1.1327	0.0125	0.539	0.711
	64.174	*1.1355*	*0.0140*	*0.320*	*0.800*
	64.530	1.1419	0.0103	0.324	0.515
MSTM	2.911	1.4166	0.2305	1.452	13.188
	2.544	*1.2380*	*0.2381*	*-1.566*	*13.648*
	2.471	1.2024	0.1651	-1.222	7.864
MTM	12.442	1.1498	0.0435	-2.283	2.492
	12.433	*1.1490*	*0.0489*	*-0.811*	*2.808*
	12.511	1.1561	0.0361	-1.148	1.792
MSQM	1.751	1.0134	0.1566	-4.758	8.956
	1.935	*1.1196*	*0.1737*	*1.359*	*9.956*
	1.840	1.0647	0.1293	0.361	6.954
Pole-Tide Regresssion		1.162 ± 1.041	(1993/96)		
		0.855 ± 0.581	*(1992/97)*		
		1.127 ± 0.518	*(1992/98)*		

The following evolution may be considered:

1. The standard deviations for the yearly wave SA are decreasing for δ and κ.
2. The δ-factors values of MSM and MF are increasing but decreasing for MSTM.
3. The phase differences of MM and MSF are reduced.

The mean square errors of the most significant long period constituents MM, MF and MTM are in the order of one, three and four percent respectively. The decrease with the extension of the measurement length is so slow, that an essential improvement may be expected only in something like a lifetime.

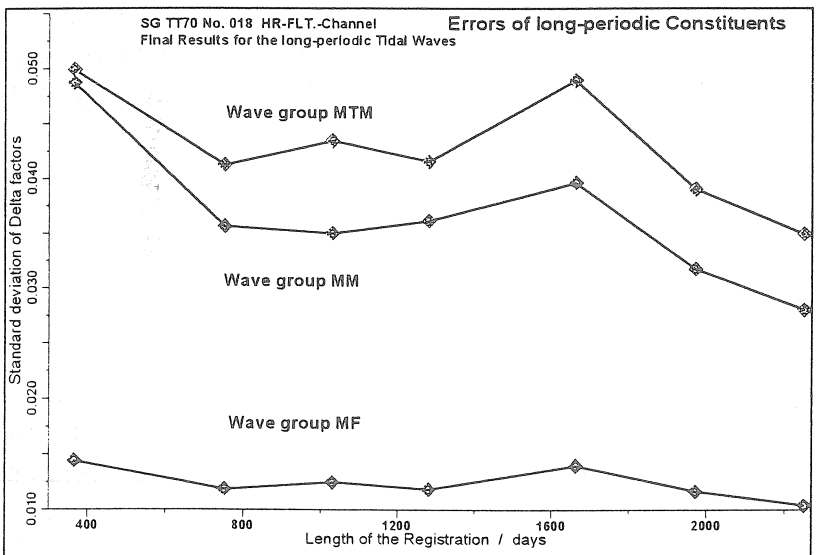

Fig. 6 Errors for some long-periodic tides during prolongation of the measurement

Naturally this is valid for this individual instrument working in a given environment and with a station maintenance as good as possible during the six years of measurement.
So we have to use our experience and try to improve the instruments and the installations in order to get in the future any significant success.

6. Influences of environmental parameters

Air pressure was registrated from the beginning with a sensor installed by GWR INSTRUMENTS inside the electronic rack of the data acquisition unit. All results mentioned before refer to air pressure corrected data. A correction was first applied during the remove-restore procedure of data despiking and degapping by the PRETERNA software (*Wenzel*, 1994). The tidal analyses gave air pressure regression coefficients of :

-2.7762 ± 0.0044 nm/s² per hPa for the final analysis with long period constituents and

-3.3153 ± 0.0041 nm/s² per hPa for the corresponding analysis with only 47 wave groups.

Other parameters as for instance the instrument tilt and different temperatures in- and outside of the gravimeter were measured every two minutes but almost not considered during this former evaluation. After the end of the measurement a special evaluation concerning room-temperature was performed.

Groundwater level measurements were carried out since a long time as monthly single readings about 300 meter northwards (Hy P 117/85) and, since 1992, also 1300 meter southwards (Hy Bgh Rb 120/84) of the gravimeter site, in each case at different horizons. Figure 7 shows the readings versus time till 1998. The variations are smaller than 0.5 meter and occur about 50 meters beneath the gravimeter. At a first sight, it seems that there are common long-term tendencies to the north as well as to the south, so that the situation may be considered as homogeneous concerning the water levels around the station. The only exception is the lower level of the near Potsdam gauge HyP117/85 (lowermost broken line in Fig. 7) which may be used by a drinking water pumping station. Therefore this gauge was equipped since 1996 with an automatic digital data logger, measuring the water level every ten minutes. Its readings were used for the following Checks.

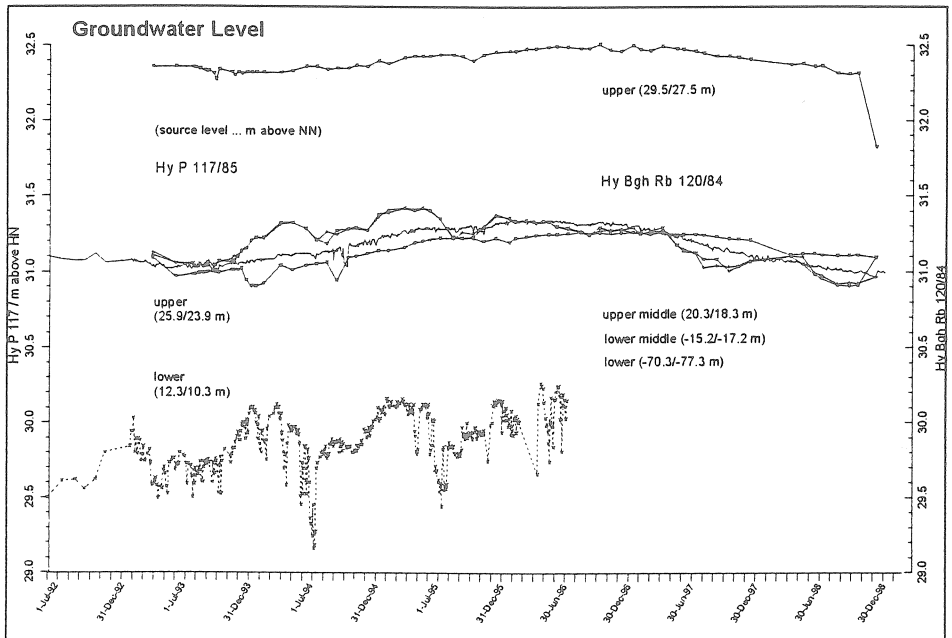

Fig. 7 Groundwater level measurements

Very small but persistent amplitudes in the diurnal and semidiurnal bands were found by tidal analyses . These analyses were performed with only two wave groups (diurnal, semidiurnal) as well as with a higher resolution to get the tidal frequencies S1 and S2 separately. Tidal amplitudes in the lower aquifer are smaller than 1.5 cm for the diurnal and smaller than 0.5 cm for the semidiurnal band respectively (last column in the following table).

Corresponding analyses were performed for the room-temperature too. The resulting amplitudes are in the order of some 10^{-3} degree Celsius except for S1 which reaches nearly 0.05 °C (see also table at following page).

Environmental Parameters
Room-Temperature and Groundwater-Level

	Room-Temperature above TT70	Groundwater- Level HyP117/85
Amplitude diurnal	0.0039°C	0.747 cm
Amplitude S1	0.0463°C	1.440 cm
Amplitude semid.	0.0028°C	0.184 cm
Amplitude S2	0.0087°C	0.486 cm
Regression 2143 days	-0.234 nm/s² / °C ±0.096	----------
Regression 1086 days	+0.872 nm/s² / °C ±0.065	----------
Regression 841 days	-0.32 nm/s² / °C ±0.06	-0.130 nm/s² / cm ±0.004
433 days	-1.09 nm/m² / °C ±0.10	-0.114 nm/s² / cm ±0.005

Adding the room temperature as an additional parameter to the analysis gave significant but different coefficients for the whole period (2143 days) and for the first half of it (1086 days) respectively. The coefficient for the room-temperature is in the first part more than three times bigger and with opposite sign compared to the whole period. That is a very significant difference.

The groundwater level data set is shorter. It was analysed using both correlation parameters i.e. groundwater level and room-temperature, in the same way as mentioned, first as a whole with 841 days and then with about the half of it (433 days). The regression coefficients for the groundwater influence are close to each other for both periods but nevertheless with a significant difference from a statistical point of view.
Also for this part of the measurement, which belongs to the second half of the data, the regression coefficients for the influence of the room-temperature differ by a factor of about three.

We can conclude that the effects of the mentioned parameters are generally too small and/or not enough persistent to provide significant regression parameters and an improvement of the results. A more detailed investigation especially concerning eventual temporal variations of the intensity of those influences may be useful.

7. Acknowledgements

Dr. J. Neumeyer, Dipl.-Ing. H. Pflug and the mechanician H. Mittmann have been involved like the author in the maintenance of the gravimeter and the data handling of the measurements analysed in this paper. Other members of Section 1.3 / GFZ "Gravity Field and Figure of the Earth" have continuously supported this work. All this is gratefully acknowledged.

References

Dehant, V., 1987. *Tidal parameters for an inelastic earth.* Phys. Earth Planet. Inter., 49, 97-116

Dittfeld, H.-J., 1998a. *The long-periodic constituents in the SG TT70 record at Potsdam.* Proceedings 13th Int. Symp. on Earth Tides, Brussels 1997, 599 – 605.

Dittfeld, H.-J., 1998b. *Recent Results of the Gravimetric Tidal Station Potsdam.* Proceedings 13th Int. Symp. on Earth Tides, Brussels 1997, 215 – 222.

Wenzel, H.-G., 1994. *PRETERNA - a pre-processor for digitally recorded tidal data.* BIM, 118, 8724 - 8734.

Wenzel, H.-G., 1996. *The nanogal software: Earthtide data processing package ETERNA 3.3.* BIM, 124, 9425 - 9439.

Appendix 1 Tidal analysis results – 47 Wave groups

```
#######################################################################
# Gravimetric Earth tide station Potsdam no.765 Germany               #
# GeoForschungsZentrum Potsdam                                        #
# 52.3805N 13.0682E H81M P2M D180KM   VERTICALCOMPONENT               #
# SL-GRAVIMETER TT70 NR. 018 - HR channel                             #
# INSTALLATION:      R. REINEMANN, San DIEGO                          #
# MAINTENANCE:       H.-J. DITTFELD;  J. NEUMEYER                     #
# CALIBRATED BY COMPARISON of TIDE RESULTS                            #
# INSTRUMENTAL LAG CORRECTED FOR 0.063 DEG O1 AND 0.130 DEG M2        #
#######################################################################

 Summary of observation data :
 19920630100000...19931127 30000  19931228 50000...19940629 30000
 19940708210000...19981008 50000

 Number of recorded days in total :  2250.08
 Hartmann+Wenzel (1995) tidal potential used with threshold  0.10E-04
 WAHR-DEHANT-ZSCHAU inelastic Earth model used.
 Inertial correction not applied
 UNITY window used for least squares adjustment.
 Numerical filter is  PERTZEV59   with  51 coefficients.
 Spectral condition number of normal equations:                 5.563

 Estimation of noise by FOURIER-spectrum of residuals
 0.1 cpd band99999.9990 nm/s**2        1.0 cpd band    0.0208 nm/s**2
 2.0 cpd band    0.0095 nm/s**2        3.0 cpd band    0.0068 nm/s**2
 4.0 cpd band    0.0065 nm/s**2        white  noise    0.0080 nm/s**2

 adjusted tidal parameters :
 from      to       wave    ampl.  ampl.fac.  stdv.  ph. lead    stdv.
 [cpd]     [cpd]         [nm/s**2]                      [deg]     [deg]
 0.721500 0.833113 SMQ1    2.5660   1.15646  0.00697  -1.2488   0.3452
 0.851183 0.859690 2Q1     8.7301   1.14632  0.00219  -0.8369   0.1095
 0.860896 0.892184 SIG1   10.5570   1.14953  0.00177  -0.3992   0.0881
 0.892331 0.892935 3MK1*   2.6759   1.08193  0.00791   1.6076   0.4189
 0.892950 0.894010 Q1     65.9710   1.14631  0.00030  -0.1785   0.0148
 0.895216 0.906315 RO1    12.5206   1.14619  0.00144  -0.1024   0.0717
 0.921941 0.932893 O1    345.6103   1.14980  0.00005   0.1317   0.0025
 0.934245 0.940487 TAU1    4.5237   1.15462  0.00280  -0.1074   0.1391
 0.958085 0.965827 "499"   9.8109   1.15453  0.00218   0.4757   0.1085
 0.965843 0.966284 M1*     8.3983   1.08540  0.00196   0.6813   0.1033
 0.966299 0.966756 M1     27.2048   1.15142  0.00081   0.2025   0.0402
 0.968565 0.974188 CHI1    5.2026   1.15073  0.00334  -0.0807   0.1665
 0.989049 0.995143 PI1     9.3685   1.14604  0.00161   0.2237   0.0807
 0.996968 0.998028 P1    160.8661   1.15039  0.00009   0.0941   0.0047
 0.999853 1.000147 S1      4.2711   1.29200  0.00568   2.8621   0.2519
 1.001825 1.003651 K1    480.6059   1.13738  0.00003   0.1966   0.0017
 1.005329 1.005623 PSI1    4.1523   1.25546  0.00402   0.5275   0.1837
 1.007595 1.013689 PHI1    7.0829   1.17708  0.00217  -0.1809   0.1057
 1.028550 1.034467 THE1    5.2493   1.16140  0.00331   0.3162   0.1631
 1.036292 1.039192 J1     27.3670   1.15786  0.00071   0.1586   0.0352
 1.039324 1.039649 3MO1*   3.0708   1.08735  0.00691   1.3552   0.3644
 1.039795 1.073349 SO1     4.5314   1.15598  0.00416   0.3563   0.2064
 1.075174 1.080944 OO1    14.9232   1.15425  0.00149   0.0101   0.0737
 1.099161 1.216397 NY1     2.8485   1.15050  0.00754  -0.2243   0.3757
 1.719381 1.823399 3N2     0.9114   1.14121  0.00757   2.3134   0.3799
 1.825518 1.856953 EPS2    2.3747   1.14715  0.00306   2.1392   0.1528
 1.858777 1.859381 3MJ2*   1.5737   1.06052  0.00538  -0.0501   0.2906
 1.859543 1.862428 2N2     8.2438   1.16135  0.00095   2.4619   0.0470
 1.863634 1.872142 MY2     9.9658   1.16325  0.00072   2.3558   0.0352
 1.888387 1.895069 "839"   0.5402   1.19803  0.01175   1.5287   0.5620
 1.895363 1.895673 N2*     5.6978   1.05376  0.00142  -0.1792   0.0770
```

1.895673	1.898720	N2	63.1798	1.17781	0.00012	1.9311	0.0060
1.900529	1.906462	NY2	12.0106	1.17870	0.00058	1.8426	0.0284
1.923766	1.942753	M2	332.2638	1.18596	0.00002	1.3609	0.0010
1.958233	1.966593	LMB2	2.4302	1.17631	0.00282	0.8254	0.1373
1.968271	1.968727	L2	9.5134	1.20125	0.00081	1.3593	0.0386
1.968875	1.969037	L2*	5.5442	1.11163	0.00150	0.8589	0.0774
1.969169	1.998287	T2	8.9900	1.17994	0.00078	0.0464	0.0381
1.999706	2.002885	S2	154.4668	1.18516	0.00005	0.1585	0.0023
2.003032	2.013689	K2	41.9921	1.18570	0.00021	0.4188	0.0100
2.031287	2.047391	ETA2	2.3312	1.17675	0.00414	-0.2113	0.2013
2.067579	2.182843	2K2	0.6221	1.20007	0.01360	-0.8253	0.6496
2.753244	2.869713	MN3*	0.9854	1.06898	0.00447	0.2052	0.2398
2.892641	2.903886	M3 *	3.6106	1.07339	0.00121	0.3221	0.0645
2.927107	2.940325	ML3*	0.2145	1.12616	0.01734	0.7961	0.8822
2.965990	3.081254	MK3*	0.4711	1.07502	0.01179	0.4184	0.6282
3.791964	3.937897	M4	0.0140	0.37453	0.09639	-4.9458	14.7458

Adjusted meteorological or hydrological parameters:

no.	regr.coeff.	stdv.	parameter	unit
1	-3.31526	0.00412	Airpress.	nm/s**2 / hPa

Degree of freedom: 53757
Max. correlation: -0.598 Y-wave-M1 with Y-wave M1*
Standard deviation: 0.837 nm/s**2

Appendix 2 Results with long period constituents
57 wave groups

```
#########################################################################
# Gravimetric Earth Tide Station Potsdam No. 765 Germany                #
# GeoForschungsZentrum Potsdam                                          #
# 52.3805N  13.0682E   H81M    P002M   D180KM    Gravity                #
# Superconducting Gravity Meter  TT70 No. 018                           #
# 1992.06.30 - 1998.10.08                                               #
# Installation: R. Reinemann, San Diego                                 #
# Maintenance:  H.-J. Dittfeld, J. Neumeyer, H. Mittmann                #
# Calibrated to Wenzel et al. 1992                                      #
# 16.2 SEC instrumental time lag corrected                              #
#########################################################################
```

Summary of observation data :
19920630100000...19931127 30000 19931228 50000...19940629 30000
19940708210000...19981008 50000

Number of recorded days in total : 2250.08
Hartmann+Wenzel (1995) tidal potential used with threshold 0.10E-04
WAHR-DEHANT-ZSCHAU inelastic Earth model used.
Inertial correction not applied
UNITY window used for least squares adjustment.
Numerical filter is no filter   with   1 coefficients.
Spectral condition number of normal equations: 380.675

Estimation of noise by FOURIER-spectrum of residuals

0.1 cpd band	0.2163 nm/s**2	1.0 cpd band	0.0300 nm/s**2
2.0 cpd band	0.0116 nm/s**2	3.0 cpd band	0.0069 nm/s**2
4.0 cpd band	0.0070 nm/s**2	white noise	0.0370 nm/s**2

adjusted tidal parameters :

from [cpd]	to [cpd]	wave	ampl. [nm/s**2]	ampl.fac.	stdv.	ph. lead [deg]	stdv. [deg]
0.002428	0.003425	SA	18.4503	4.41794	3.68889	-40.4209	46.4758
0.004710	0.005917	SSA	29.7456	1.13123	0.23450	-2.2203	11.7666
0.007595	0.010951	STA	2.1144	1.37725	2.61348	62.3824	107.2836
0.025812	0.031744	MSM	6.0211	1.05474	0.16538	3.7476	8.9667
0.033407	0.044653	MM	33.9715	1.13793	0.02801	0.6155	1.4012
0.060132	0.070611	MSF	5.9890	1.20931	0.09730	-3.0624	4.6030
0.072436	0.080797	MF	64.3895	1.13926	0.01027	0.3244	0.5152
0.096423	0.104931	MSTM	2.4712	1.20258	0.16507	-1.2219	7.8639
0.106137	0.115411	MTM	12.5106	1.15609	0.03615	-1.1475	1.7916
0.130596	0.249951	MSQM	1.8403	1.06473	0.12933	0.3606	6.9540
0.501370	0.911390	Q1	65.9525	1.14599	0.00087	-0.2222	0.0434
0.911391	0.947991	O1	345.6280	1.14986	0.00017	0.1300	0.0086
0.947992	0.981854	M1	27.2488	1.15328	0.00162	0.3047	0.0806
0.981855	0.998631	P1	160.8672	1.15040	0.00032	0.1202	0.0160
0.998632	1.001369	S1	4.2293	1.27936	0.01928	2.0156	0.8633
1.001370	1.004107	K1	480.6254	1.13743	0.00012	0.2049	0.0058
1.004108	1.006845	PSI1	4.1662	1.25967	0.01372	0.6317	0.6241
1.006846	1.023622	PHI1	7.0880	1.17794	0.00737	-0.1271	0.3586
1.023623	1.057485	J1	27.3592	1.15753	0.00217	0.1378	0.1074
1.057486	1.470243	OO1	14.8978	1.15228	0.00444	0.1227	0.2207
1.470244	1.880264	2N2	9.9550	1.16199	0.00153	2.4007	0.0752
1.880265	1.914128	N2	63.2311	1.17877	0.00032	1.9928	0.0155
1.914129	1.950419	M2	332.2691	1.18598	0.00006	1.3629	0.0029
1.950420	1.984282	L2	9.2852	1.17243	0.00159	0.6109	0.0775
1.984283	2.002736	S2	154.5598	1.18588	0.00013	0.2079	0.0065
2.002737	2.451943	K2	42.0089	1.18618	0.00060	0.4456	0.0287
2.451944	7.000000	M3M6	3.6101	1.07327	0.00284	0.3357	0.1515

Adjusted meteorological or hydrological parameters:

no.	regr.coeff.	stdv.	parameter	unit
1	-2.77617	0.00441	airpress.	nm/s**2 / hPa
2	1.12681	0.51776	pole tide	nm/s**2 /nm/s**2
3	1.80371	29.29407	dpoltid/dt	nm/s**2 /nm/s**2/d

Correlation matrix of meteorological regression parameters:

	airpress.	pole tide	dpoltid/dt
airpress.	1.000	-0.027	0.073
pole tide	-0.027	1.000	-0.048
dpoltid/dt	0.073	-0.048	1.000

Adjusted TSCHEBYSCHEFF polynomial bias parameters :

block	degree	bias	stdv.
1	0	404.722830 nm/s**2	0.367641 nm/s**2
1	1	17.713859 nm/s**2	0.149289 nm/s**2
1	2	31.786830 nm/s**2	0.184715 nm/s**2
2	0	-130.943602 nm/s**2	0.374169 nm/s**2
2	1	65.231643 nm/s**2	0.273233 nm/s**2
2	2	5.500268 nm/s**2	0.250314 nm/s**2
3	0	-1465.662712 nm/s**2	0.350433 nm/s**2
3	1	77.604048 nm/s**2	0.082763 nm/s**2
3	2	-28.819849 nm/s**2	0.084738 nm/s**2

Degree of freedom:	53936
Standard deviation:	9.128 nm/s**2